R-07-64

Quantitative assessment of radionuclide retention in the near-surface system at Forsmark

Development of a reactive transport model using Forsmark 1.2 data

Fidel Grandia, Clara Sena, David Arcos, Jorge Molinero,
Lara Duro, Jordi Bruno
Amphos XXI Consulting S.L.

December 2007

SKB

Quantitative assessment of radionuclide retention in the near-surface system at Forsmark

Development of a reactive transport model using Forsmark 1.2 data

Fidel Grandia, Clara Sena, David Arcos, Jorge Molinero,
Lara Duro, Jordi Bruno
Amphos XXI Consulting S.L.

December 2007

Summary

The Swedish Nuclear Fuel and Waste Management Company (SKB) is conducting a comprehensive geoscientific characterization of two alternative sites to locate a deep geological repository of high level nuclear waste. The site characterization program also includes the near-surface systems, which are expected to constitute the last geological barrier between the repository system and the earth's surface. The evaluation of the retention capacity of the near-surface systems is, therefore, highly relevant for the site characterization program. The main objective of this work is to assess the migration behaviour of selected long-lived radionuclides through the near-surface system of Forsmark, with special focus on the evaluation of the capacity of the Quaternary deposits and sediments for radionuclide retention. The work reported here is based on data and information from Forsmark Site Descriptive Model version 1.2.

From the geological point of view, the near-surface systems in the Forsmark area consist of Quaternary deposits and sediments that overlay the granitic bedrock. Glacial till is the more abundant outcropping Quaternary deposit (~ 75% of surface extension) and the remainder is made of clayey deposits (glacial and post-glacial clays). These types of near-surface sediments show distinctive hydraulic and geochemical features. The main reactive mineral in the till deposits, for the time horizons considered in this work, is calcium carbonate together with minor amounts of clay minerals (e.g. illite). The till deposits forms aquifers with relatively high hydraulic conductivities. In contrast, glacial and post-glacial clays are basically composed of illite with low to very low amounts of calcium carbonate, and containing organic matter-rich layers (*gyttja*), which can promote reducing conditions in the porewaters. All these clays exhibits relatively low hydraulic conductivity values.

Five radionuclides have been selected for conceptualization and qualitative evaluation of retention process: U as an actinide, Se as a redox-sensitive radionuclide, Cs as a monovalent cation, Sr as a divalent cation, and I as an anion radionuclide. Overall, radionuclide retention capacity in the surface systems at Forsmark can be provided by sorption on charged surfaces of clays and oxyhydroxides, co-precipitation with sulphates, sulphides, oxyhydroxides and carbonates, and sorption on organic matter.

The adsorption on ferrihydrite is the more plausible retention mechanism for uranium in the till deposits. Elemental analysis of this soil type at Forsmark supports this hypothesis, since the till deposits have relatively high uranium concentrations showing a rough correlation with the iron content. In more reducing glacial and postglacial clays, ferrihydrite is unstable and uranium is expected to be retained via precipitation of U(IV) solid phases. It is worth taking into account, however, that the uranium complexation with organic acids (e.g. humic acids) can reduce the availability of free aqueous uranium preventing a quick saturation with these phases.

Similar to uranium, selenium retention will be strongly related to redox conditions. Under reducing conditions, microbial activity is able to reduce both selenite and selenate to elemental selenium, which subsequently precipitates as iron selenide or co-precipitates with pyrite or amorphous FeS. In contrast, the retention capacity in more oxidising conditions as in the till can be much lower, although some mechanisms such as incorporation into carbonate minerals and adsorption onto organic matter may be effective.

Caesium competes with other monovalent and divalent cations in the interlayer of clay minerals. Particularly, this element has a strong affinity with frayed edge sites (FES) in clay minerals such as illite, which is a major component in Quaternary deposits at Forsmark. Therefore, cation exchange is expected to be the main retention mechanism for caesium in both glacial clays and till.

Strontium is also involved in cation exchange reactions in illite, competing with other divalent cations for the so-called "planar" sites. In addition, strontium can co-precipitate with calcium

forming $Sr_xCa_{1-x}CO_3$ solid solutions, although the incorporation of strontium into calcite lattice is very limited to molar fractions below 3.5×10^{-3}. This limitation is caused by the non-ideal behaviour of this solid solution series.

Iodine is a highly mobile element that can be present in soils as organic and inorganic complexes. The retention processes affecting this element are dependent on the aqueous speciation. Sorption onto hematite and kaolinite is an effective retention mechanism for iodate, whereas iodine can be adsorbed on illite. In organic matter-rich soils, iodine is effectively complexed by humic acids. Microbial activity can drive the methylation of iodide (CH_3I), which is volatile.

Two-dimensional coupled hydrogeological and reactive solute transport models have been developed to simulate the geochemical behaviour of U, Cs and Sr. These three radionuclides have been selected for quantitative modelling based on the availability of data and parameters. Two distinct geological and hydrogeological domains have been considered: (1) the till system and (2) the clay system. The first case simulates the intrusion of a radionuclide-bearing fluid from granite bedrock into a relatively dynamic till aquifer. In the second case, the radionuclide-bearing fluid interacts with a low permeability, reducing clay layer that is present at the bottom of a discharge zone (such as a lake or the Baltic Sea, for instance), overlying the till deposit.

Groundwater flow and transport modelling results highlight the different behaviour of the two simulated systems. The till system constitutes a dynamic aquifer, which reaches the transport steady-state in less than 8 years. On the other hand, the clay system constitutes a relatively low permeability aquitard in which the transport steady state needs hundreds of years to be reached.

Reactive transport results indicate that caesium is very strongly retained in the FES of illite in both till and clay systems. Most of the caesium mass entering the system from the deep source is effectively retained in the very close vicinity of the source, independently of the hydrogeological conditions. In the case of uranium, the most effective processes for retention are very different depending on the two considered hydrogeological systems. In the till aquifer, the dissolved uranium is mainly adsorbed onto the charged surfaces of ferrihydrite. It is seen that this dynamic aquifer system still exhibits a uranium retention efficiency of about 50% even after about 100 years of simulation time.

On the other hand, the simulated clay system is much more efficient than the till aquifer for uranium retention due to the precipitation of amorphous uranium (IV) oxides. Uranium retention efficiencies higher than 95% are computed for the clay system, even after more than 400 years. As in the case of caesium, most of the uranium mass entering the system from the deep source is effectively retained (in this case precipitated into solid phases) in the vicinity of the source.

Finally, model results indicate that strontium is retained by two different geochemical processes: (1) cation exchange within illite interlayers and (2) precipitation into a $Sr_xCa_{1-x}CO_3$ solid solution. Even though there are two distinct retention mechanisms affecting strontium, the clay system exhibits the lowest efficiency for retention of this radionuclide compared to the other two simulated radionuclides. Cation exchange is the dominating retention process in both the clay and the till system, but the contribution of carbonate solid solution is not negligible; its relative importance depends on the initial pool of carbonate minerals in the system. The overall efficiency of both systems to retain strontium shows a clear decrease with time. However, the efficiency for strontium retention of both systems is still higher than 60% after simulation times of hundreds of years.

From this study it can be concluded that the near-surface system at Forsmark constitutes a geochemically reactive barrier able to retain radionuclides by several key processes. Such retention mechanisms produce an effective overall retardation of the migration of the studied radionuclides.

Contents

1   Introduction

1.1   Motivation and context

The Swedish Nuclear Fuel and Waste Management Company (SKB) is investigating two alternative sites to locate a deep geological repository for the disposal of high level radioactive waste. SKB's intention is to assemble all the information that is required to choose one of the sites, and to submit a license application for a deep repository. In this context, SKB is conducting a comprehensive geoscientific characterization and modeling work. The results from the investigations at the sites are used as a basic input to the site descriptive modelling. A Site Descriptive Model (SDM) is an integrated description of the site and its regional setting as well as ongoing natural processes of importance for long term safety. The SDM shall summarise the current state of knowledge of the site, and provide parameters and models to be used in further analyses within Safety Assessment, Repository Design and Environmental Impact Assessment.

One important component of the site descriptive modelling approach is the so-called near-surface system, mainly composed of Quaternary deposits. The near-surface system is actually the transitional zone between the deep bedrock (also referred to as the geosphere) and the surface system (also referred to as the biosphere). The near-surface system would be the last natural barrier for an eventual radionuclides release from the repository to the surface. To evaluate and describe the radionuclide retention capacity of the near-surface system is therefore an important part of the site descriptive modelling.

1.2   Objectives

This work has two main objectives:

(1) To assess the migration behaviour of selected long-lived radionuclides through the near-surface system with special focus on the evaluation of the capacity of of the Forsmark Quaternary deposits for radionuclide retention.

(2) To test the ability of coupled reactive transport modelling technique as a tool for quantitative evaluation of the radionuclide retention efficiency of the near-surface system at the Forsmark site.

1.3   Scope

The work reported here is based on "data freeze" 1.2 and the corresponding Site Descriptive Model version 1.2 of Forsmark site, as it is described in /SKB 2005/. It is worth mentioning that major conceptual updates have been produced recently in Forsmark, mainly concerning the bedrock hydrogeological model. This fact could lead to some discrepancies with the hydrogeological assumptions adopted here. It is emphasised that the aim of this work is to produce quantitative and realistic results, but that these results are not "site descriptive" in the sense that they describe a particular catchment or place at the Forsmark candidate site. This is why the main insights from this work can be regarded as valid irrespectively of the updates in the hydrogeological conceptual model of the site.

The behaviour of selected long-lived radionuclides in the near-surface Quaternary deposits (including lake and wetland sediments) of the Forsmark site is conceptually evaluated and numerically modelled in this report. Due to their different chemical nature, these elements will be selectively retained by distinct mechanisms. From the available data and comparing with other examples in similar environments, the more favourable retention mechanisms are

determined. The evaluation is made considering that radionuclides would migrate from deep bedrock to the surface (Figure 1-1) so that the near-surface system Quaternary deposits will eventually interact with these radionuclides.

This report starts with a review of the available data for surface and shallow waters as well as for Quaternary deposits in the Forsmark area (Chapter 2). Possible retardation mechanisms for selected radionuclides are evaluated in Chapter 3, and a discussion to establish the geochemical conceptual model is given in Chapter 4. The radionuclide retention capacity of the Quaternary deposits and sediments is simulated by means of two-dimensional coupled groundwater flow and reactive solute transport models. Chapter 5 shows all the details related to the setup of the numerical models, including scoping flow simulations to establish the hydrogeological frame-work for the subsequently coupled models. Reactive transport model results are presented and discussed in Chapter 6. Finally, the main conclusions are summarized in Chapter 7 of the report.

1.4   Selection of radionuclides

Concepts of deep geological disposal are designed to retard for long periods of time the migration of radionuclides to the surface. During this retention time, the concentration of many radionuclides decreases to negligible levels since their half lives are relatively short. These short-lived radionuclides are only relevant in studies dealing with nuclear plants effluents or accidental releases (e.g. ^{90}Sr, ^{137}Cs). In performance and safety assessment of deep repositories of high-level nuclear waste, only radionuclides with long half lives are expected to reach the surface and, therefore, need to be taken into consideration in such studies. Among these long-lived radionuclides, we select here five for modelling purposes, based on the following considerations:

(1) uranium as a redox-sensitive actinide,

(2) selenium (^{79}Se) as a redox sensitive radionuclide forming oxyanions under anoxic and oxidising conditions,

(3) iodine (^{129}I) as an anionic radionuclide,

(4) caesium (^{135}Cs) as a monovalent cation radionuclide,

(5) strontium as a divalent cation radionuclide.
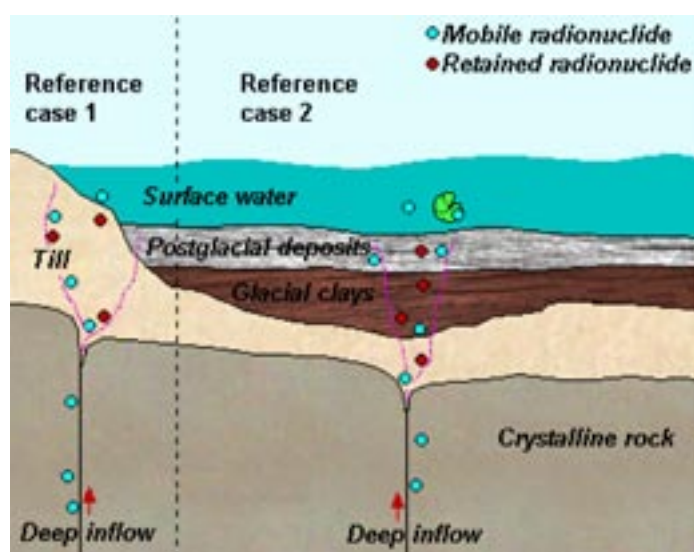
Figure 1-1. *Transition zones between bedrock and surface systems in the Forsmark area. Radionuclides migration can be retarded in glacial (till and lacustrine clays) and post-glacial deposits between rock and surface waters.*

2   Summary of surface and near-surface water chemistry and geology in the Forsmark area

The raw data used in this work correspond to the "data frezee" version 1.2 of Forsmark, as it was delivered by the ChemNet group of SKB. In the Forsmark area, direct contact between the crystalline bedrock and the surface systems/atmosphere occur regularly (13% of total land area, see /Sohlenius et al. 2004/). More commonly, Quaternary deposits and sediments separate bedrock outcrops from surface environments (Figure 2-1).

Glacial till is the most abundant outcropping Quaternary deposit (~ 65% of total land area; Figure 2-1). Other types of deposits, usually overlying till, are related to wetland areas, and consist of glacial clays and biogenic-derived sediments (gyttja). These wetlands have similar stratigraphy to sediments found presently in lakes. The thickness of Quaternary deposits is highly variable, usually from 0 to 2–3 m, although in some places it can exceed 10 m (Figure 2-2).

2.1   Till

Till features have been characterised in several reports from SKB, see e.g. /Sohlenius et al. 2004, Albrecht 2005, Lokrantz and Hedenström 2006/. It is believed to be deposited during the latest ice age and rest directly upon the crystalline bed rock. Several types of till have been described from the granulometric point of view /Albrecht 2005/; in general, the till is poorly sorted and consists of sand with variable amounts of boulders, and of clay.
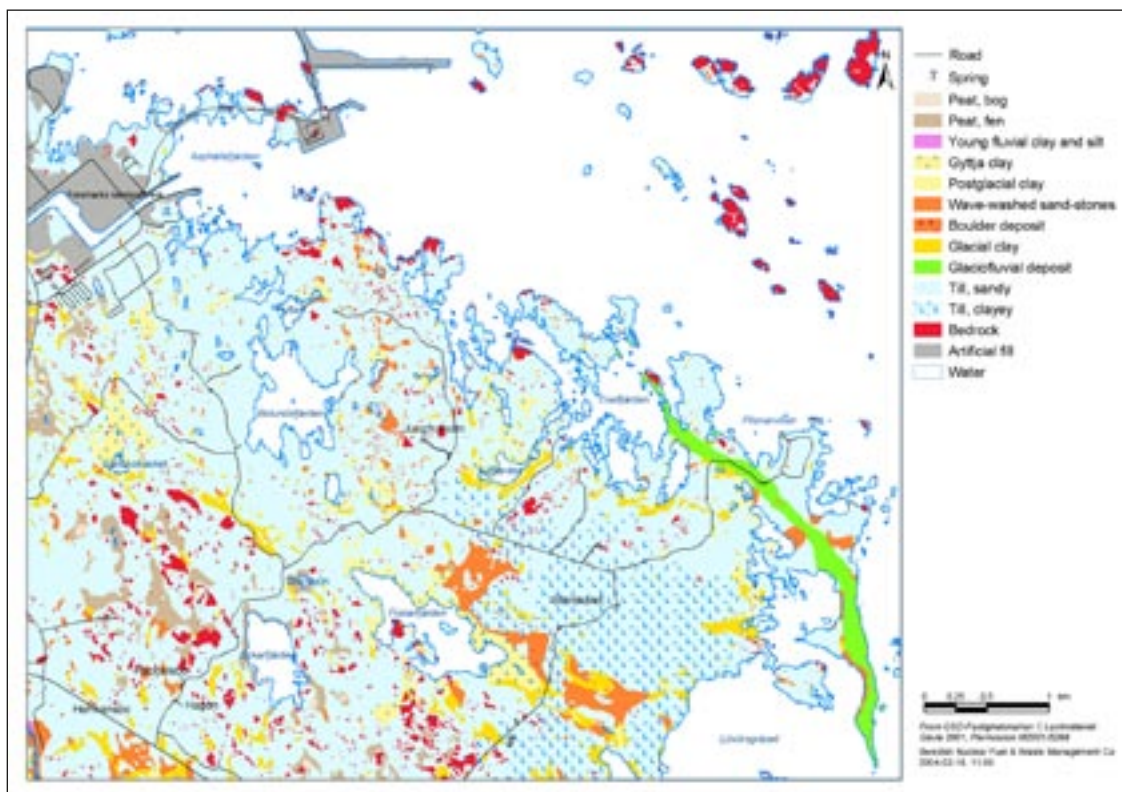
Figure 2-1. *Map of the Forsmark area showing the spatial distribution of Quaternary deposits /Sohlenius et al. 2004/.*
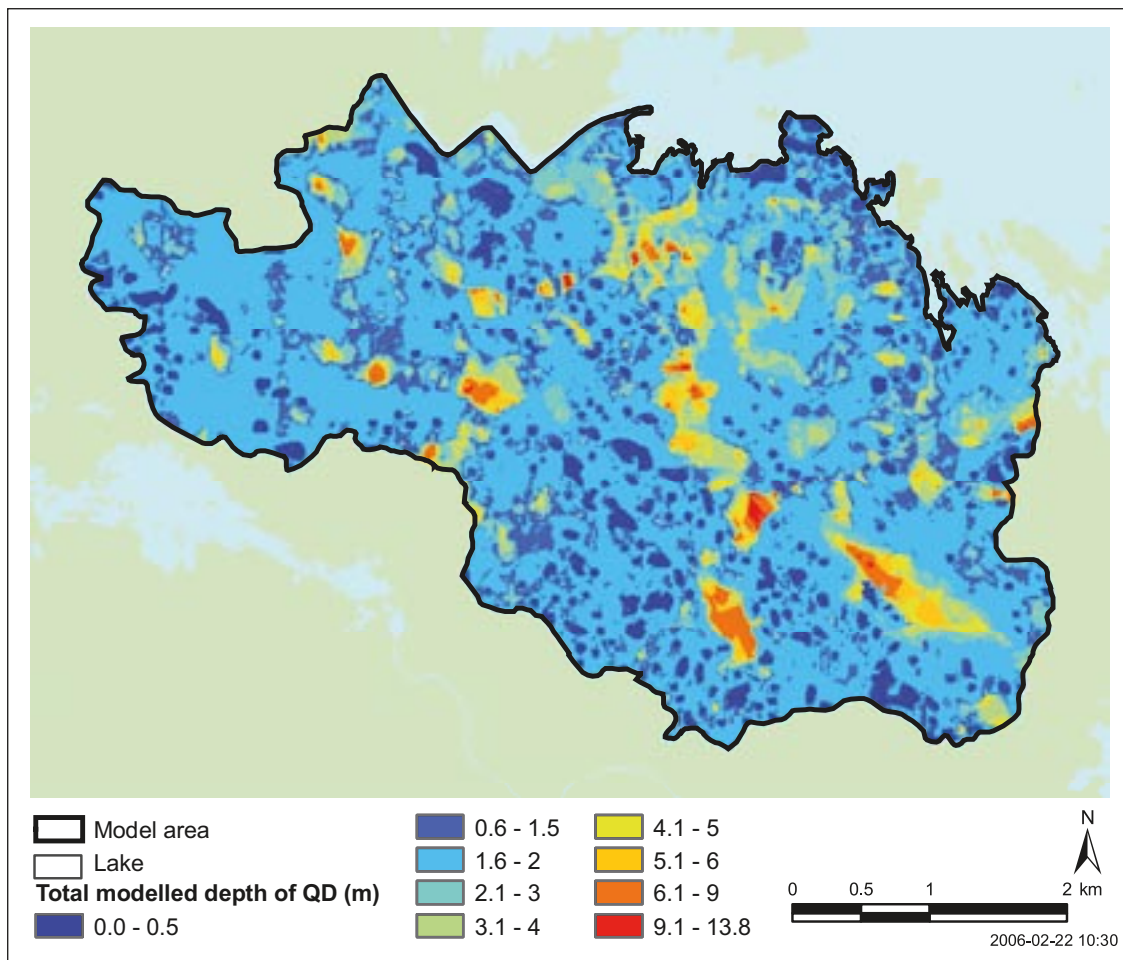
Figure 2-2. *Depth to bedrock, i.e. total thickness of Quaternary deposits, in the Lake Bolundsfjärden catchment area in Forsmark; figure from /SKB 2006/ based on model described in /Vikström 2005/.*

The origin of this till is associated with the glacial erosion and transport of Paleozoic carbonate rocks located northwards from Forsmark. Consequently, it contains significant concentrations of $CaCO_3$ (from 23 to 30 wt%). This is an outstanding geochemical feature from the perspective of the work developed in this project. In addition to calcite, the till is basically made up of clays, although no precise mineralogical description is provided in characterisation studies.

From analyses of the elemental content in the till /Tröjbom and Söderbäck 2006/, it can be inferred that other mineral phases could be present, such as Fe-Mn oxyhydroxides (see section 2.5), but no direct evidence exists. The uppermost level, consisting of gravelly sand, is carbonate-free due to recent surface weathering. Hydraulic conductivities of till are variable, from 5×10^{-9} m·s^{-1} in the sediments with higher clay content to 5×10^{-5} m·s^{-1} in the sandy-gravel levels. The uppermost level is highly conductive with a hydraulic conductivity of c 1×10^{-4} m·s^{-1}) /Johansson et al. 2005/.

2.2 Glacial and post-glacial clays

These materials are mainly related to reworking and deposition in low-energy environments during the post-glacial period; they typically contain organic layers (*gyttja*). These deposits are spatially associated with wetlands and lake sediments /Hedenström 2004, Vikström 2005,

10

Lokrantz and Hedenström 2006/, which show a very similar stratigraphy (Table 2-1). The composition of these sediments differs significantly from the till, since the amount of calcium carbonate is much lower, usually less than 1 wt%. However, it is worth mentioning that glacial clays with high carbonate contents (as high as 60 wt%) also are found at the bottom of many lakes.

Sampling in the Börstilåsen esker revealed that carbonate content in varved glacial clays varied seasonally, due to greater calcite precipitation during the formation of winter layers. Finally, a calcareous gyttja layer is found in some lakes, e.g. Lake Stocksjön /Strömgren and Brunberg 2006/, containing up to 65 wt% of $CaCO_3$. XRD analyses of glacial and postglacial clays in lake sediments show that the more abundant mineral is illite, and calcite is only present in glacial material /Hedenström 2004/. Other minerals detected in the analyses are quartz and chlorite (as clinochlore, $(Mg,Fe^{2+})_5Al[(OH)_8|AlSi_3O_{10}]$. It is worth mentioning that mineral phases that may be indicative of redox conditions, such as Fe-Mn oxyhydroxides or Fe sulphides have not been detected. However, this does not mean that they are absent.

Elemental concentrations of carbon, nitrogen and sulphur in these lake sediments increase from bottom to top of the stratigraphy; algal *gyttja* sediments are rich in carbon (up to 27%), nitrogen (up to 2.9%) and sulphur (up to 3.3%), whereas glacial clays are poor in carbon (up to 1.2%) and almost free of nitrogen and sulphur.

The most detailed characterisation of the elemental content in lake sediments is from Lake Stocksjön, recently reported by /Strömgren and Brunberg 2006/. The stratigraphy of the studied core (70 cm deep) shows very high contents of organic material in the upper levels, and reducing conditions are believed to be confined to the deepest levels. Calcium is preferentially found in the upper levels due to calcite precipitation, closely related to organic activity. Manganese is also enriched in the upper levels (perhaps as oxyhydroxides). On the other hand, many cations (Si, Al, Fe, K, Mg, Na) increase their concentrations at depth in the sediments, either forming a part of or being absorbed onto clay material. Deeper sediments are also richer in sulphur, although it is unknown whether it is present as solid sulphides or associated with the organic material.

From the geochemical information summarised in the previous paragraphs it can be postulated that the near-surface system in the Forsmark area consists of two hydraulically and chemically distinct environments, the till and the fine-grained sediments (including wetlands and lake sediments). In terms of hydraulic conductivity, the till is much more conductive compared to the fine-grained sediments. With respect to their chemical composition, the till is rich in calcium carbonate, whereas the glacial and postglacial clays are poorer in calcium carbonate but much richer in organic material. The evaluation of the behaviour of the selected radionuclides is made considering the chemical properties of these environments.

Table 2-1. General stratigraphy of glacial and postglacial deposits in the Forsmark area /Hedenström 2003/.

Environment	Lithology	Time
Freshwater lake	Gyttja	Recent
Postglacial Baltic basin	Gyttja clay	
Shallow coast	Sand, gravel	↑
Postglacial Baltic basin	Postglacial clay	
Late glacial Baltic basin	Glacial clay	Ancient

## 2.3　Water chemistry and its relationship with the Quaternary deposits

2.3.1　Major ions

In an initial characterisation, waters in the Forsmark area were divided into surface waters (lakes and streams) and shallow groundwaters. The latter type basically refers to waters flowing through the Quaternary till, since they have been collected at shallow depths (< 10 m). The chemistry of groundwaters is of special interest since it may give an insight into the radionuclide retention capacity of the Quaternary deposits.

The origin of water in both types is essentially the same (i.e. meteoric origin), so that major ion chemistry is quite similar. There are, however, substantial differences between water types. Firstly, some surface waters show large temporal changes in many ions (Cl, Br, Na, K and Mg), see Figure 2-3. These changes have been interpreted to be caused by saline inflow from relict or present-day seawater (e.g. in Lake Bolundsfjärden). Similar large variations are not as evident in individual shallow groundwater sampling points (Figure 2-4).

Secondly, surface waters show a very large temporal variability in both bicarbonate and calcium concentrations. This variability is caused by organic activity: the loss of dissolved CO_2 due to photosynthetic activity leads to a decrease of HCO_3^-, which in turn consumes protons to maintain the carbonate equilibrium, increasing pH. In periods with low organic productivity, putrefaction releases CO_2 and pH decreases. Figure 2-5 shows the inverse correlation between pH and bicarbonate.

The calcium concentration is also inversely correlated to the bicarbonate concentration. Shallow groundwaters show a reverse calcium and bicarbonate correlation to that from lakes and streams, so that higher calcium concentrations are found in those waters with lower bicarbonate
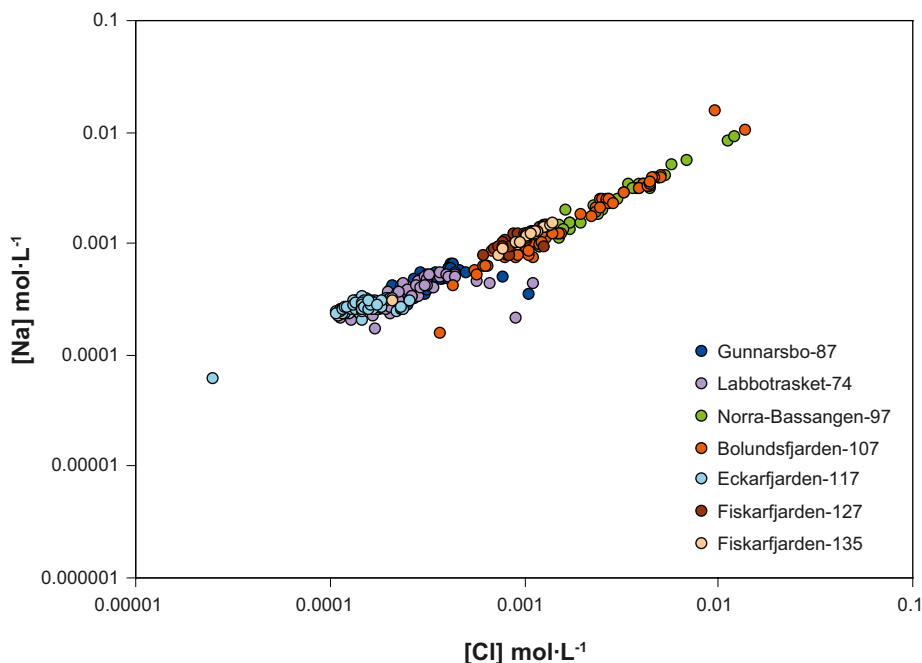
Figure 2-3. *Na vs Cl concentrations in lake waters. Note the wide ranges in composition in lakes such as Bolundsfjärden and Norra Bassängen. The numbers in the legend refer to PFM ID numbers.*
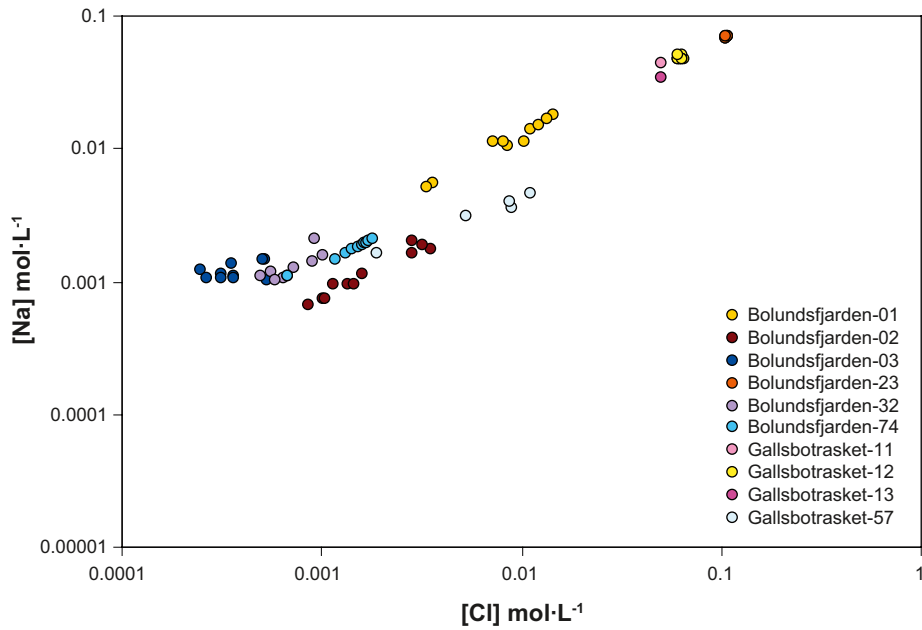
Figure 2-4. *Na vs Cl concentrations in shallow groundwaters in the Bolundsfjärden subcatchment. The numbers in the legend refer to SFM ID numbers. Water in groundwater monitoring wells SFM0011, SFM0012, SFM0013 and SFM0023 may have a substantial contribution from old saline waters.*
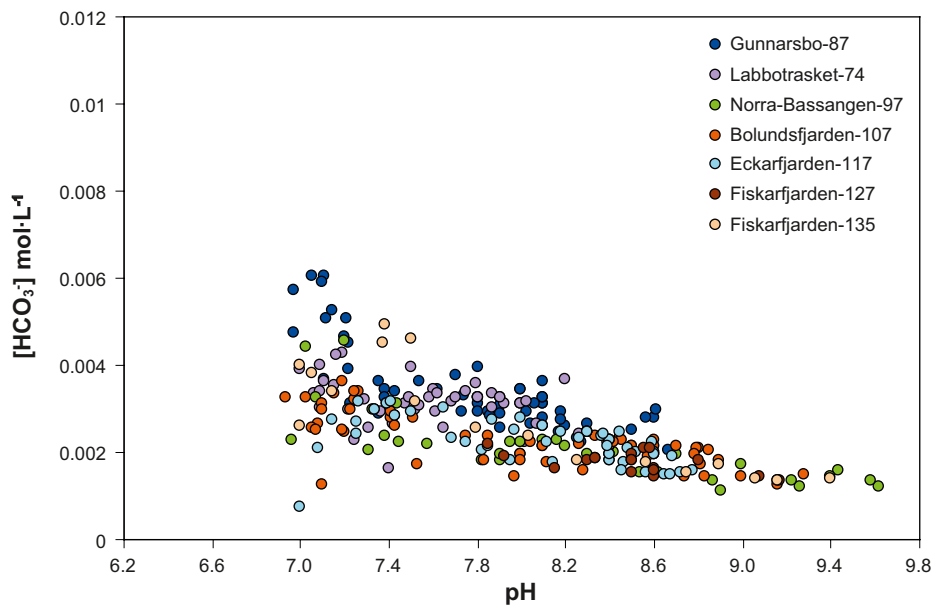
Figure 2-5. *Bicarbonate vs pH in lakes in the Forsmark area. The numbers in the legend refer to PFM ID numbers.*

content. In addition, individual wells show a small variability. pH in shallow groundwaters is relatively constant compared to lakes and streams and shows a positive correlation with HCO_3^- and calcium (Figure 2-6). These data suggest that pH in shallow groundwaters is not controlled by organic processes, but is directly influenced by carbonate mineral equilibrium.

Figure 2-6. *pH vs bicarbonate in shallow groundwaters in Lake Bolundsfjärden catchment. The numbers in the legend refer to SFM ID numbers.*
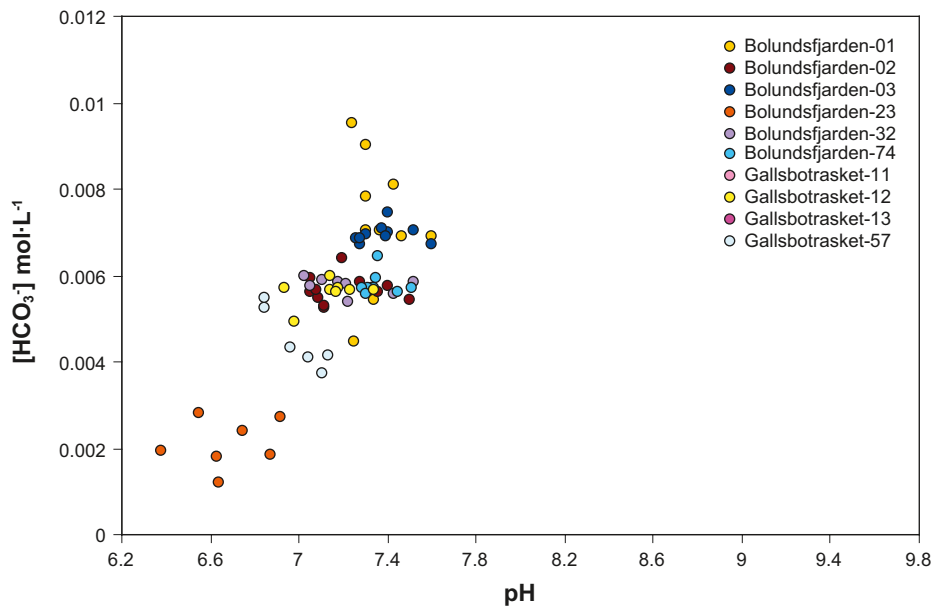
Calculated saturation indices for calcite and dolomite in shallow groundwaters are close to zero confirming the pH buffering exerted by the Quaternary deposits, which are very rich in $CaCO_3$ (Figure 2-7). The only exception is found in saline groundwater (well SFM0023 from Lake Bolundsfjärden area), which is slightly undersaturated. On the other hand, shallow groundwaters are close to saturation in SiO_2, reflecting the interaction with siliceous components of the soil (Figure 2-8).
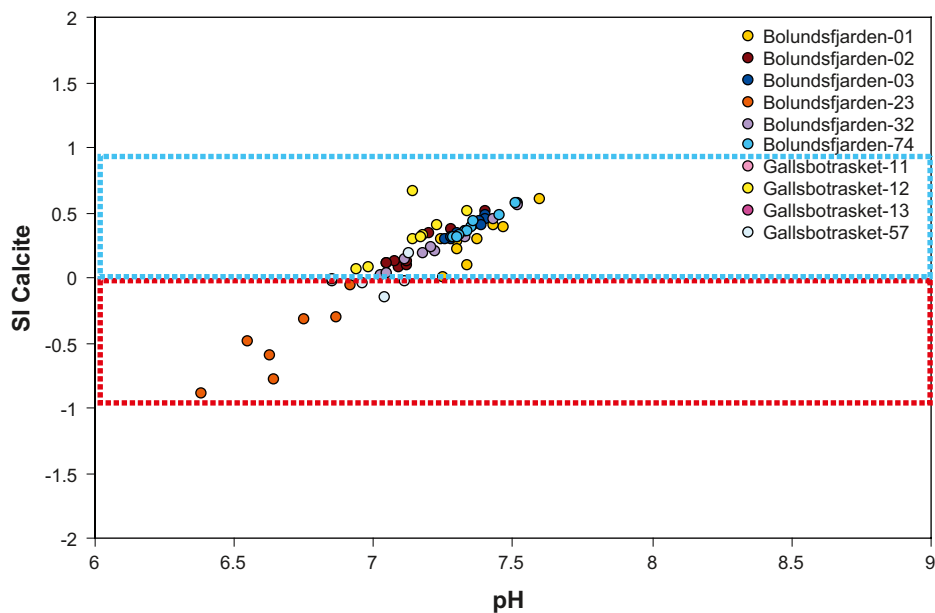
Figure 2-7. *Saturation indices of calcite for shallow groundwaters in the Lake Bolundsfjärden area. Except for saline waters (well SFM0023), all groundwaters are saturated or slightly oversaturated. The numbers in the legend refer to SFM ID numbers.*

14
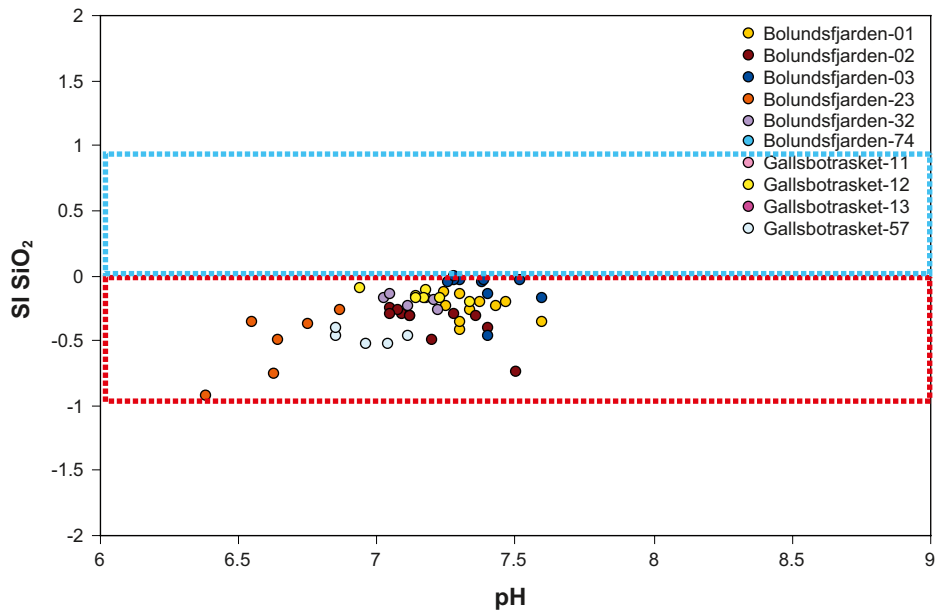
Figure 2-8. *Saturation indices of SiO₂ for shallow groundwaters in the Lake Bolundsfjärden area. All groundwaters are saturated or slightly undersaturated. The numbers in the legend refer to SFM ID numbers.*

The chemical buffer exerted by the Quaternary deposits, basically the till, is well illustrated in Figure 2-9, in which the composition of some shallow groundwater is represented in Stiff diagrams. This type of diagrams shows the composition of 6 major ions from a water sample providing a quick visualisation of the relative proportions between them. The concentration of each component is referred to the scale on the X axis.
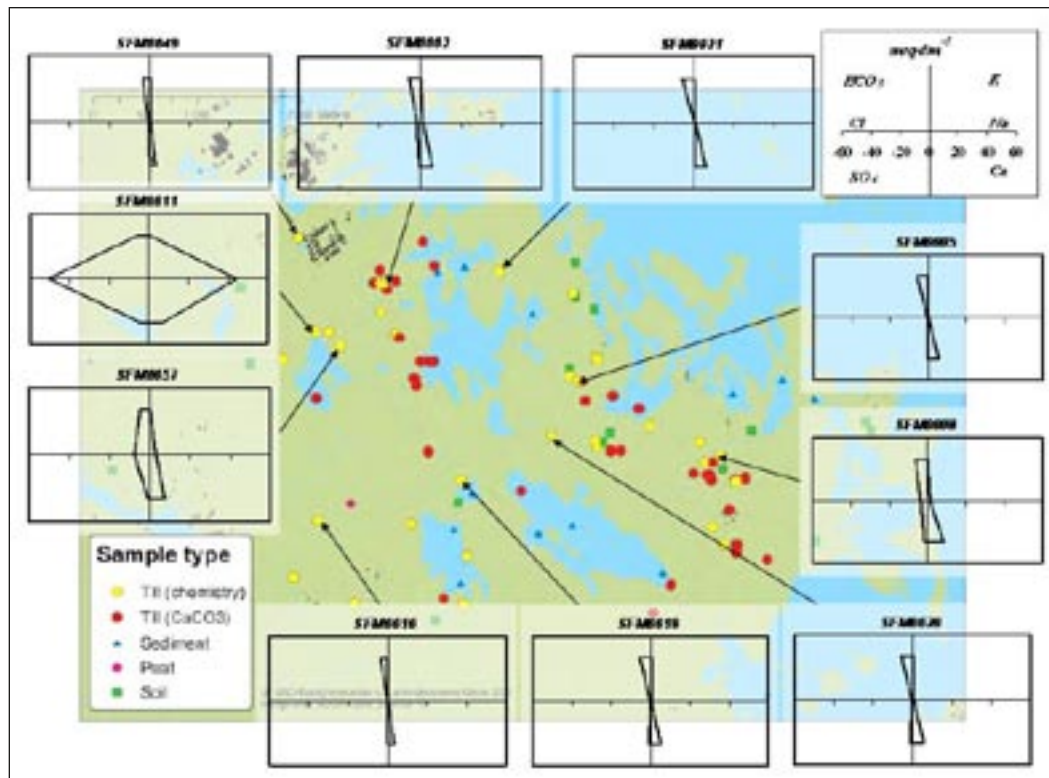
Figure 2-9. *Stiff diagrams of major ions for some shallow groundwaters in the Forsmark area. Except SFM0011, which likely has contributions from saline fluids, all waters show a striking homogeneity.*

15

Except for one sample (from SFM0011), which is much more saline, all waters show almost identical Ca-HCO_3^- composition. Samples from SFM0011 have geochemical signatures consistent with old saline groundwaters flowing in crystalline rocks in the Forsmark area. Sample SFM0057 is also of Ca-HCO_3^- nature but with higher chloride content, suggesting contribution of Cl from deep or marine sources.

2.3.2 Uranium

Uranium in shallow groundwaters in the Forsmark area has concentrations ranging from 1.0×10^{-11} to 1.5×10^{-7} M. This wide range indicates variable redox conditions in Quaternary porewaters. Lake and stream waters have similar uranium concentrations (average$_{stream}$ = 1.3×10^{-8} M, average$_{lake}$ = 8.8×10^{-9} M). Plotting the uranium concentration against ions concentrations such as bicarbonate, phosphate, iron and DOC (dissolved organic carbon), some clues on uranium mobility may come to light. Uranium commonly is transported forming complexes with these ions (see section 3.1). However, none of these parameters shows a clear correlation with the uranium concentration (Figure 2-10 and Figure 2-11).

2.3.3 Selenium

No data on selenium concentrations in surface waters or groundwaters in the Forsmark area were available at the start of the present work.

2.3.4 Iodide

Like Cl$^-$, the iodide concentration in shallow groundwaters is mainly controlled by the contribution of saline fluids of deep or marine origin (Figure 2-12). Concentrations in shallow groundwaters range from 1×10^{-8} to 8×10^{-7} M. The highest temporal variations are observed in dilute samples suggesting that other processes than mixing with saline waters may control iodide transport.
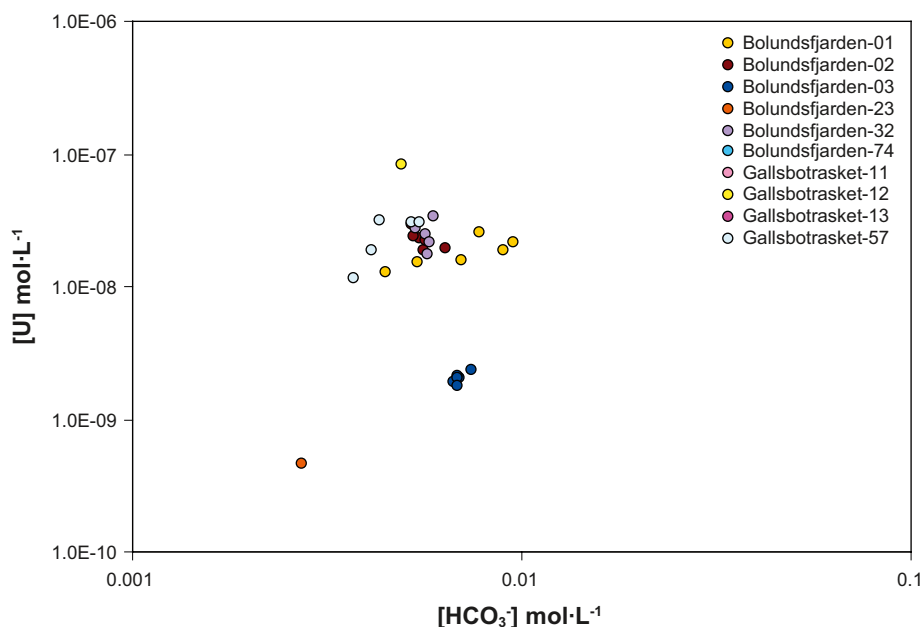
Figure 2-10. *[U] vs [HCO$_3^-$] in shallow groundwaters from the Lake Bolundsfjärden area. No correlation is observed. Data from /Tröjbom and Söderbäck 2006/. The numbers in the legend refer to SFM ID numbers.*
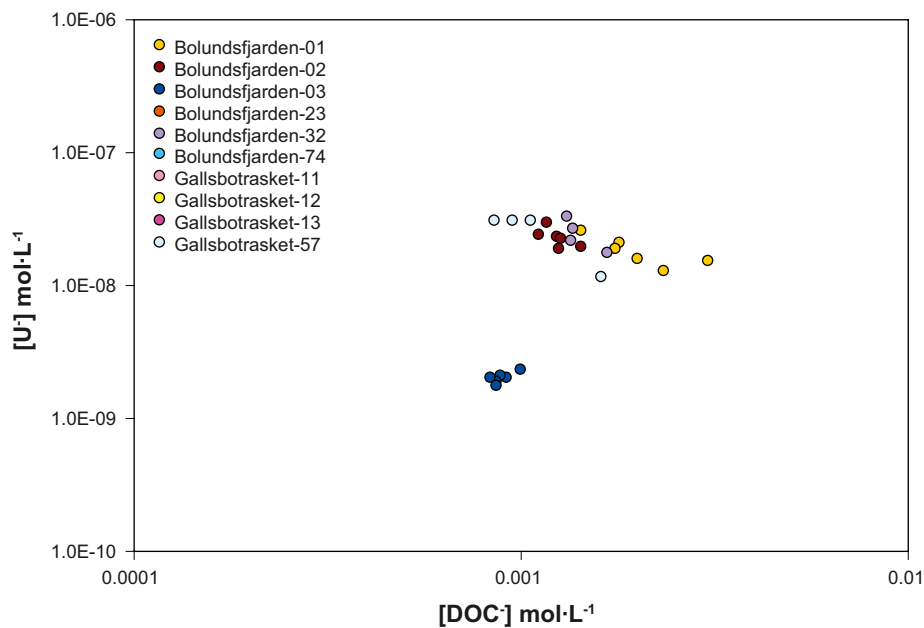
Figure 2-11. *[U] vs [DOC] in shallow groundwaters from the Lake Bolundsfjärden area. Data from /Tröjbom and Söderbäck 2006/. No clear correlation is observed. The numbers in the legend refer to SFM ID numbers.*
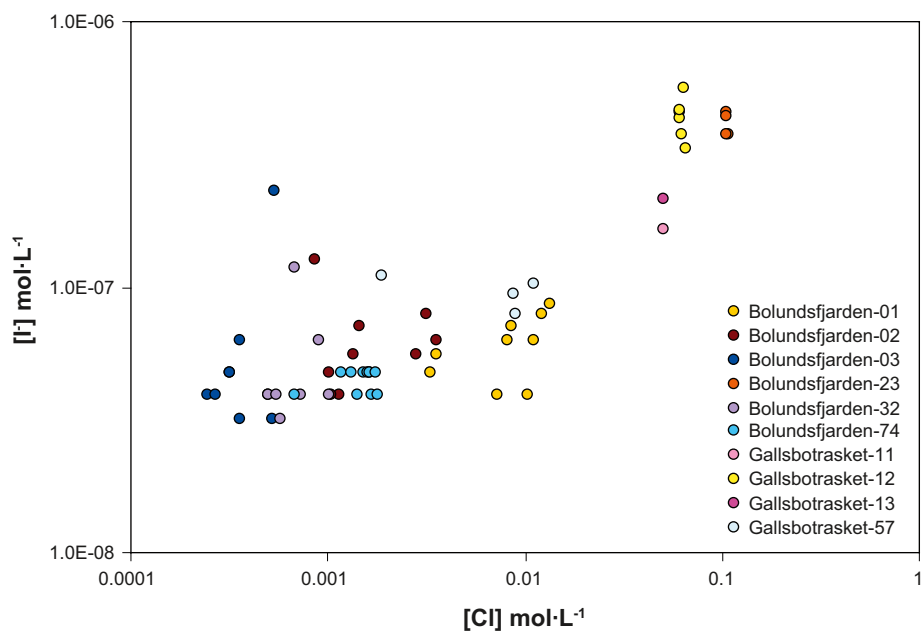
Figure 2-12. *[I⁻] vs [Cl⁻] in shallow groundwaters from the Lake Bolundsfjärden area. Data from /Tröjbom and Söderbäck 2006/. The numbers in the legend refer to SFM ID numbers.*

2.3.5 Caesium

Data on caesium concentrations are scarce in shallow groundwaters in the Forsmark area, ranging from 5×10^{-11} to 1×10^{-9} M. With the available data no clear correlations with other ions have been observed.

2.3.6   Strontium

Strontium concentrations in shallow groundwaters range between 8×10^{-7} to 5×10^{-5} M. Taking into account the interaction between water and the till, a correlation between strontium and calcium is expected. Indeed, looking in detail at waters in the Lake Bolundsfjärden subcatchment, two different trends are observed when strontium concentrations are plotted against Ca (Figure 2-13).

One trend involves high salinity waters (e.g. samples from well SFM0023), and represents a mixing trend. The most saline end-member is not necessarily equilibrated with calcite, and, actually, it is undersaturated (see Figure 2-7). On the other hand, the correlation observed in dilute waters is consistent with Sr-bearing calcite from till. In fact, the Sr/Ca ratios in these waters and in solid phases in the till are quite comparable (see Figure 2-21 below), confirming the role of carbonate rocks in the strontium transport.

2.4   Metal distribution and cycle in lacustrine sediments

The understanding of the geochemical processes of Quaternary deposits is essential to evaluate the radionuclide retention capacity of the near-surface systems. As a starting point, the nature of these sediments can be assumed to be similar to that in other areas where geological and paleoclimatic history can be comparable to Forsmark (e.g. Artic and Canadian regions).

In many lacustrine and marine environments, the distribution of many metals in soils and lake sediments is strongly dependent on the redox cycles /Boudreau 1999/. Manganese and iron are commonly used to follow such cycles as they constitute the main redox drivers. In common sediments, metals are accumulated as oxides at the top of the sediment column, together with organic matter. Since the sediment-water interface is oxidising, these solid phases are stable. As these solids are buried into the sediment pile, the available O_2 is quickly consumed by microbes that use the organic matter (exemplified by CH_2O in Equation 2-1) as electron donor.
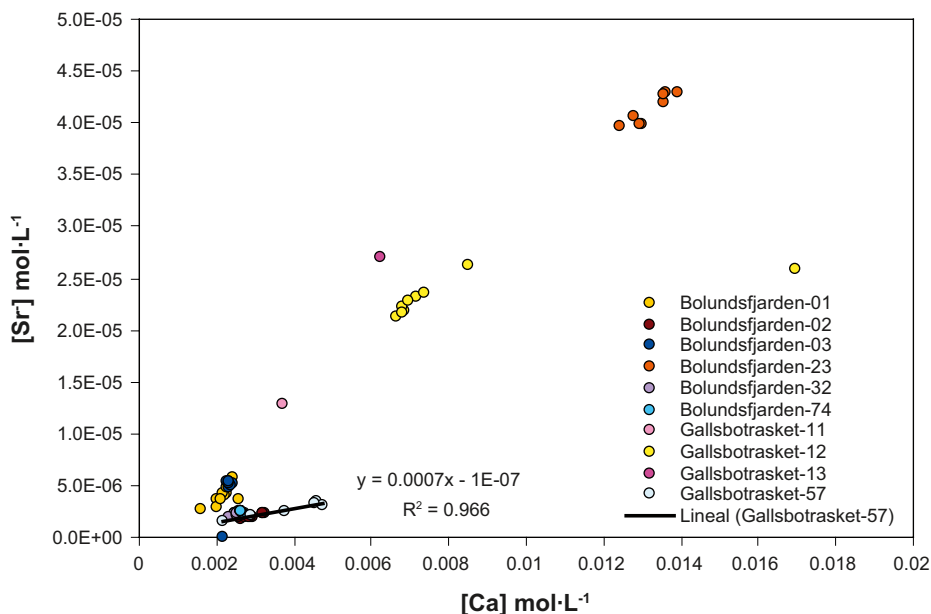

Figure 2-13. *Ca-Sr concentrations in shallow groundwaters from the Lake Bolundsfjärden area. Data from /Tröjbom and Söderbäck 2006/. The numbers in the legend refer to SFM ID numbers. Linear correlation for well SFM0057 is shown.*

After O_2 disappearance, microbial activity forces the reduction of metal oxides following the next reaction (manganese is taken as example):

$$CH_2O + 2MnO_2 + 3CO_2 + H_2O \rightarrow 2MN^{2+} + 4HCO_3^-$$ Equation 2-1

This results in the release of metals in the porewater at some depth into the sediment. Since surface sediments are free of dissolved metals, a diffusion flux of metals is established from depth to top of the sediment. The cycle is closed by new oxidation processes of the metals when they reach the oxic zone. Together with Fe and Mn, many other minor and trace metals follow this cycle. They are immobilised by adsorption into or co-precipitation with iron and manganese oxyhydroxides, and released back to porewater when these phases are reduced and dissolved. Phosphate also participates in this cycle and adsorption/desorption to iron oxides plays an essential role to phosphate fluxes in lakes.

Only a small part of these metals leaves the cycle by permanent immobilisation into sediments by precipitation (and co-precipitation) as sulphides and carbonates. This cycle may be repeated many times by a single atom of a particular element. /Dhakar and Burdige 1996/ concluded that one atom of Mn may cycle up to 70 times. In principle, this metal cycle can be applicable to sediments in the Forsmark area. A sketch of this redox cycle is shown in Figure 2-14.

In this project, we assume that the radionuclides susceptible to take part in this cycle, mainly uranium and selenium, are not introduced in the system from surface environments (e.g. atmosphere, streams and wetlands), but they come from the deep geosphere. Consequently, they are not going to enter in the cycle if they are (co)precipitated in reducing zones (see Chapter 3). If reducing zones are absent or with insufficient retention capacity, these radionuclides will eventually participate in the redox cycle. The existence of reducing zones at Forsmark is still to be proven, but it has been observed in many examples of lacustrine sediments in other areas in the world.
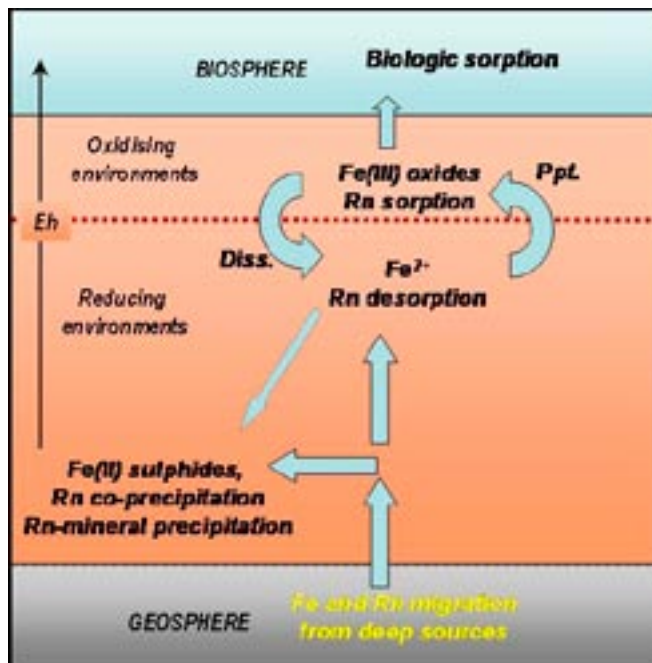
Figure 2-14. Metal cycle in the near-surface system. Iron is used to represent metals. Radionuclides such as U and Se enter the Quaternary deposits from deep sources and can be immobilised in the more reducing zones forming pure phases or co-precipitated with iron sulphides. If not retained, they start to cycle driven by the redox state of the system. They may eventually be precipitated in sediments or released and adsorbed in biota.

However, few can be related to those in the Forsmark area; lakes in this area are very shallow, leading to an easy oxygen access to the sediment and deeper anoxic interface. This situation (cool, shallow, oligotrophic lakes) is not commonly found in literature. In a comparable example, /Percival et al. 2001/ found high contents (up to 12 wt% in untreated samples) of pyrite in glacial lake sediments in Canada. From the point of view of long-lived radionuclide transfer to the surface systems, these sulphides are very relevant for the retention of selenium. In addition, its formation is an indicator of reducing conditions that are essential to immobilise other radionuclides like uranium.

Unfortunately, the authors did not report the depth of the sampling point in the sediment. They also analysed till samples from different locations in the Canadian Shield, but the sampled materials are not comparable to the till in the Forsmark area. Pyrite has also been observed in varved sediments in Lake DV-09, situated in the eastern Canadian High Arctic /Outridge et al. 2005/. This mineral was found at 30–32 cm depth, and it was interpreted as an indicator of early diagenesis. The evolution and dynamics of this lake can be comparable to lakes in the Forsmark area.

Another interesting example is Lake MacFarlane (Canada), since it has many of the geochemical features apparent in lakes in the Forsmark area. In this lake, /Belzile et al. 2000/ found freshly-formed amorphous iron and pyrite at relatively shallow depths into the sediment, and they suggest that these phases were responsible for the scavenging of selenium (see below). Based on these examples, reducing zones could be expected in the deepest sediments in lakes and wetlands in the Forsmark area.

2.5 Radionuclide concentrations in Quaternary deposits

2.5.1 Uranium

Elemental composition of till in Forsmark is summarised in /Tröjbom and Söderbäck 2006/. Although mineral composition is not fully reported, an idea of the incorporation of radionuclides of interest into mineral phases can be obtained by coupling elemental compositions. In addition to major elements, data for U, Se and Sr are also available. In the case of uranium, very rough correlations between this element and Fe, Mn and P could possibly be identified (Figure 2-15 and Figure 2-16). This indicates that uranium could be preferentially incorporated to Fe-Mn oxides or phosphates, although other phases containing Fe, Mn and P could be uranium-free.

Iron and manganese correlate well with each other (Figure 2-17), suggesting that, indeed, both can be present as oxyhydroxide mixtures. The lack of correlation between Fe-Mn and Ca may be indicative of the absence of ankerite-siderite and rhodochrosite.

The possible correlation between uranium and Fe-Mn oxides is not supported by the observation that uranium in some cases is stronger retained in samples from larger depths (Figure 2-18). Considering that no significant differences in mineral paragenesis exist throughout the till column, this could indicate that uranium is not fixed at surfaces by oxyhydroxides, but that it is progressively incorporated into sediments via reduction.

This assumption does not rule out other hypotheses for the uranium retention. A relatively good correlation is seen if we compare uranium and sodium contents. Actually, two different trends are observed that could correspond to distinct mineral phases (Figure 2-19). A candidate mineral group could be clays, but no U-Ca correlation exists. However, this correlation is not expected since several minerals contribute to the bulk analysis of calcium (e.g. calcite, clays and feldspars) and their concentration can vary from one sample to another. So, the dilution effect of uranium-free minerals can mask any correlation. Instead, Na is essentially found in clays and albite; the former could be a candidate for uranium retention.
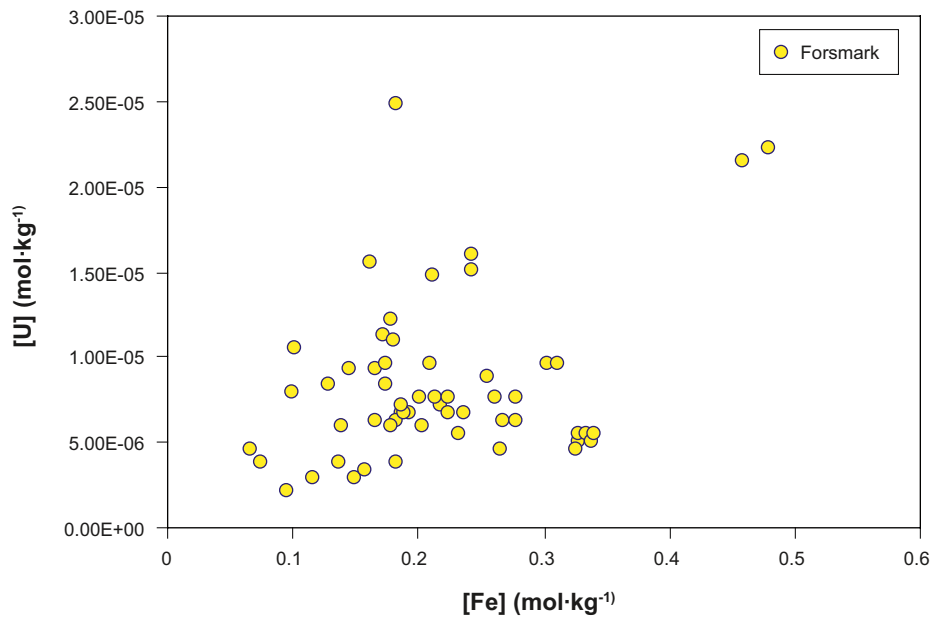
Figure 2-15. *Comparison between uranium and iron contents in till from Forsmark. A very rough correlation between these elements could possibly be identified. Data from /Tröjbom and Söderbäck 2006/.*
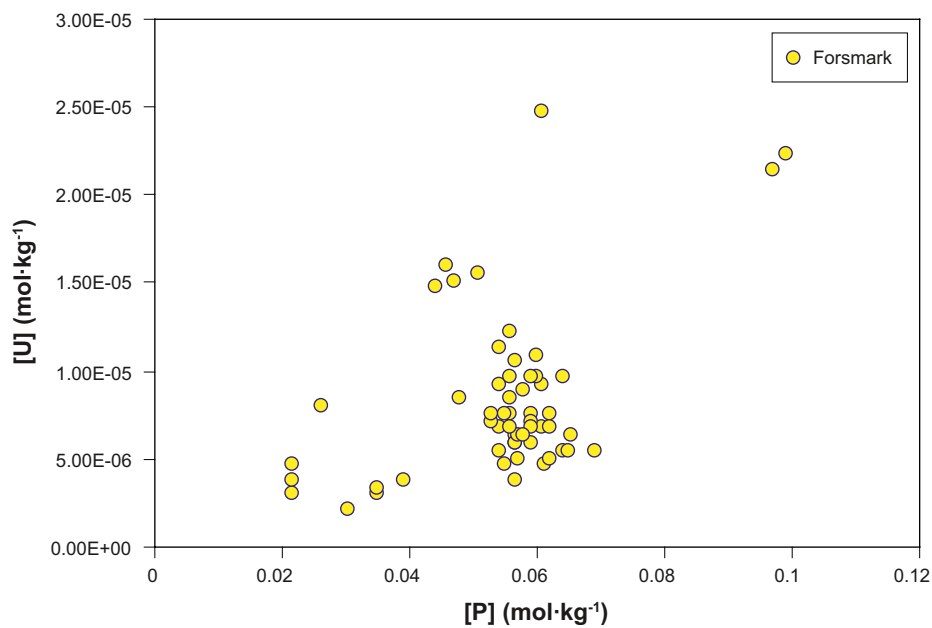
Figure 2-16. *Comparison between uranium and phosphate contents in till from Forsmark. A very rough correlation could possibly be identified. Data from /Tröjbom and Söderbäck 2006/.*

Uranium concentration in fine-grained sediments is limited to the data reported by /Strömgren and Brunberg 2006/ from Lake Stocksjön. Uranium distribution in these sediments shows a marked increase down to depths of 40–50 cm, and a decrease down to 55 cm. These variations could be attributed to changes in the redox conditions, in which speciation of uranium may significantly change.
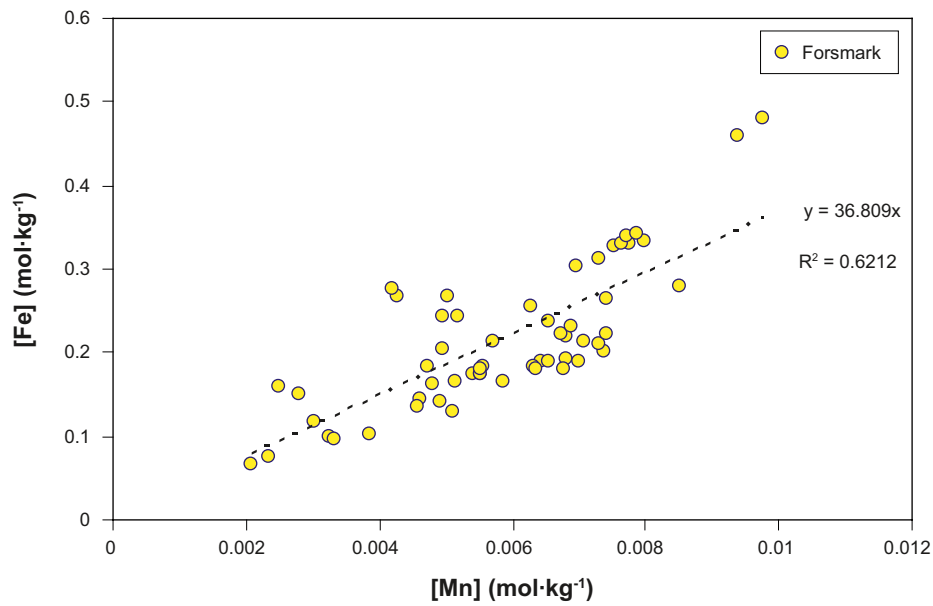
Figure 2-17. *Positive linear correlation between iron and manganese contents in sample of till from the Forsmark area. This could be an evidence of the existence of Fe-Mn oxyhydroxides. Data from /Tröjbom and Söderbäck 2006/.*
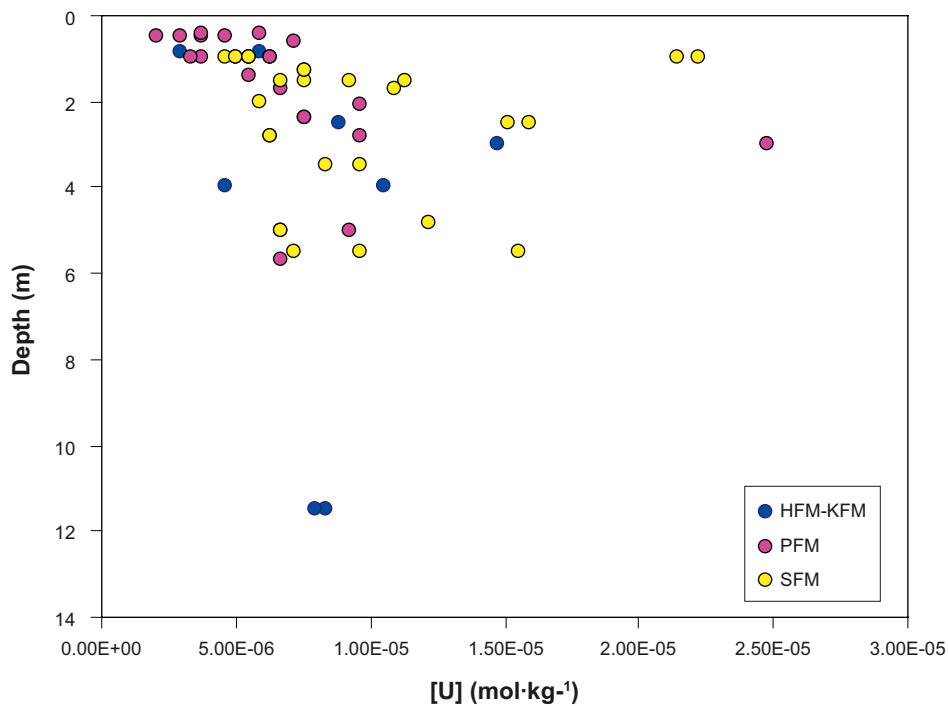
Figure 2-18. *Uranium concentrations in the near-surface system (till and upper bedrock) vs depth of sampling. The samples have been divided according to the type sampling point. KFM stands for samples collected in core-drilled boreholes, HFM in percussion drilled boreholes, and SFM and PFM in drilling in Quaternary deposits.*
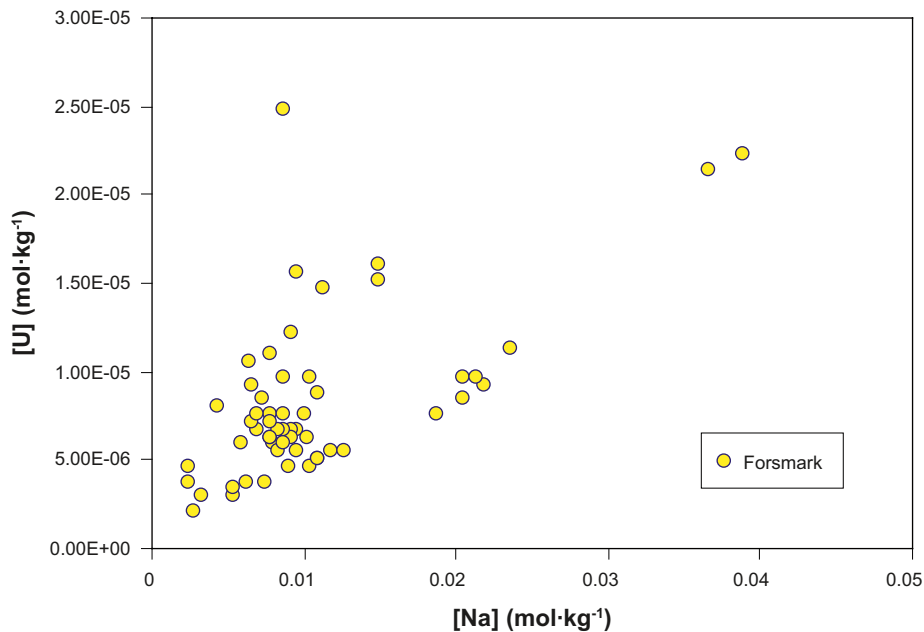
Figure 2-19. *Correlations between uranium and sodium contents in sample of till from the Forsmark area. Two different trends are observed, suggesting two distinct host minerals for uranium in the till. Data from /Tröjbom and Söderbäck 2006/.*

2.5.2   Selenium

Selenium deserves a special attention in radionuclide-biosphere studies since it is quickly transferred from water to biota as nutrient. Data on selenium contents in the till at Forsmark /Tröjbom and Söderbäck 2006/ show small amounts of this element in till minerals (up to 7×10^{-6} $mol_{Se} \cdot kg_{rock}^{-1}$). A detailed review of these data shows a rough positive correlation between Se and Fe (Figure 2-20), suggesting that both elements are found in the same mineral phase.

Under reducing conditions, selenium can be precipitated as native selenium or sulphide-selenide solid solutions (see below). However, no correlation between Se and S contents is observed in till. This does not mean that both elements do not occur together in the same mineral. Instead, this could suggest that analysed sulphur is found in more than one solid phase, some of which are selenium-free (e.g. sulphates). On the other hand, correlation of Se with other elements is not observed.

2.5.3   Iodide

No data on iodide contents in Quaternary deposits are available in the dataset considered in this work.

2.5.4   Caesium

No data on caesium concentrations in Quaternary deposits are available in the dataset considered in this work.
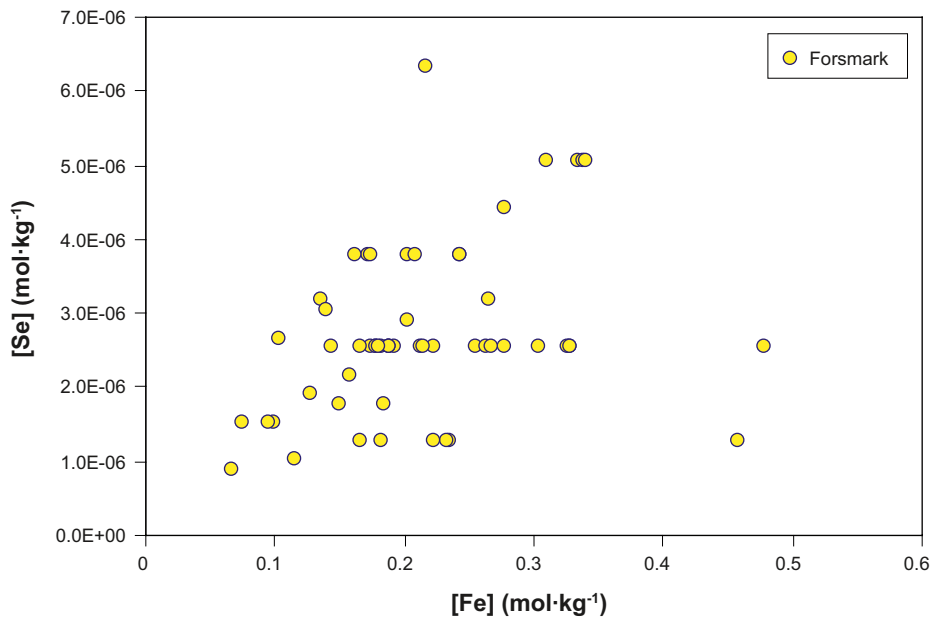
Figure 2-20. *Comparison between selenium and iron content in till samples from the Forsmark area. Data from /Tröjbom and Söderbäck 2006/.*

2.5.5 Strontium

Near-surface systems at Forsmark have high contents of calcium carbonate mainly in till and glacial clay sediments. Consequently, calcite could be considered a very relevant sink for strontium. Looking at the till composition /Tröjbom and Söderbäck 2006/, it is observed that the strontium content in the till samples from the Forsmark area is highly variable but indistinctly liked to calcium. In Figure 2-21, a highly positive correlation of strontium and calcium is observed, not only at Forsmark but also at Simpevarp. This correlation suggests a unique host mineral with fixed Sr/Ca ratio (4×10^{-4} and 8.7×10^{-3} at Forsmark and Simpevarp, respectively).
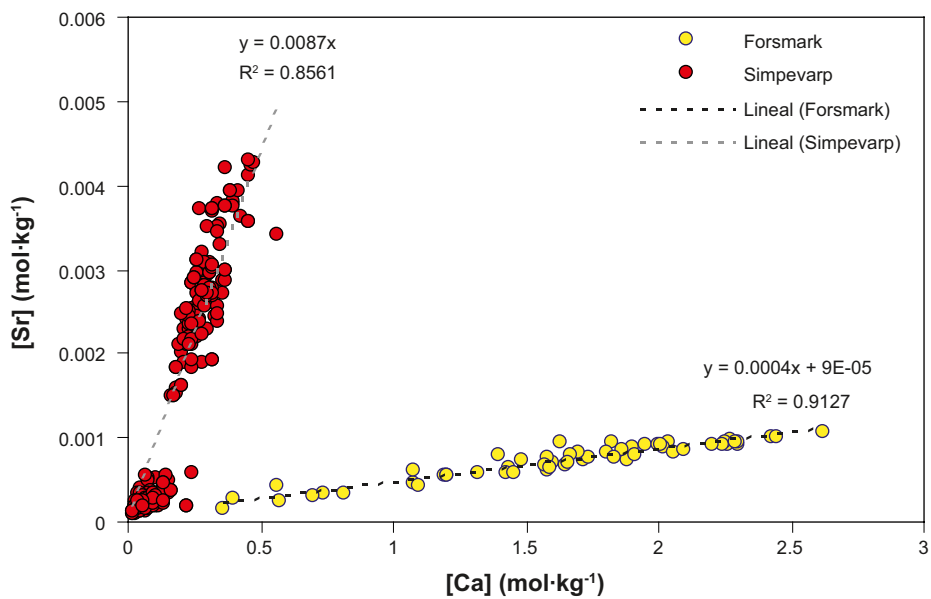
Figure 2-21. *Ca-Sr linear concentrations in till samples from Forsmark and Simpevarp. The high positive correlations are indicative of a unique solubility limiting phase, likely calcite or clays.*

24

These clear correlations are not seen when comparing strontium with other exchangeable cations in charged mineral surfaces (Na, K and Mg). Moreover, the lack of correlation with K also rules K-feldspar out. Calcite is a reasonable candidate as a solubility limiting phase for strontium rather than strontium minerals such as celestite or strontianite. The two distinct slopes between Simpevarp and Forsmark can not be univocally interpreted at this stage. One hypothesis can be distinct calcite-water partition coefficients between both sites, leading to two specific $(Ca,Sr)CO_3$ solid solutions, but further analysis is needed for a definitive explanation.

Clays are also a common component in the Quaternary deposits at Forsmark (e.g. illite); consequently, strontium can be retained via ion exchange. However, no data from these fine-grained sediments are available.

3 Processes affecting radionuclide retention-release in the near-surface system

The capacity of the near-surface system to retain radionuclides via sorption or precipitation (basically co-precipitation with major ion solid phases) depends essentially on the pH and redox state of the porewater. Both parameters, together with the water composition, control the speciation of the radionuclides and the stability of the organic and mineral surfaces where they can be attached. In organic matter-rich sediments, biological fixation of some radionuclides (e.g. uranium) may be even more relevant than inorganic retention. Therefore, in order to establish the main chemical constraints of the near-surface system, Pourbaix (Eh, pH) diagrams of the selected radionuclides are plotted under the possible chemical conditions of the system. The diagrams have been calculated by using the MEDUSA code package /Puigdomènech 2002/. References for the thermodynamic data used in the calculations are provided in the text.

Concerning the dynamic redox conditions of the near-surface system, data for lakes in the Forsmark area indicate that the whole water column is under oxidising conditions in periods of high organic production (spring-summer). In addition, at least in some lakes (e.g. Lake Stocksjön), the upper levels of the sediments are also oxidising. These conditions are favourable to mobilisation of radionuclides but also to the formation of mineral phases able to retain them (mainly Fe-Mn oxyhydroxides).

Reducing conditions in deeper sediments have not been reported from the Forsmark area, but their existence cannot be ruled out. It is important to keep in mind that the Quaternary deposits could be the last natural barrier to be encountered by ascending radionuclides from the bedrock, and, therefore, an exhaustive evaluation of the potential retention mechanisms in this zone is relevant. On the other hand, in till deposits, shallow groundwaters could have relatively high dissolved oxygen contents (from 9×10^{-6} to 3×10^{-4} M), although data for many wells are not available or are incomplete.

The proton concentrations in lakes, wetlands and groundwaters flowing through the till are thought to be buffered by the presence of calcium carbonate, so that acidic waters are not present in the Forsmark area. In fact, the pH in shallow-groundwaters in the Forsmark area ranges from 6.8 to 8.2, except in some saline groundwaters (pH from 6.4 to 6.9).

In general, radionuclide retention capacity is provided by sorption on charged surfaces as in clays and oxyhydroxides, co-precipitation with sulphates, sulphides, oxyhydroxides and with carbonates, and sorption into organic tissues. Precipitation of pure phases (e.g. strontium sulphates, iron selenides, $UO2_{(s)}$) is also worth considering in spite of the very low concentrations of these radionuclides.

3.1 Uranium

The behaviour of uranium in natural waters has been long studied. Uranium occurs in nature as two different oxidation states: U(IV) and U(VI). The former is found in reducing environments and the latter in oxidising conditions. U(IV) is rather immobile so that waters with low Eh are not able to transport much uranium, e.g. $< 10^{-8}$ M according to /Langmuir 1997/. U(IV) solid phases are mainly oxides, especially uraninite (or amorphous analogues; Figure 3-1). Coffinite ($USiO_4 \cdot n(H_2O)$) is a very common U(IV) phase in many uranium ores but its formation has long been debated. Direct precipitation from U(IV)-bearing solutions is believed to be kinetically limited since laboratory experiments failed to synthesize it /Robit-Pointeau et al. 2006/.

$[SO_4^{2-}]_{TOT} = 0.19$ mM $[UO_2^{2+}]_{TOT} = 1.00$ µM
$[CO_3^{2-}]_{TOT} = 3.00$ mM $[H_4SiO_4]_{TOT} = 61.40$ µM
$[Ca^{2+}]_{TOT} = 1.40$ mM $[Cl^-]_{TOT} = 0.65$ mM

Becquerelite

Uranophane

$UO_2 \cdot 2H_2O$ (am)
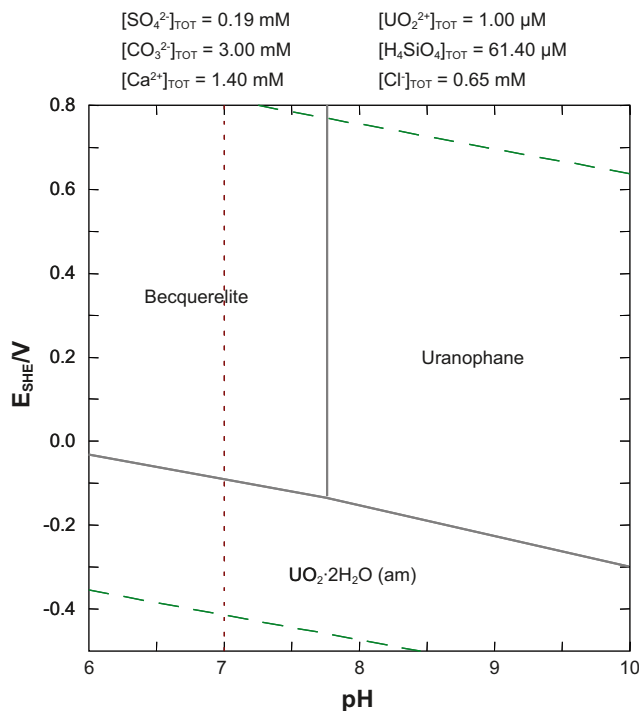
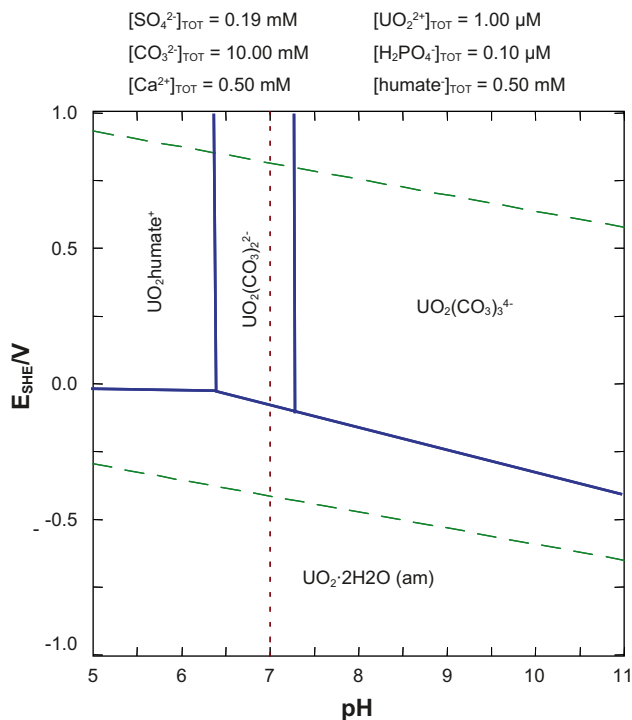*Figure 3-1.* *Eh-pH diagram for uranium in the range of environmental conditions expected in the near-surface systems at Forsmark. Water composition used for diagram construction is taken from data from Lake Bolundsfjärden (January 2004) /Tröjbom and Söderbäck 2006/. Uranium concentration is 1×10^{-6} M, which is higher than present-day concentrations in surface waters at Forsmark.*

It is likely that a previous U(VI) reduction step is required before coffinite precipitates /Goldhaber et al. 1987/. The reduction would be favoured by uranyl adsorption onto mineral surfaces and organic matter. Both uraninite and coffinite can be expected to form if uranium from the bedrock, transported as U(VI), interacts with a potentially reducing environment at the bottom of the near-surface system.

If uranium from a deep repository eventually reaches shallower, oxidising conditions, its mobility is enhanced. Under these conditions, uranium is found as U(VI), forming soluble hydroxide and carbonate complexes at pH > 5 (Figure 3-2). At high pCO_2 conditions, U(VI) is mainly transported as carbonate complexes. The presence of CO_2 is, therefore, very relevant to retention processes at circumneutral pH.

Another important element that commonly forms complexes with uranium is phosphorous. At very high phosphorous concentrations with respect to carbonate ($[PO_4^{3-}]/[CO_3^{2-}] > 10^{-1}$), uranium-phosphate complexes predominate over uranium-carbonate complexes /Sandino and Bruno 1992/.

Solubility limiting phases under aerobic conditions depend on the chemistry of water. In silica and calcium-rich waters at neutral to alkaline pH, uranium is commonly precipitated as uranophane ($Ca(UO_2)(SiO_3OH)_2(H_2O)_5$) /Finch and Murakami 1999/. At low Si concentrations, becquerelite ($Ca(UO_2)_6O_4(OH)_6 \cdot 8H_2O$) precipitation is favoured /Duro et al. 2006a/, cf Figure 3-1. Uranophane can be replaced by soddyite ($(UO_2)_2SiO_4(H_2O)_2$) if pCO_2 is low enough /Finch 1994, Casas et al. 1994/. In many oxidised halos around uranium ores, the occurrence of vanadium in groundwaters forces a quick precipitation of uranium as vanadates (carnotite, $K_2(UO_2)_2(V_2O_8)(H_2O)_3$, tyuyamunite, $Ca(UO_2)_2(V_2O_8)(H_2O)_8$), due to the low solubility of these phases. Phosphates, such as saléeite ($Mg[(UO_2)(PO_4)]_2(H_2O)_{10}$), can be a sink for uranium even if groundwater is, apparently, undersaturated in these phases. /Murakami et al. 1997/ suggested that local release of P adsorbed onto ferrihydrite when this mineral is replaced by other Fe (III) phases (hematite and goethite) can cause uranyl phosphate precipitation.

Figure 3-2. *Eh-pH diagram for uranium in water under high-PCO₂ conditions. Total concentration of humic acids is 5×10^{-4} M. Thermodynamic data are based on /Grenthe et al. 1992/ and /Guillaumont et al. 2003/ for the inorganic compounds, on /Choppin and Shanbhag 1981/ for calcium complexation with humic acids, and /Shanbhag and Choppin 1981/ for the uranium-humic acid complexes.*

The co-precipitation of uranium with iron oxides is proven to be a very effective process that controls the uranium concentration in natural waters. Results from projects dealing with natural analogues, e.g. /Bruno et al. 1998, 2002/ show that uranium concentration in groundwaters flowing through uranium-rich rocks are best explained if mixed Fe(III)-U(VI) oxides are considered as the solubility limiting phases.

U(VI) may be involved in many sorption reactions, especially sorption onto clays /Turner et al. 1996/, aluminium /Pabalan et al. 1998/ and iron oxides /Hsi and Langmuir 1985, Payne et al. 1996, Duff et al. 2002/, hydroxyapatite /Seaman et al. 2001, Fuller et al. 2002, Krestou et al. 2004/ and organic compounds /Lenhart et al. 2000, Reiller 2005/.

Unlike the inorganic geochemistry of uranium, the interaction with organic substances (Natural Organic Matter, NOM) is still not fully understood. The retention of uranium in organic compounds, mainly humic substances, in soil and sediments has been evaluated recently by /Reiller 2005/. Humic substances are anionic polyelectrolytes that can form complexes with many metal ions. In principle, uranium could be strongly complexed by these acids. However, in many surface waters, major cations, especially calcium, are expected to compete with uranium and other trace metals for these binding sites, limiting the organic complexation of these elements.

Figure 3-2 and Figure 3-3 show the predominance of the uranium complexes in a water with a moderate calcium concentration (5×10^{-4} M) and a high uranium content (1×10^{-6} M). Under acidic conditions, uranium-humate species are predominant, whereas under more alkaline conditions, uranium is bound to mobile carbonate complexes. The total concentration of humic acids used in these speciation calculations is 5×10^{-4} M. At higher concentrations, the uranium complexation with humic acids increases significantly, as shown in Figure 3-4, and it predominates at concentrations higher than 2.5×10^{-3} M. More details on the thermodynamic properties of the humate complexes used in these diagrams are provided in section 5.3.2.
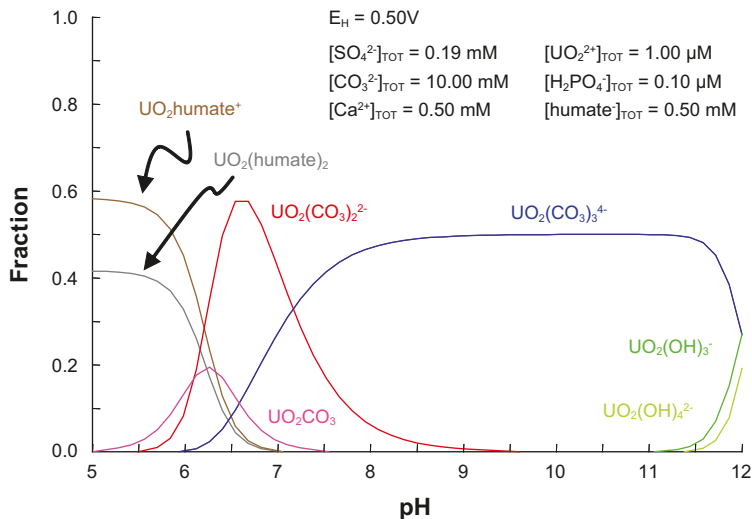
Figure 3-3. *Fraction diagram of uranium species as a function of pH under oxidising conditions (Eh = 500 mV). Uranium speciation is controlled by the association with humic acids at acidic to circumneutral pH, whereas carbonate complexes dominate at circumneutral and alkaline conditions.*
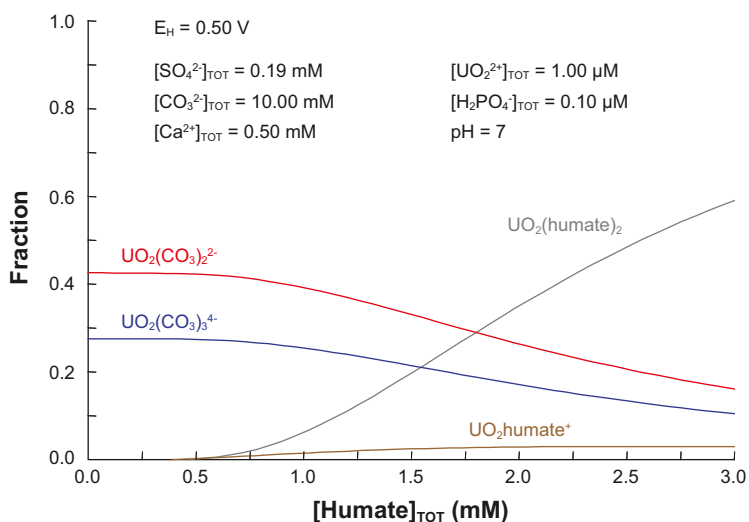
Figure 3-4. *Changes in the uranium speciation in water with variable humic acid concentration at neutral pH.*

On the other hand, adsorption of U(VI) onto humic substances seems to play a significant role for the availability of uranium to metal-reducing microbes, which subsequently may reduce and immobilise it, see, e.g. /Gu and Chen 2003/.

3.2   Selenium

Dissolved selenium in surface waters and groundwater mainly occurs as Se(IV) (selenite) and Se(VI) (selenate) (Figure 3-5). Under oxidising and alkaline conditions, selenate predominates. Only under reducing or acidic conditions, selenium is found as elemental Se (Figure 3-5) or as Se(-II). At circumneutral pH values, selenium speciation is highly dependent to redox state in water. In lakes and wetlands in the Forsmark area, oxidising conditions are present during the whole year, and selenate is expected to be the predominant dissolved species.

If oxygen is consumed by organic activity, Eh may be reduced enough to make selenite to be the predominant species. This situation is expected during periods of high organic production or at moderate depths within the sediment column. In shallow groundwaters, selenate is expected to be more abundant than selenite. Data from /Alfthan et al. 1995/ showed that selenate is the predominant species in Finnish groundwaters.

The determination of the selenium speciation is crucial to evaluate the retention potential of the near-surface system. If selenium migrating from the bedrock first meets an anoxic near-surface system, selenium can be microbially reduced and precipitated as native Se, FeSe or $FeSe_2$, or co-precipitated with pyrite, e.g. /Masscheleyn et al. 1991, Bruggeman et al. 2005/. If selenium as selenite reaches oxidised soils and sediments, it can be scavenged by Fe-Al-Mn oxyhydroxides, see /Duc et al. 2003, Templeton et al. 2003, Peak 2006/, via adsorption as inner-sphere complexes. In contrast, if selenium has been oxidised to selenate, it is not well absorbed into these phases. However, it is worth mentioning that in aerobic soils, some bacteria strains are able to reduce selenite and selenate to Se(-II), which is incorporated to cell structures and immobilised /Garbisu et al. 1996, Siddique et al. 2006/.

In calcite-rich till, selenium could be co-precipitated with calcite, although few studies have been focused on quantifying the extent of solid carbonate-selenium interactions. /Lamble et al. 1995/ and /Wang and Liu 2005/ performed with significant success adsorption (co-precipitation) experiments of selenium in calcite, showing the ability of a calcium carbonate lattice to accommodate this element. Clay minerals are not considered important phases for selenium retention due to the anionic character of the main species of this element.

The sorption of selenium on organic compounds has long been considered as one of the more significant retention mechanisms and laboratory, and field studies have been developed, cf /Zhang and Moore 1997, Belzile et al. 2000/. Recently, /Chabroullet et al. 2006/ carried out experiments in selenite-doped soils, and determined that most selenium was adsorbed in organic particulate. However, they also found a clear correlation with iron and they suggest that adsorption of iron oxides within the particulate could be the real retention mechanism.

$[CO_3^{2-}]_{TOT} = 3.00$ mM $[SeO_4^{2-}]_{TOT} = 10.00$ nM
$[Mg_2^+]_{TOT} = 0.20$ mM $[SO_4^{2-}]_{TOT} = 0.20$ mM
$[Ca_2^+]_{TOT} = 1.40$ mM $[Fe^{3+}]_{TOT} = 5.00$ µM
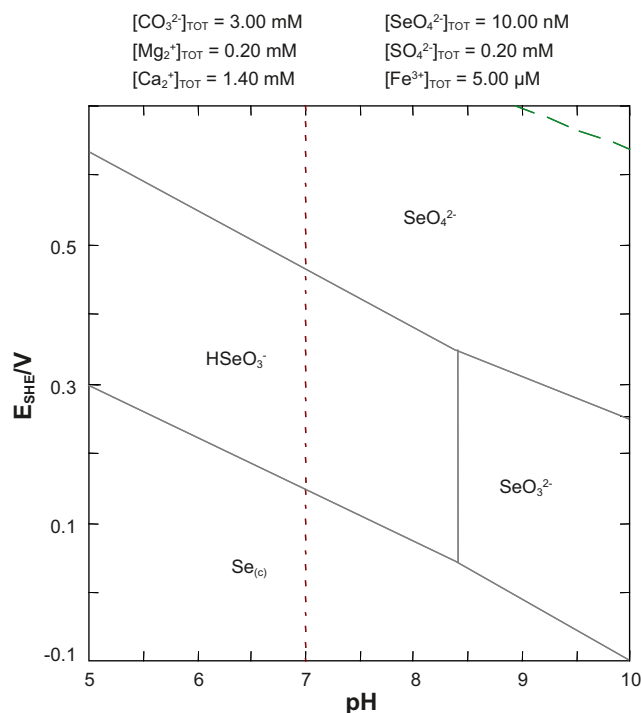
Figure 3-5. Eh-pH diagram for selenium. Water composition used for diagram construction is taken from data from Lake Bolundsfjärden (January 2004) /Tröjbom and Söderbäck 2006/. Selenium concentration is 10^{-8} M. Thermodynamic data for selenium is based on /Olin et al. 2005/.
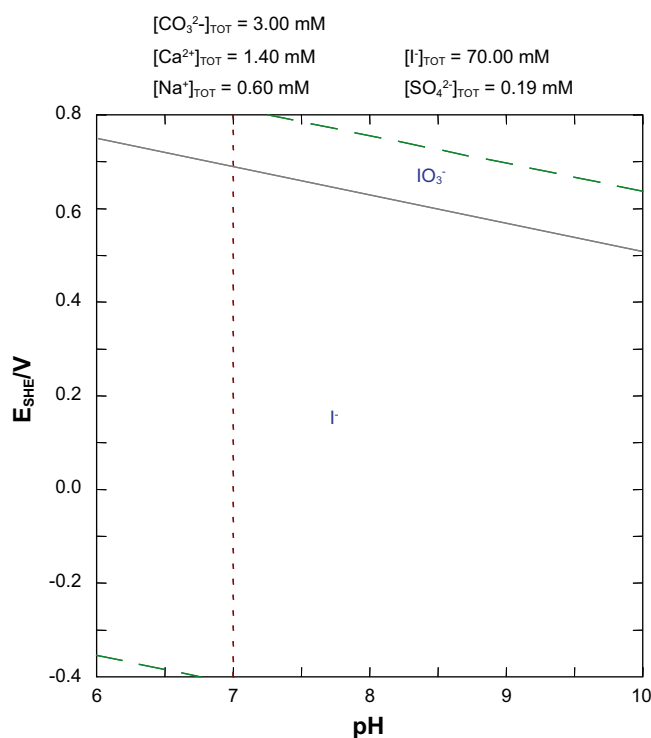
Methylation reactions are also of importance in the selenium cycle as a mobilisation process. Methylation via microbial activity leads to volatile gaseous species such as dimethyl selenide and dimethyl diselenide /Oremland et al. 1989, Losi and Frankenberger 1998, Martens and Suarez 1999/. These species can subsequently be oxidised (e.g. by MnO_2), and selenium then be adsorbed back onto the soil.

The studies of selenium retention in wetlands developed by /Zhang and Moore 1996, 1997/ are of particular interest when assessing the conditions in the Forsmark area. They found that the governing processes of selenium retention in wetland sediments were the adsorption to organic compounds and the bacterial reduction to elemental Se. In contrast, adsorption onto oxyhydroxide surfaces was minor.

3.3 Iodide

In a similar way as selenium, iodine is an essential micronutrient in living organisms and its incorporation into biosphere is, therefore, of major concern. Iodine is a highly mobile element that can be present in soils as organic and inorganic complexes. The speciation of iodine in natural waters is simple since in almost all cases I^- (iodide) is the dominant species (Figure 3-6). Iodate (IO_3^-) predominates only at high redox states and alkaline conditions. The iodine retention capacity of a soil is mainly related to the saturation of the sorption sites and to the microbial activity. The speciation of iodine is important in the adsorption onto some mineral phases. Iodate is readily adsorbed onto hematite and kaolinite /Couture and Seitz 1983, Hu et al. 2005/, but little iodide is retained.

In soils with low organic content, the retention of iodine is essentially linked to illite, substantially increasing as pH decreases /Kaplan et al. 2000/. Even at alkaline conditions (pH > 9), illite adsorbs more iodine (basically iodate) than other clay minerals (chlorite, montmorillonite,

$[CO_3^{2-}]_{TOT}$ = 3.00 mM

$[Ca^{2+}]_{TOT}$ = 1.40 mM $[I^-]_{TOT}$ = 70.00 mM

$[Na^+]_{TOT}$ = 0.60 mM $[SO_4^{2-}]_{TOT}$ = 0.19 mM

Figure 3-6. *Eh-pH diagram for iodine. Water composition used for diagram construction is taken from data from Lake Bolundsfjärden (January 2004) /Tröjbom and Söderbäck 2006/. Iodate (IO_3^-) is only found at high redox and under alkaline conditions.*

vermiculite), oxides (goethite) or carbonates (calcite), which do not show any significant retention at circumneutral-alkaline pH values /Ticknor and Cho 1990, Kaplan et al. 2000/. In soils rich in organic matter, iodine is effectively retained by humic acids /Tikhomirov et al. 1980, Rädlinger and Heumann 2000, Bostock et al. 2003/.

In addition to adsorption onto mineral phases or in organisms, iodine may be released from groundwater via volatilisation of methyl iodide (CH_3I). This compound is formed by microbially-mediated conversion from inorganic iodine /Muramatsu and Yoshida 1995, Muramatsu et al. 2004/. The iodide methylation is thought to occur in both oxidising and reducing environments, suggesting that this process can be conducted by aerobic and anaerobic microbes. The efficiency of microbes to absorb iodine is limited by the toxicity of this element at high concentrations. /Sheppard and Hawkins 1995/ found a threshold of 8×10^{-4} M of I for toxicity to microbes in experiments of iodine in soils with high organic contents. Their experiments also showed that iodine adsorption is lowered under reducing conditions.

3.4   Caesium

The relevance of studying caesium in near-surface systems like the one of concern here is mainly based on (1) the ready incorporation to organisms due to its similarity to K and ammonium, (2) the very high solubility in natural waters and (3) the concern about the presence in soils of two radioactive isotopes related to nuclear waste and operations (long-lived ^{135}Cs and short-lived ^{137}Cs) /Avery 1996/.

The retention capacity of caesium in soils and sediments is commonly related to some silicates; particularly, the adsorption on zeolites and clays has been long known, e.g. /Sawhney 1972/. These minerals are a powerful sink for caesium, leading to a confinement of Cs pollution in areas surrounding the source /Seaman et al. 2001/. Two different mechanisms of retention in clays are known: (1) cation exchange with hydrated cations on planar sites on expansible layer silicates (e.g. smectites), and (2) sorption on wedge or frayed edge sites (FES) in non-expandable phyllosilicates (mica, illite, kaolinite, etc) /Bradbury and Baeyens 2000/. Figure 3-7 shows an example of the enrichment of Cs in exchangeable FES in muscovite. These sites are located at the edge of the layers.

The most important minerals are 2:1 clays, especially illite and vermicullite, which have large layer charge. A detailed study of Cs sorption on illite over a range of pH, [Cs] and salinity was performed by /Poinssot et al. 1999/; their results showed quick sorption kinetics. In these
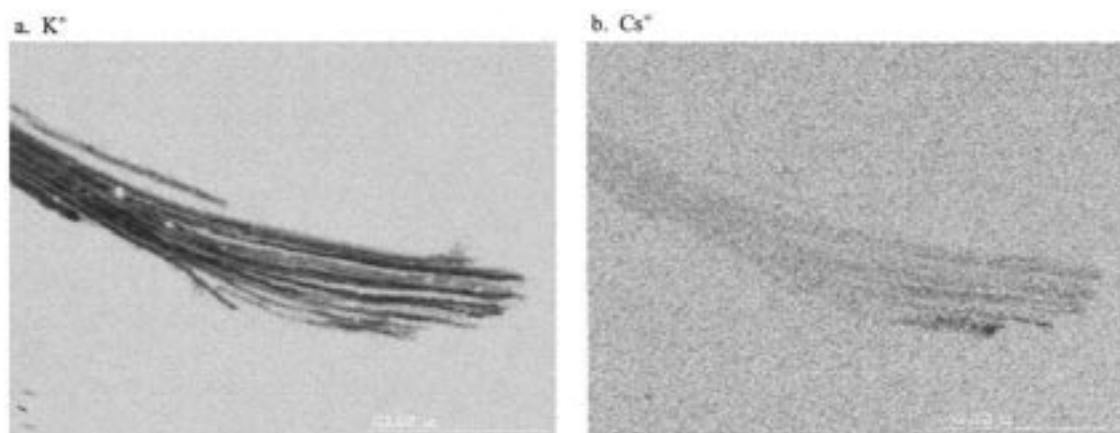
Figure 3-7. *EMP (electron microprobe) images of Cs (left) and K (right) distributions in muscovite from soil affected by Cs contamination at Hanford /Zachara et al. 2002/. Enhanced Cs sorption on frayed edge sites is observed.*

minerals, though, Cs^+ competes with K^+ and NH_4^+ for sorption sites /Comans et al. 1989, Shaw and Bell 1991, Poinssot et al. 1999/. /Shenber and Eriksson 1993/ show that ammonium can be more effective than K^+ in competing with caesium for binding sites.

Many studies reveal that the Cs sorption on clays may be strongly reduced by the influence of NOM, see review by /Staunton et al. 2002/. /Hird et al. 1995/ noted that some illite-bearing soils were not able to immobilise much caesium and they suspected that interaction with organic compounds could be responsible for such anomalous behaviour. This was subsequently confirmed by a number of experimental approaches, see references in /Staunton et al. 2002/. As an example, /Dumat and Staunton 1999/ observed a significant decrease of Cs sorption on illite due to the presence of humic acids. The results from all these studies are in disagreement with recent data from /Loft et al. 2002/. These authors found that illite is able to retain much more caesium than organic substances even at very high concentrations of humic acids.

The adsorption of caesium in other solid soil constituents, such as quartz, carbonates and Fe-Mn-Al oxyhydroxides is very limited when compared with the sorption on clays. Consequently, they are usually not considered as relevant sorption phases for caesium in studies of near-surface systems.

3.5   Strontium

The strontium speciation in most natural waters is dominated by cation Sr^{2+} (Figure 3-8). Except in special geological and anthropogenic environments, saturation of pure strontium-bearing phases such as celestite ($SrSO_4$) or strontianite ($SrCO_3$) is rarely achieved. Instead, carbonates (especially calcite) are considered the common solubility limiting phases /Lorens 1981,
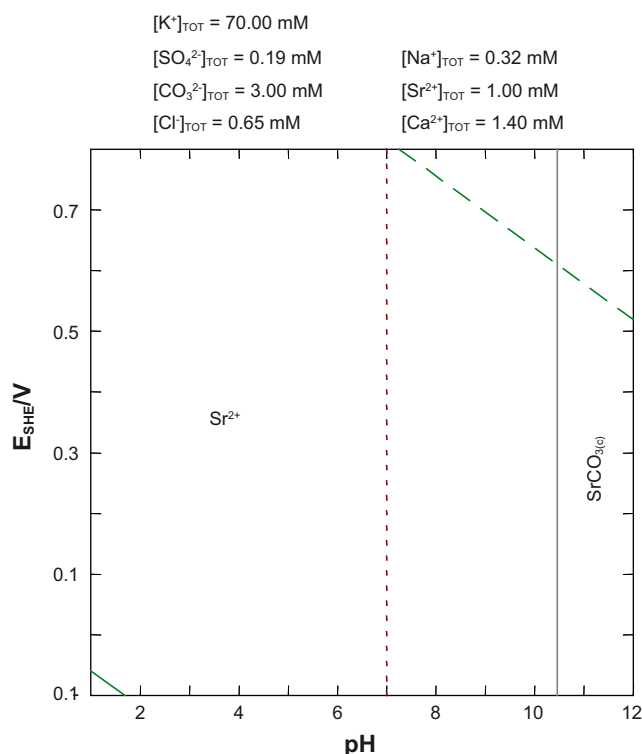
Figure 3-8. Speciation of strontium in an Eh-pH diagram. Except for highly alkaline conditions, strontium is found as Sr^{2+}. The relative low Sr concentration (10^{-6} M) prevents the precipitation of solid phases. Water composition used for diagram construction is taken from data from Lake Bolundsfjärden (January 2004) /Tröjbom and Söderbäck 2006/.

Tesoriero and Pankow 1996, Bruno et al. 1998/. The similar geochemical behaviour of Sr and Ca allows the formation of a set of $(Ca,Sr)CO_3$ solid solutions. Consequently, calcite-bearing rocks and soils will be favourable host aquifers for radiostrontium retention if fluid saturation of these solid solutions is reached.

Recent studies have shown that strontium can be retained in carbonate minerals that result from biogenic reduction of iron and manganese oxides, following the reaction (Equation 3-1):

$$CH_2O + 2MnO_2 + 3CO_2 + H_2O \rightarrow 2Mn^{2+} + 4HCO_3^-$$
Equation 3-1

The bicarbonate production from the reduction may lead to siderite or calcite precipitation, with strontium co-precipitation /Roden et al. 2002/.

Strontium can also be adsorbed by these oxides. Such adsorption can be described to take place into two steps /Trivedi and Axe 1999, Van Beinum et al. 2005/: (1) a rapid and reversible adsorption reaction to the external surface including the macropores, and (2) a slow surface diffusion along the micropore walls of the oxides.

In addition to calcite, strontium is known to be readily exchanged within surface-charged, layered silicates (e.g. montmorillonite, kaolinite, and illite), see /Chen and Hayes 1999, Lu and Mason 2001/. The problem with this mechanism is the reversibility that can easily release strontium back to solution if the ambient conditions change.

4 Summary and discussion of the radionuclide retention processes

For many radionuclides, their retention in Quaternary deposits (including lake and wetland sediments) is closely related to the establishment of anoxic conditions. The only exceptions are iodine, which is more mobile as iodide (I^-) than as iodate (IO_3^-), and strontium, which seems to be mainly linked to calcium carbonate precipitation and cation exchange.

The most efficient mechanisms for uranium retention in Quaternary sediments in the Forsmark area would be found in those places where anaerobic conditions are met; there, uranium can be reduced to U(IV and immobilised as uraninite or coffinite, e.g. /Abdelouas et al. 2000/. The main unknown is the redox state in the deepest sediments in lakes and wetlands and in the till. The only available data on sediment composition is from Lake Stocksjön /Strömgren and Brunberg 2006/. To our present knowledge, no data on sediment porewater exist.

In shallower environments, U(VI) can be adsorbed onto NOM and deposited and buried in the lake bottom. These sediments contain high concentrations of humic acids, which are products of decomposition of organisms. The adsorption of uranium onto humic acids is a favourable mechanism at slightly acidic pH, whereas at alkaline conditions carbonate complexes will predominate, even during periods of low organic activity. In this case, the main retention process will be the adsorption onto inorganic phases such as iron oxides, apatite and clays. No data on iron oxide contents in sediments or in wetlands are available for the Forsmark area. Fe-Mn correlations in till samples suggest their presence in this Quaternary soil (see section 3.5.1).

The formation of these oxides is ubiquitous in almost all aquatic oxidising environments. On the other hand, U(VI) is not expected to be transported as uranium-phosphate complexes since the ratio between carbonate and phosphate is too large according to /Sandino and Bruno 1992/. However, some lake bottoms and wetlands may retain enough phosphate to reach apatite saturation (Figure 4-1); if so, apatite can be a sink for uranium via adsorption. In soils from granite alteration, apatite can be a common phase leading to the retention of uranium by phosphate phases. Examples of this retention mechanism are common in weathered horizons covering uranium ores /Jerden et al. 2003/, and in uranium-polluted sediments /Seaman et al. 2001/.

Another possible mechanism of uranium retention is the adsorption onto clays. In the Forsmark area, illite is the rock-forming mineral of glacial and post-glacial clays. The ability of this mineral to adsorb uranium is not well characterised in the literature. /Davis et al. 2006/ concluded that illite/smectite in alluvial sediments in Colorado (USA) did not significantly contribute to uranium sorption. In addition to glacial clays, soils derived from granite alteration are rich in clays such as kaolinite. The retention capacity of this mineral to uranium has been tested in many experimental investigations, e.g. /Payne et al. 1998/. /Ohnuki et al. 2005/ performed experiments to test the competition for uranium between kaolinite and microbial activity. Their results indicate that uranium was mainly retained by bacteria. This may suggest that in organic-rich environments, the organic activity has much more significance than adsorption onto common clays.

Selenium geochemistry is expected to be strongly controlled by microbially-mediated processes, especially in lake sediments and wetlands. Adsorption and reduction of both selenite and selenate to Se(0) by microbes is the most effective way to retain selenium into soils and sediments. Subsequent precipitation as iron selenides or co-precipitation with pyrite could occur under more reducing conditions. Another mechanism to take into consideration is the adsorption onto iron oxyhydroxides, although it is only effective if selenium is found as selenite. Similar to uranium, the capacity of the till to retain selenium is debated. No detailed data on the amount and type of organic matter exist, although the concentrations of TOC are comparable (slightly
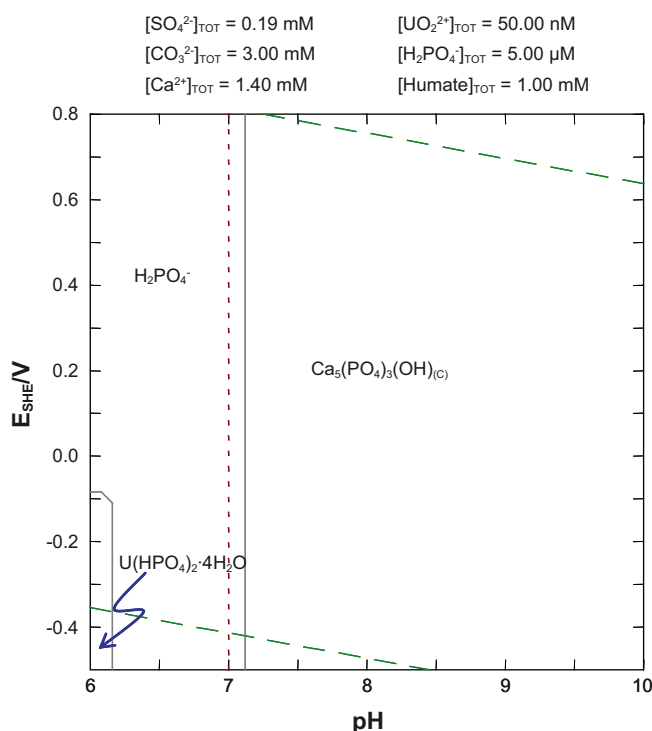
Figure 4-1. *Phosphate speciation in the Lake Bolundsfjärden waters. Higher concentrations of phosphate than those found in the lake are considered in the diagram (5×10^{-6} M) to achieve apatite equilibrium. This mineral is the controlling phase for phosphate at pH values higher than 7. U(VI) may readily be adsorbed on this mineral. Under more acidic conditions, uranium can precipitate as phosphate minerals.*

smaller) to lakes and streams. Another retention mechanism in the till is the incorporation of selenium anions into carbonate minerals, although its relevance needs further analytical investigations.

Iodine behaviour in the near-surface system would also be strongly dependent on the microbial activity, since this element is readily adsorbed as a nutrient even at very high concentrations. Iodine concentration in shallow groundwaters and in lakes ranges from 1×10^{-8} to 7×10^{-7} M. As already mentioned in section 2.3.4, the highest levels are related to saline monitoring wells (SFM0012, SFM0015, SFM0022 and SFM0023), which likely have influence of iodine deep or marine sources. In any case, these concentrations are low enough to prevent toxicity of microbes. In shallow groundwaters and surface waters in Forsmark, iodine is expected to be found as iodate due to the relative high contents of oxygen. Under these conditions, iodine can be adsorbed in humic acids and, more significantly, in illite-rich soils of post-glacial sediments. In deep sediments in lakes and wetlands, iodide is likely the predominant species, and in such cases the retention capacity of the media is much more reduced.

Despite the apparent uselessness of caesium in the organisms, its uptake is markedly fast. In lake environments such as those in the Forsmark area, this uptake should basically be associated with cyanobacteria and green algae. This quick transfer from surface water to living organisms implies that the soil adsorption processes are highly relevant. Sediments in wetlands and lakes contain glacial and post-glacial clays with important amounts of illite. As mentioned above, this mineral is a strong sink for caesium. However, an interesting factor to be evaluated for the Quaternary deposits in the Forsmark area, especially the lake sediments and wetlands, is the influence of NH_4^+ on Cs adsorption/desorption on illite and in organic compounds.

Ammonium concentrations in surface waters are relatively high, mainly during low productivity periods (autumn-winter), as high as 2×10^{-5} M. Potassium can also interfere with caesium

adsorption, but its concentrations are lower than the ammonium concentrations. On the other hand, the effect of discharge of radiocaesium from deep disposal into the till is difficult to evaluate since little information on the nature of the clay fraction in this soil exists. However, clay minerals such as illite are present in the till and, therefore, they should be the main sink for caesium.

Finally, strontium could be effectively retained by soils via co-precipitation with calcite, which is a major mineral in the till and glacial clays, and via ion exchange in clays, although in the latter case, strontium can be easily desorbed. Table 4-1 summarises the more relevant retention processes for the selected radionuclides in the near-surface system at Forsmark.

This preliminary evaluation could be significantly refined if more detailed data on (1) redox potentials in sediments, (2) mineral compositions of soils and sediments, and (3) porewater geochemistry become available. Another important unknown is the nature of the organic compounds in sediments and soils; a precise characterisation of NOM could lead to a better understanding of the retention potential of the near-surface system.

Table 4-1. Retention processes that may be relevant under the conditions of interest in this work. The mechanisms that are "able to retain" and are likely to occur under the conditions found in the Quaternary soils and sediments at Forsmark are indicated by black cells. "Able to retain" processes but of questionable occurrence at Forsmark are grey-shadowed. Processes that are "unable to retain" and/or unlikely are indicated by colourless cells in the table. Many processes occurring at low redox potentials (e.g. precipitation of selenium in sulphides) are in grey since reducing conditions are not confirmed to occur in the Forsmark near-surface system.

Retention process	Radionuclide				
	U	^{79}Se	^{129}I	^{135}Cs	Sr
Precipitation as pure phases	grey	grey	white	white	white
Sorption onto phyllosilicates	grey	white	black	black	black
Sorption on organic matter	black	white	black	white	white
Sorption onto Fe-Mn-Al oxyhydroxydes	black	grey	black	white	white
Association with carbonates	white	grey	white	white	black
Association with phosphates	grey	white	white	white	white
Association with sulphides	white	grey	white	white	white

black	Favourable and possible
grey	Favourable but perhaps unlikely
white	Unfavourable and/or unlikely

5 Numerical model setup

5.1 Reference cases and radionuclide selection

The retention capacity of the near-surface system of Quaternary deposits is evaluated, for selected radionuclides, by means of reactive solute transport simulations. Two distinct domains have been selected:

(1) The first reference case simulates a Quaternary till deposit overlying a granite bedrock. The bottom boundary of the modelled domain is the contact between the till and the granite bedrock. Deep groundwater containing dissolved radionuclides is assumed to migrate upwards through a fracture in the granite rock and eventually come into contact with Quaternary deposits. The Quaternary deposits are assumed to be hydraulically connected to a surface discharge zone (theoretically it could be a river, a lake, a wetland or the Baltic coast). Figure 5-1 shows the conceptual sketch of the first reference case. Most likely, the equilibrium with Fe(III) oxyhydroxides will control the redox state of the system in this example. Therefore, for redox-sensitive radionuclides (e.g. uranium), the main retention processes can be expected to be related to adsorption to these mineral surfaces.

(2) The second reference case simulates a clay layer that is present at the bottom of a discharge zone (such as a lake or the Baltic estuary for instance), and is overlying the till deposit. In order to evaluate the retention capacity of the clay, it is assumed that deep groundwater can flow through a preferential path in the till, that contacts directly with the bottom of the clay layer. Figure 5-2 shows the conceptual sketch of the second reference case. In contrast to reference case #1, the porewater redox in reference case #2 is assumed to be controlled by the equilibrium with pyrite, leading to more reducing conditions. Consequently, the radionuclide retention via precipitation of mineral phases, especially for uranium, will be evaluated in this case. In addition, the effect of organic acids on the mobilisation of uranium will be tested.
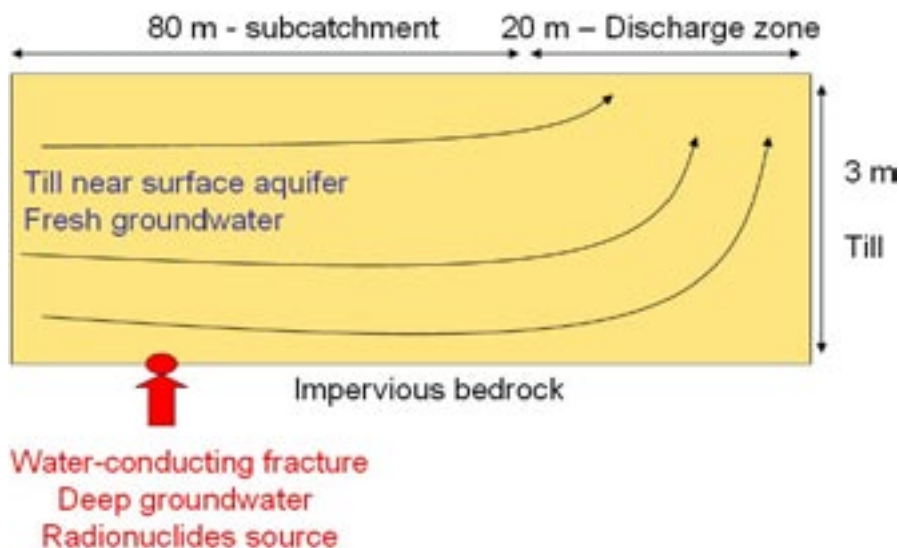

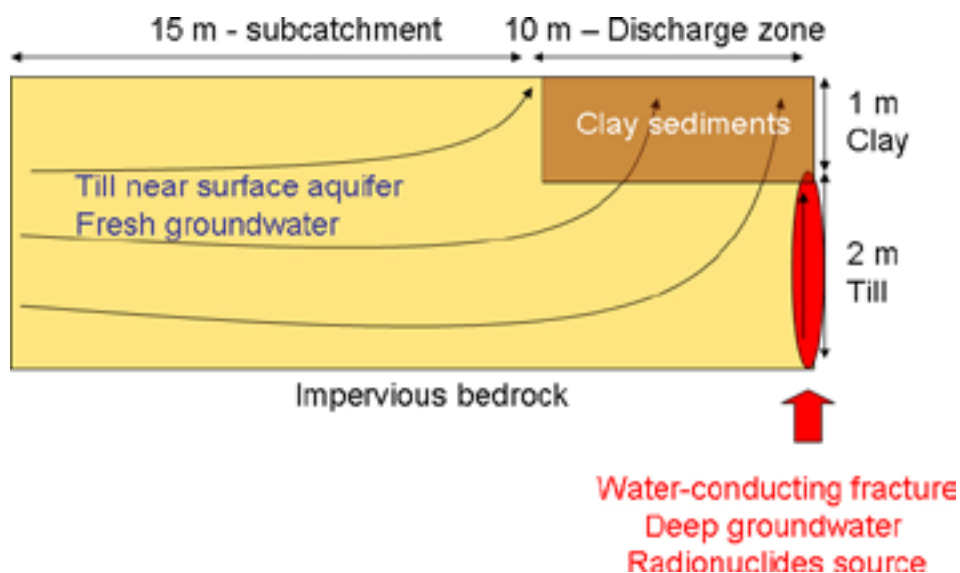*Figure 5-1.* Sketch of the reference case #1.

Figure 5-2. *Sketch of the reference case #2.*

Three different waters are considered in the numerical models:

Till shallow groundwater: Overall, the chemistry of shallow groundwaters flowing through till is fairly constant, with a predominance of Ca and HCO_3 that reflects the equilibrium with the host rock. The average composition of water sampled in well SFM0002 has been selected as the till reference water for numerical calculations. This selection is made according to the following considerations:

(1) This soil pipe has been repeatedly sampled (11 measurements),

(2) It shows small seasonal changes,

(3) It is saturated with calcite (i.e. equilibrium with the till),

(4) It contains analytical data on redox sensitive elements (Fe, Mn, U), and data on other elements of interest in the present work (Sr, Cs, NH_4^+) are available.

Points 2 and 3 provide evidence that the residence time of this groundwater in the till is relatively long. The availability of data on redox sensitive elements is especially relevant to determine the redox state of the water since little information on the redox potential is provided. The complete chemical composition of the SFM0002 soil pipe is listed in Table 5-1.

Clay porewater: In contrast to till groundwaters, compositions of clay porewaters in the Forsmark area have not been reported. As an alternative, the water composition from surface water sampled near the bottom of Lake Eckarfjärden (sampling point PFM117) has been selected; it is expected that the lake water interacts with the bottom sediments, influencing its hydrochemistry. Since this water sample is from a surface water body with short residence time, and therefore with little influence from water/rock interactions, it was decided to equilibrate the sample (using the PHREEQC code) with the minerals that are expected to interact with porewater in the sediments (cation exchange in illite, calcite, siderite, pyrite and quartz). After equilibration of the water sample from PFM117 with the mineral phases, the resulting composition will reflect water/rock interactions and therefore approach a clay porewater composition. This resulting water composition will be used as the reference water for the clay porewater.

Table 5-1. Chemistry of the waters selected for numerical calculations; concentrations in mol·L^{-1}.

	SFM0002	PFM117 bottom	SFM0023
pH	7.20	8.00	6.68
$[Na^+]_{total}$	1.22×10^{-3}	2.65×10^{-4}	6.93×10^{-2}
$[K^+]_{total}$	1.22×10^{-4}	5.20×10^{-5}	1.67×10^{-3}
$[Ca^{2+}]_{total}$	2.89×10^{-3}	1.19×10^{-3}	1.32×10^{-2}
$[Mg^{2+}]_{total}$	3.53×10^{-4}	1.17×10^{-4}	7.18×10^{-3}
$[CO_3^{2-}]_{total}$	5.66×10^{-3}	2.51×10^{-3}	2.14×10^{-3}
$[Cl^-]_{total}$	1.90×10^{-3}	1.53×10^{-4}	1.07×10^{-1}
$[SO_4^{2-}]_{total}$	2.41×10^{-4}	6.39×10^{-5}	3.73×10^{-3}
$[Si(IV)]_{total}$	9.74×10^{-5}	4.63×10^{-5}	7.56×10^{-5}
$[Fe]_{total}$	3.46×10^{-4}	8.34×10^{-7}	4.91×10^{-4}
$[Fe(II)]_{total}$	3.44×10^{-5}	–	–
$[Mn]_{total}$	3.86×10^{-6}	–	1.56×10^{-5}
$[Sr^{2+}]_{total}$	2.09×10^{-6}	6.23×10^{-7}	4.13×10^{-5}
$[U]_{total}$	2.27×10^{-8}	5.02×10^{-9}	4.62×10^{-10}
$[Cs^+]_{total}$	6.47×10^{-11}	4.51×10^{-11}	–
$[NH_4^+]_{total}$	6.61×10^{-6}	1.82×10^{-5}	1.95×10^{-4}
$[PO_4^{3-}]_{total}$	1.39×10^{-7}	4.80×10^{-8}	3.80×10^{-8}
$[O_2]$	4.27×10^{-5}	–	–
DOC	1.22×10^{-3}	1.49×10^{-3}	3.29×10^{-4}

Radionuclide-bearing groundwater: It is difficult to select a single sample for the bottom boundary condition since several chemically different waters occur underground in the Forsmark area. For the calculations, we have selected the average composition of water sampled in soil pipe SFM0023. Despite its relatively shallow occurrence, this groundwater shares many geochemical features with deep groundwaters: It is a Na-Cl water with a moderate salinity (ionic strength = 0.2 mol·L^{-1}; Table 5-1) and long residence time according to ^{3}H and ^{14}C data.

Three radionuclides have been selected for numerical modelling: U, Cs and Sr. The reason for this selection is related to the fact that experimental data for the retention mechanisms, mainly cation exchange and surface complexation, are available in scientific literature. This means that the retention processes can be implemented properly in the calculations.

5.2 Hydrodynamic processes and parameters

In this work, groundwater flow through porous media is assumed to be governed by Darcy's Law, which in its most general form relates water flux, **q**, to the gradient of water pressure, p, and elevation z, as

$$\mathbf{q} = -\frac{k}{\mu}\left(\nabla p + \rho\,\mathbf{g}\right) \qquad \text{(Equation 5-1)}$$

where ρ and μ are water density (volume per unit mass) and dynamic viscosity, respectively, k is intrinsic permeability and **g** is a vertical vector pointing downwards of modulus equal to gravity acceleration. When density changes are negligible, Darcy's Law can be written in terms of hydraulic head, h, as:

$$\mathbf{q} = -\mathbf{K}\nabla h \qquad \text{(Equation 5-2)}$$

where

$$\mathbf{K} = \frac{k\rho\,g}{\mu} \qquad\qquad \text{(Equation 5-3)}$$

and

$$h = \frac{p}{\rho g} + z \qquad\qquad \text{(Equation 5-4)}$$

Here, **K** is hydraulic conductivity tensor. By combining Darcy's Law and the mass balance equation one has the groundwater flow equation:

$$\nabla \cdot (\mathbf{K}\,\nabla h) + w = S_s\,\frac{\partial h}{\partial t} \qquad\qquad \text{(Equation 5-5)}$$

where W represents fluid sink/sources per unit volume of medium and S_s the is specific storage coefficient, defined as the volume of water delivered per unit time and unit volume of medium in response to a unit change of hydraulic head.

The solute transport processes considered in the model are: (1) advection, (2) molecular diffusion and (3) hydrodynamic dispersion. The equation governing solute transport through porous media is derived from the principle of mass conservation accounting for the mass fluxes due to the three above mentioned processes, leading to the well know advection-dispersion equation:

$$\nabla \cdot (\theta\mathbf{D}\nabla c) - c\nabla \cdot \mathbf{q} - \nabla c \cdot \mathbf{q} = \frac{\partial(\theta c)}{\partial t} \qquad\qquad \text{(Equation 5-6)}$$

where the solute concentration in water, c, is the unknown of the equation, θ denotes the volumetric water content of the porous media (porosity in a fully saturated case such as the models performed here), and **D** is the lumped dispersion tensor which accounts both for hydrodynamic dispersion and molecular diffusion processes. In this work, as in many other transport modelling studies, hydrodynamic dispersion is quantified by longitudinal and transverse dispersivities, denoted α_L and α_T, respectively, and molecular diffusion by an effective diffusion coefficient, denoted D_m.

Solute sinks and sources are added to the left-hand-side of the equation. For a fluid source r having a concentration, c*, and a solute sink/source term, R (solute mass added per unit time and unit fluid volume), the transport equation, as considered in the current models becomes:

$$\nabla \cdot (\theta\mathbf{D}\nabla c) - \mathbf{q} \cdot \nabla c + r(c^* - c) + \theta R = \theta\,\frac{\partial c}{\partial t} \qquad\qquad \text{(Equation 5-7)}$$

In the current models it is assumed that the till deposits host a near-surface aquifer with an average recharge of 66 mm/year. On the other hand, from the fracture in the underlying granitic bedrock, 2 mm/year of deep groundwater is transferred into the phreatic till aquifer. All these values are obtained from water balance calculations in the Forsmark area MIKE SHE models in /Johansson et al. 2005/. In accordance with the available characterisation data of the Quaternary deposits reported there, a thickness of 3 m has been assumed in the model for the till.

Following /Johansson et al. 2005/, the modelled till domain was divided along the vertical axis into three layers (Figure 5-3). The top 0.8-m layer and the bottom 0.8-m layer are more conductive than the intermediate layer (1.4 m). The whole till domain is here assumed anisotropic with a vertical hydraulic conductivity 10 times lower than the horizontal hydraulic conductivity. The effective porosity is also stratified with higher porosity values in the surface layer, reflecting a higher level of weathering and physical degradation closer to the surface /Johansson et al. 2005/. Table 5-2 shows all the hydrodynamic parameters used in the numerical simulations.

Table 5-2. Values of the hydrodynamic parameters used in the numerical models; K_h and K_v are the horizontal and vertical hydraulic conductivities, respectively, α_L and α_T the longitudinal and transverse dispersivities, respectively, θ_s the porosity (water content at saturation), and D_m the molecular diffusivity.

Material		K_h (m/s)	K_v (m/s)	α_L (m)	α_T (m)	θ_s (–)	D_m (m²/s)
Till	Layer 1	1.5×10^{-5}	1.5×10^{-6}	0.5	0.2	0.15	5×10^{-10}
	Layer 2	1.5×10^{-6}	1.5×10^{-7}	0.5	0.2	0.05	5×10^{-10}
	Layer 3	1.5×10^{-5}	1.5×10^{-6}	0.5	0.2	0.05	5×10^{-10}
Clay		1.0×10^{-8}	1.0×10^{-9}	0.5	0.2	0.2	5×10^{-10}

5.3 Geochemical processes and parameters

5.3.1 Reference case #1: The till system

Aqueous speciation

The thermodynamic database used in the calculations is described in section 5.6. Since the studied groundwaters are rich in aqueous carbonate, Fe(III) carbonate complexes have been added in the calculations. The species added are $Fe(CO_3)_3^{3-}$ and $FeOHCO_3$. The complexation reactions for these species with the corresponding constants are shown in Table 5-3. Constants are obtained from /Grivé 2005/.

Activity coefficients for charged species have been calculated by using the Davies equation:

$$\log\gamma_{ai} = -Az_i^2\left(\frac{(I)^{\frac{1}{2}}}{1+(I)^{\frac{1}{2}}} - 0.3I\right) \qquad \text{(Equation 5-8)}$$

where I is the ionic strength of the solution, z_i is the electric charge of the species in solution. A is a constant that depends on temperature.

For uncharged species, the Extended Debbye-Hückel equation has been used:

$$\log\gamma_{ai} = -\frac{Az_i^2(I)^{\frac{1}{2}}}{1+Ba_i(I)^{\frac{1}{2}}} + bI \qquad \text{(Equation 5-9)}$$

where a_i is the ionic radius of the species in solution. A and B are constants that depend on temperature and dielectric water constant. Unless otherwise specified, b is assumed to be 0.1 for all uncharged species.

Equilibrium with pure mineral phases and solid solutions

Mineralogical composition in the till shows the existence of calcite, quartz and illite as major minerals (> 5 wt%) /SKB 2005/. In the reactive transport calculations, calcite is considered to contain trace amounts of Sr forming a solid solution. The initial amount of Sr-bearing calcite is assumed to be in excess given the very high content in the till and the low water-rock ratio. Similarly, quartz concentration in the till is high enough to consider it as an infinite reservoir.

Table 5-3. Complexation reaction of aqueous Fe(II) carbonates and corresponding thermodynamic constant from /Grivé 2005/.

Reaction	LogK (25°C)
$3HCO_3^- + Fe^{2+} \leftrightarrow Fe(CO_3)_3^{3-} + 3H^+ + e^-$	−19.77
$HCO_3^- + H_2O + Fe^{2+} \leftrightarrow FeOHCO_3 + 2H^+ + e^-$	−12.59

Illite dissolution kinetics are very slow under the environmental conditions modelled in this study. /Köhler et al. 2003/ found very slow dissolution rates in circumneutral pH values, from 10^{-14} to 10^{-15} mol·m^{-2}·s^{-1}. Consequently, dissolution of illite is not considered in the numerical simulations; it only participates as a charged surface for cation exchange.

As discussed in section 2.5, it is very likely that other phases exist at minor and trace concentrations, some of which can play a very important role in the control of the redox conditions and radionuclide retention. Among these, Fe(III)-hydroxide (ferrihydrite) is thought to be the controlling phase for the redox of the till porewater and also to be the main uranium sorbent. In the reactive transport, it has been arbitrarily (due to the lack of field data), but reasonably, considered an initial concentration of 0.1 wt% in the till.

The log K of the reaction involving this mineral has been discussed in the literature, and a wide range of values has been reported. The disparity in the log K values is mainly caused by the variable crystallinity of the samples used in the laboratory experiments. For the numerical simulations in the present study, we have selected the following constant:

$$Fe(OH)_3(s) + 3H^+ = Fe^{3+} + 3H_2O \qquad \log K = 5.00$$
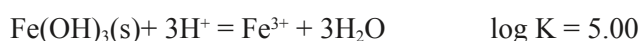
which corresponds to an amorphous ferrihydrite. The reason for this selection is that the reference water is close to the saturation with this phase.

Another mineral that is not cited in the mineralogical inspections of the till samples is siderite ($FeCO_3$). This mineral is redox sensitive and can precipitate in the till domain after the deep inflow. Therefore, in the reactive transport model it is allowed to precipitate if this mineral reaches over-saturation in the water. It is worth mentioning that this mineral rarely precipitates as a pure $FeCO_3$ but it forms solid solutions with calcium (ankerite, $CaFe(CO_3)$). The thermodynamics of this solid solution series are still not well known, which is why the pure phase is selected for the current model calculations.

According to section 3.1, apatite ($Ca_5(OH)(PO_4)_3$) is a good sorbent for uranium, which implies that it could be interesting to include it in the reactive transport calculations. There is no evidence of apatite in the till, but deep groundwater intrusion could lead to precipitation of this phase, and that it becomes a potential uranium sorbent. For this reason, the predicted evolution of the saturation index of this mineral has been monitored in the preliminary simulations. The phosphate concentration is low enough to keep the porewater undersaturated in apatite. However, apatite precipitation is allowed in the model if oversaturation is reached.

A set of minerals has been selected as possible solubility-limiting phases of aqueous uranium. For U(IV), a hydrated, amorphous phase ($UO_2 \cdot 2H_2O$) has been preferred instead of a crystalline phase (e.g. uraninite, UO_2). Moreover, coffinite (($USiO_4 \cdot nH_2O$) formation is not allowed since it is considered that its precipitation is not kinetically favoured (see section 3.1). For U(VI) schoepite ($UO_2(OH)_2$), soddyite (($UO_2)_2SiO_4(H_2O)_2$), uranophane ($Ca(UO_2)(SiO_3OH)_2(H_2O)_5$) and becquerelite ($Ca(UO_2)_6O_4(OH)_6 \cdot 8H_2O$) are allowed to precipitate if the solution becomes oversaturated in these phases.

In Table 5-4, the dissolution reactions of all minerals considered in the numerical simulations with the corresponding thermodynamic constants have been listed. All reactions are simulated under local equilibrium approach.

Pure mineral phases are rarely found in natural environments. Instead, many solid phases are "mixtures" of two or more end-members at variable proportions forming solid solutions. A well known example of solid solution is the uptake of strontium in calcite, forming $Ca_{1-x}Sr_xCO_3$, where x is the molar fraction of strontium. At Forsmark, strontium concentration in shallow groundwaters is thought to be influenced by the equilibrium with host rock.

The till is made of carbonate particles derived from the erosion of Cambro-Ordovician marine carbonate rocks, and contains significant amounts of strontium (see section 2.5). The Sr/Ca molar ratio observed in these rocks in the Forsmark area is fairly constant, around 4×10^{-4} (see section 2.5). On the other hand, two distinct Sr/Ca molar ratios in shallow groundwaters can be

Table 5-4. Dissolution reactions of the reactive solid phases in the numerical simulations. Thermodynamic equilibrium constants and references are also listed.

Reaction	Log K (25°C)	Reference
Mineral solubility		
Calcite: $CaCO_3 + H^+ \leftrightarrow Ca^{2+} + HCO_3^{-\,(*)}$	+1.85	(1)
Strontianite: $SrCO_3 + H^+ \leftrightarrow Sr^{2+} + HCO_3^{-\,(*)}$	+1.05	(1)
Siderite: $FeCO_3 + H^+ \leftrightarrow Fe^{2+} + HCO_3^-$	−0.47	(2)
Gypsum: $CaSO_4 \cdot 2H_2O \leftrightarrow Ca^{2+} + SO_4^{2-} + 2H_2O$	−4.85	(2)
Quartz: $SiO_2 + H_2O \leftrightarrow Si(OH)_4$	−3.75	(3)
Pyrite: $FeS_2 + 2H^+ + 2e^- \leftrightarrow Fe^{2+} + 2HS^-$	−18.50	(4)
Hydroxilapatite: $Ca_5(OH)(PO_4)_3 + 4H^+ \leftrightarrow H_2O + 3HPO_4^{2-} + 5Ca^{2+}$	−3.07	(5)
$UO_2 \cdot 2H_2O_{\,(am)} + 4H^+ \leftrightarrow U^{4+} + 4H_2O$	+1.50	(6)
Ferrihydrite: $Fe(OH)_{3\,(am)} + 3H^+ \leftrightarrow Fe^{3+} + 3H_2O$	+5.00	(7)
Uranophane: $Ca(UO_2)_2(SiO_3OH)_2 \cdot 5H_2O + 6H^+ \leftrightarrow Ca^{2+} + 2UO_2^{2+} + 2Si(OH)_4 + 5H_2O$	+9.42	(8)
Becquerelite: $Ca(UO_2)_6O_4(OH)_6 : 8H_2O + 14\,H^+ \leftrightarrow Ca^{2+} + 6UO_2^{2+} + 18H_2O$	+29.00	(9)
Soddyite: $(UO_2)_2SiO_4 \cdot 2H_2O + 4H^+ \leftrightarrow 2UO_2^{2+} + Si(OH)_4 + 2H_2O$	+5.00	(10)
Schoepite: $UO_3 \cdot 2H_2O + 2H^+ \leftrightarrow UO_2^{2+} + 3H_2O$	+5.96	(11)

(*) Minerals involved in the $Ca_{1-x}Sr_xCO_3$ solid solutions.

(1) /Plummer and Busenberg 1982/.

(2) /Nordstrom et al. 1990/.

(3) /Cox et al. 1989/.

(4) /Robie and Waldbaum 1968/.

(5) /Johnson et al. 2000/.

(6) /Guillamont et al. 2003/.

(7) /Hummel et al. 2002/.

(8) /Nguyen et al. 1992/.

(9) /Casas et al. 1997/.

(10) /Pérez et al. 1997/.

(11) /Bruno and Sandino 1989/.

defined (Figure 2-21): the first one is around 7×10^{-4} and it is found in samples from soil pipes SFM0002, -32 and -57 in the Lake Bolundsfjärden area. The second ratio is lower, and seems to reflect the mixing between shallow dilute groundwaters and more saline waters.

The incorporation of strontium in the calcium carbonate lattice has widely been studied, since it was suggested that $(Ca,Sr)CO_3$ solid solutions could control the strontium concentrations in seawater /Stumm and Morgan 1996/. This solid solution series is highly non-ideal, i.e. the activity coefficients of the end-members are not equal to 1 (Equation 5-10 and Equation 5-11):

$$\{Ca^{2+}\}\{CO_3^{2-}\} = K_{CaCO_3}a_{CaCO_3} = K_{CaCO_3}x_{CaCO_3}f_{CaCO_3} \qquad \text{(Equation 5-10)}$$

$$\{Sr^{2+}\}\{CO_3^{2-}\} = K_{SrCO_3}a_{SrCO_3} = K_{SrCO_3}x_{SrCO_3}f_{SrCO_3} \qquad \text{(Equation 5-11)}$$

where $\{CO_3^{2-}\}$, $\{Ca^{2+}\}$, $\{Sr^{2+}\}$ are the aqueous activities of CO_3^{2-}, Ca^{2+} and Sr^{2+}; respectively, K_{CaCO_3} and K_{SrCO_3} are the solubility products of pure $CaCO_3$ and $SrCO_3$ end members with activities a_{CaCO_3}, a_{SrCO_3}, mole fractions x_{CaCO_3}, x_{SrCO_3}, and activity coefficients f_{CaCO_3}, f_{SrCO_3}, respectively.

Non-ideality of a solid solution implies a dependence of the activity coefficients of the end members on the composition of the solid solution. This dependence can be quantified following the /Redlich and Kister 1948/ equations, cf Equations 5-12 and 5-13 below, which in turn were derived from Equation 5-14 suggested by /Guggenheim 1937/.

$$\ln f_{CaCO_3} = x^2_{SrCO_3}\left[a_0 + a_1\left(3x_{CaCO_3} - x_{SrCO_3}\right) + a_2\left(x_{CaCO_3} - x_{SrCO_3}\right)\left(5x_{CaCO_3} - x_{SrCO_3}\right) + ...\right]\text{ (Equation 5-12)}$$

$$\ln f_{SrCO_3} = x^2_{CaCO_3}\left[a_0 + a_1\left(3x_{SrCO_3} - x_{CaCO_3}\right) + a_2\left(x_{SrCO_3} - x_{CaCO_3}\right)\left(5x_{SrCO_3} - x_{CaCO_3}\right) + ...\right]\text{ (Equation 5-13)}$$

$$G^E = x_{SrCO_3} x_{CaCO_3} RT\left[a_0 + a_1\left(x_{SrCO_3} - x_{CaCO_3}\right) + a_2\left(x_{SrCO_3} - x_{CaCO_3}\right)^2 + ...\right]\text{ (Equation 5-14)}$$

The first two coefficients (a_0 and a_1) in equation 5-12 to equation 5-14 are generally sufficient to describe the non-ideality of many solid solutions. /Plummer and Busenberg 1987/ reported values for a_0 and a_1 of 3.43 and –1.82, respectively, for the $(Ca,Sr)CO_3$ solid solutions. The calculated gap of miscibility (i.e. the set of solid solution compositions that are thermodynamically unstable) derived from these data is $0.0048 < X_{ss} < 0.857$. This means that the maximum molar fraction of strontium that can be incorporated as trace element into the solid solution is 0.0048. Similar values were reported by /Lippmann 1980/, $a_0 = 5.3$ and $0.005 < X_{ss} < 0.995$, and /Tesoriero and Pankow 1996/, $a_0 = 5.7$ and $0.0035 < X_{ss} < 0.065$.

The main difference between the work by /Plummer and Busenberg 1987/ and /Lippmann 1980/ and /Tesoriero and Pankow 1996/ is that the former considered aragonite as $CaCO_3$ end-member, whereas the latter used calcite.

The initial composition of the solid solution present in the till considered in the reactive transport calculations is $Ca_{0.9996}Sr_{0.0004}CO_3$, which is in agreement with the elemental composition measured in the till at Forsmark (Figure 2-13). The reference groundwater is not strictly in equilibrium with a solid solution of this composition, which it is with a more Sr-depleted solid solution. This could mean that present-day shallow groundwater flowing through the till is in equilibrium with the outer rim of the till grains only, which is poorer in strontium due to water-rock interaction. In this study, however, we have maintained the actual composition measured in the whole grains in the numerical simulations.

In the numerical modelling carried out in the present work, the solid solution-aqueous solution (SSAS) equilibrium is also simulated assuming the local equilibrium approach, and all the solid phase is instantaneously re-equilibrated to a most stable solid solution if the composition of the groundwater in contact changes in a given node. This approach is less realistic than considering replacement of only a rim of the mineral crystal, but the present reactive transport codes are not capable to deal with this sort of calculations. Since the inflowing deep groundwater is expected to have a lower Ca/Sr ratio, the predicted newly formed solid solutions in equilibrium with it will be progressively richer in Sr. The thermodynamic data and references of the end members are shown in Table 5-4.

Cation exchange in illite-bearing till

Like other clay minerals, illite balances its electric charge deficit through adsorption of cations in the interlayers. The composition of these interlayers is conditioned on the equilibrium with the porewater and the selectivity coefficients of each cation involved. According to available studies dealing with the adsorption of caesium on illite, it is known that cation exchange in this mineral takes place on different surface sites, see /Poinssot et al. 1999/. /Bradbury and Baeyens 2000/ proposed a model of cation exchange in illite considering three types of sites (Table 5-5).

The most abundant sites ($\sim 80\%$ of the total CEC, which is $0.2\ eq\cdot kg^{-1}$) are the so-called "planar sites", which can adsorb either divalent cations such as Ca^{2+}, Mg^{2+} and Sr^{2+} or monovalent ions (Na^+, K^+ and Cs^+); these sites are considered of "low affinity", and are usually associated with the fixed negative charge on the surface of illite arising from isomorphous substitution, e.g. Al^{3+} for Si^{4+} /Poinssot et al. 1999/. Due to steric reasons, divalent cations are only involved in this type of sites /Poinssot et al. 1999/.

Table 5-5. Cation exchange reactions in the illite interlayer.

Reaction	Log K (25°C)	Reference
Total Exchange Capacity (CEC) = 0.2 eq·kg^{-1}		
Planar sites (0.8×CEC)		
$X^- + Na^+ \leftrightarrow NaX$	0.0	(1)
$X^- + K^+ \leftrightarrow KX$	1.1	(1)
$X^- + Cs^+ \leftrightarrow CsX$	1.6	(1)
$2X^- + Sr^{2+} \leftrightarrow SrX_2$	1.5	(2)
$2X^- + Ca^{2+} \leftrightarrow CaX_2$	1.3	(3)
$2X^- + Mg^{2+} \leftrightarrow MgX_2$	1.5	(3)
Type II sites (0.2×CEC)		
$X^{II-} + Na^+ \leftrightarrow NaX^{II}$	0.0	(1)
$X^{II-} + K^+ \leftrightarrow KX^{II}$	2.1	(1)
$X^{II-} + Cs^+ \leftrightarrow CsX^{II}$	3.6	(1)
Frayed edge sites (FES) (0.0025×CEC)		
$X^{FES-} + Na^+ \leftrightarrow NaX^{FES}$	0.0	(1)
$X^{FES-} + K^+ \leftrightarrow KX^{FES}$	2.4	(1)
$X^{FES-} + Cs^+ \leftrightarrow CsX^{FES}$	7	(1)
$X^{FES-} + NH_4^+ \leftrightarrow NH_4X^{FES}$	3.5	(1)

(1) /Bradbury and Baeyens 2000/.

(2) /Cole et al. 2000/.

(3) /Tournassat et al. 2007/.

The second and the third types of sites, called "Type II" and "Frayed Edge Sites" (FES), are considered to be of "high affinity" and involve monovalent cations such as Na^+, K^+, Cs^+ and NH_4^+. The site density is much lower (20% and 0.25% of the total sites, respectively), but the uptake of some cations such as Cs^+ on these sites (especially on FES) is particularly efficient and dominant. Interestingly, these sites are not generally associated with other clay minerals, such as smectite, chlorite or kaolinite /Bradbury and Baeyens 2000/.

Uranium sorption on ferrihydrite (Fe(OH)$_3$ (am))

Under oxidising conditions, uranium (as U(VI)) transport in aquifers is mainly limited by the adsorption on mineral surfaces, and at higher concentrations by the precipitation of mineral phases. As already detailed in section 3.1, U(VI) can be absorbed in a number of mineral surfaces, especially onto clays and iron oxyhydroxides. In the reactive transport simulations, uranium is assumed to be adsorbed only on ferrihydrite (Fe(OH)$_3$(s)). The surface complexation model followed is that of /Waite et al. 1994/. This model considers two types of adsorption sites, i.e. sites of strong and weak binding, respectively.

The adsorbable species and corresponding constants are listed in Table 5-6. Note that adsorbing carbonate species also have been included in the simulations. This is because the amount of aqueous carbonate is expected to be high due to the equilibrium with the (Ca,Sr)CO$_3$ solid solution present in the till, and, under these conditions, carbonate adsorption on ferrihydrite surface can be significant /Bruno et al. 1992, Van Geen et al. 1994/. Two types of uranium complexes are included: $\equiv(HFO\_O)UO_2$ and $\equiv(HFO\_O)UO_2CO_3^{2-}$, which are capable of being adsorbed on both weak and strong sites. The total concentration of sites is 0.875 mol·mol$_{Fe}^{-1}$ /Waite et al. 1994/. Most of these sites are of low affinity (weak binding) and only 0.0018 mol·mol$_{Fe}^{-1}$ correspond to high-affinity (strong binding) sites.

Table 5-6. Complexation reactions on the ferrihydrite surface.

Reaction	Log K (25°C, I = 0.1 M)	Reference
Strong sites (1.8×10^{-3} $mol_{site} \cdot molFe^{-1}$)		
$\equiv HFO^sOH + H^+ \leftrightarrow \equiv HFO^sOH_2^+$	6.51	(1)
$\equiv HFO^sOH \leftrightarrow \equiv HFO^sO^- + H^+$	−9.13	(1)
$\equiv HFO^sOH + UO_2^{2+} \leftrightarrow \equiv (HFO^sO)2UO_2 + 2H^+$	−2.57	(1)
$\equiv HFO^sOH + UO_2^{2+} + CO_3^{2-} \leftrightarrow \equiv (HFO^sO)_2UO_2CO_3^{2-} + 2H^+$	3.67	(1)
$\equiv HFO^sOH + CO_3^{2-} + 2H^+ \leftrightarrow \equiv HFO^sCO_3H + H_2O$	19.50	(1)
$\equiv HFO^sOH + CO_3^{2-} + H^+ \leftrightarrow \equiv HFO^sCO_3^- + H_2O$	11.51	(1)
Weak sites (0.875 $mol_{site} \cdot molFe^{-1}$)		
$\equiv HFO^wOH + H^+ \leftrightarrow \equiv HFO^wOH_2^+$	6.51	(1)
$\equiv HFO^wOH \leftrightarrow \equiv HFO^wO^- + H^+$	−9.13	(1)
$\equiv HFO^wOH + UO_2^{2+} \leftrightarrow \equiv (HFO^wO)2UO_2 + 2H^+$	−6.28	(1)
$\equiv HFO^wOH + UO_2^{2+} + CO_3^{2-} \leftrightarrow \equiv (HFO^wO)2UO_2CO_3^{2-} + 2H^+$	−0.42	(1)
$\equiv HFO^wOH + CO_3^{2-} + 2H^+ \leftrightarrow \equiv HFO^wCO_3H + H_2O$	19.50	(1)
$\equiv HFO^wOH + CO_3^{2-} + H^+ \leftrightarrow \equiv HFO^wCO_3^- + H_2O$	11.51	(1)

(1) /Waite et al. 1994/.

Unlike illite surface, ferrihydrite is a reactive mineral very sensitive to changes in the redox state of the system. Intrusion of deep groundwaters into the till domain may lead to dissolution of ferrihydrite. For this reason, the total amount of sites available for adsorption in the reactive transport simulations depends on the remaining moles of ferrihydrite in each time step.

5.3.2 Reference case #2: The clay system

Aqueous speciation

The aqueous species selected and the thermodynamic database used are the same as for the reference case #1 (section 5.3.1). Moreover, organic species have been included as humic acids to simulate the metal complexation in waters with high concentration of organic compounds. The metals considered for complexation with humic acids are calcium and uranium. Six different organic species have been considered: Humate$^-$, CaHumate$^+$, UHumate^{3+}, U(Humate)$_2^{2+}$, UO$_2$Humate$^+$ and UO$_2$(Humate)$_2$. The first two complexes of uranium are for U(IV), and the last two are for U(VI). The reactions and thermodynamic constants for these species are listed in Table 5-7.

Table 5-7. Complexation reactions of organic compounds and corresponding thermodynamic constants.

Reaction	Log K (25°C)
$Ca^{2+} + Humate^- \leftrightarrow CaHumate^+$	4.7 [1]
$U^{4+} + Humate^- \leftrightarrow Uhumate^{3+}$	7.0 [2]
$2U^{4+} + Humate^- \leftrightarrow U(Humate)_2^{2+}$	11.5 [2]
$UO_2^{2+} + Humate^- \leftrightarrow UO_2Humate^+$	7.64 [3]
$2UO_2^{2+} + Humate^- + H_2O \leftrightarrow UO_2(Humate)_2$	11.54 [3]

[1] /Choppin and Shanbhag 1981/.

[2] /Li et al. 1980/.

[3] /Shanbhag and Choppin 1981/.

Equilibrium with pure mineral phases and solid solutions

According to /Hedenström 2004/, the glacial clays present in the lake sediments and the Baltic estuary of Forsmark show considerable amounts of illite, quartz and calcite. As in the previous reference case, it was considered that calcite present in the till has trace amounts of Sr forming a solid solution, which can be a sink for the incoming Sr from deep fluids. Also, the moles of Sr-rich calcite are assumed to be initially in excess. Similarly, the quartz concentration in the glacial clay is high enough to consider it as an infinite reservoir.

As explained for the reference case #1 (section 5.3.1), no reactivity is given to illite in the numerical simulations, and therefore illite only participates as a charged surface for cation exchange. As discussed in section 2.5, it is very likely that other phases exist at minor and trace concentrations, some of which can play a very important role in the control of the redox conditions and radionuclide retention. Among these, pyrite is considered to significantly affect the redox of the clay porewater. An initial concentration of 1 mol·L^{-1} of pyrite has been considered in the model, in order to ensure the relatively reducing conditions in the glacial clays.

The uranium mineral phases allowed to precipitate in the reactive transport simulations are the same as in the previous till system case. Nevertheless, due to the prevailing reducing conditions of the glacial clays, it is expected that the U(IV) mineral phases will be favoured. The initial composition of the solid solution present in the clay considered in the reactive transport calculations is $Ca_{0.9996}Sr_{0.0004}CO_3$, i.e. the same as for the previous case.

Cation exchange in illite

The configuration of the illite interlayer applied to the clay system is the same as that in the till system (Table 5-5), with the only difference being the percentage of illite in the modelled domain. In the till system an illite content of 10 wt% was used, while in the clay system an illite content of 50 wt% is considered, due to the higher clay content in this domain. The difference in the proportion of illite in the modelled domain will lead to a higher exchangeable sites density in the clay system.

5.4   Spatial and temporal discretisation

5.4.1   Reference case #1: The till system

The modelled domain of the numerical model built for the reference case #1 is a 2D vertical cross-section of the till deposits. According to the available characterization data of the Quaternary deposits /Johansson et al. 2005/ a thickness of 3 m has been assumed for the model. Taking into account the actual dimensions of the subcatchments in the Forsmark area, the horizontal length of the model domain was set to a value of 100 m. The modelled till deposit was divided into three layers following the simplified till profile proposed by /Johansson et al. 2005/ (Figure 5-3). These three layers have different hydraulic properties, as described above.

The till deposit hosts phreatic aquifers that may be locally confined, and may discharge to distinct surface water bodies, like streams, lakes and the Baltic Sea /Johansson et al. 2005/. It has been decided to simulate a confined aquifer that discharges into a surface water body located at the top-right corner of the modelled domain. The spatial discretisation of the modelled domain was adapted according to the main features of the boundary conditions, which will influence the groundwater flow directions and the groundwater chemistry of the modelled domain. In particular, the position of the deep groundwater inflow and the position of the discharge area (outflow boundary) are important boundaries.
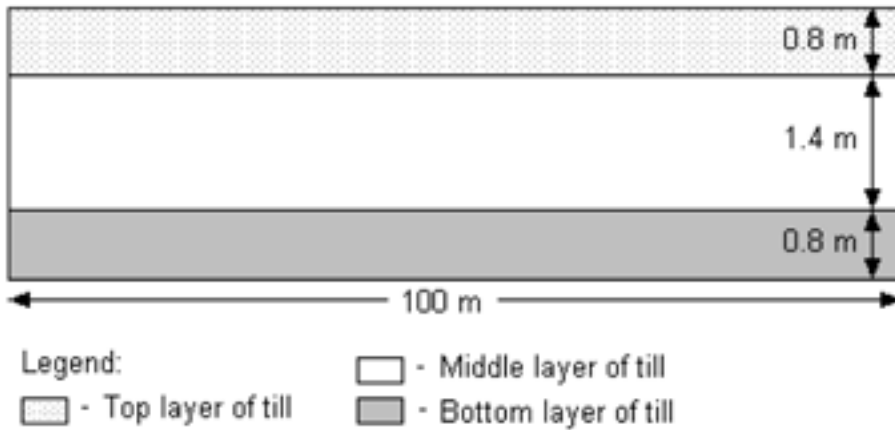
Figure 5-3. *Layering of the till domain. The till is composed of three layers that show distinct differences in hydraulic properties (Y axis magnified 15 times).*

In reference case #1, the spatial discretisation along the X axis is refined in the till directly overlying the area where the deep groundwater enters. Similarly, the discretisation is also refined under the discharge area. Underneath the section of the top boundary that represents the discharge area, the spatial discretisation along the Y axis is also finer due to high upward vertical component of the shallow groundwater flow (Figure 5-4).

It is expected that the higher chemical gradients will occur at the beginning of the simulation period and, consequently, greater changes of the water composition (aqueous species) and solid composition (composition of the illite exchanger, ferrihydrite surface, solid solutions and pure
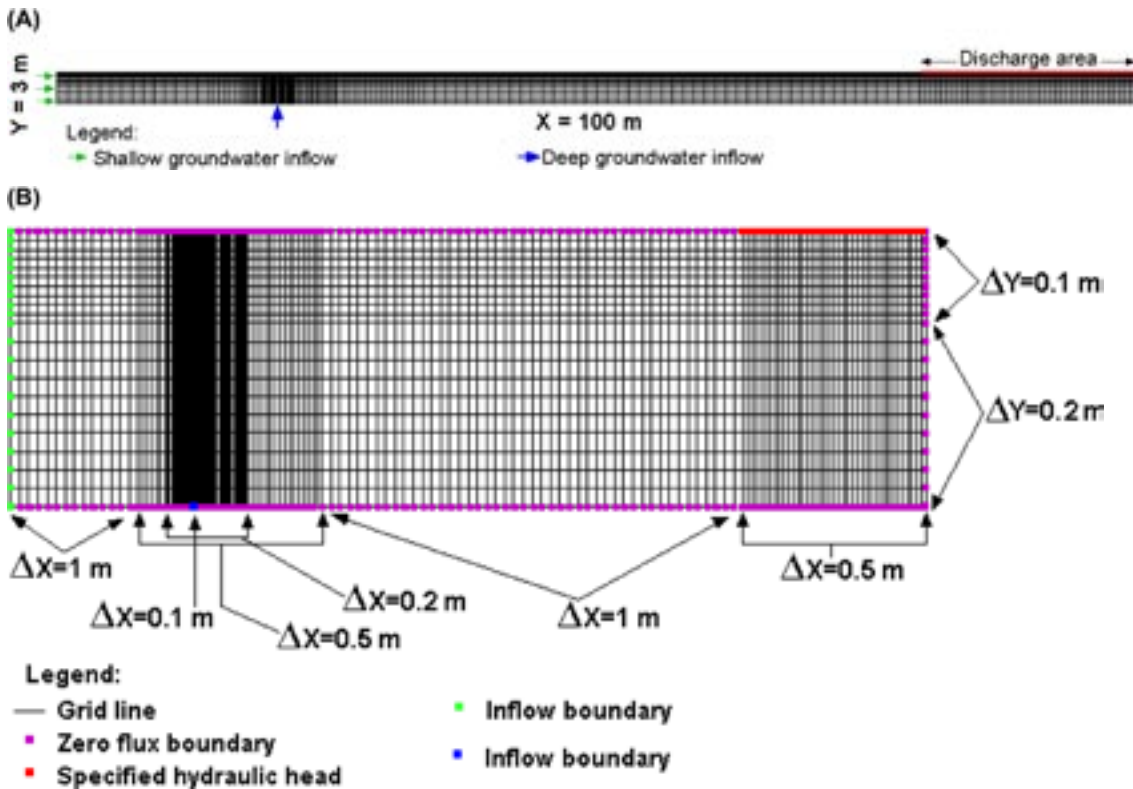
Figure 5-4. *Numerical grid showing the distinct spatial discretisations along the X and Y axis, and the boundary conditions assigned to the till system (reference case #1). Grid A shows the length of each axis, whereas grid B explains where the finer discretisations occur and the boundary conditions (Y axis is magnified 10 times).*

52

mineral phases) will occur at the beginning of the simulation period. Thus, the time discretisation was refined at the beginning of the simulation period, and then made progressively coarser towards the end of the simulation period. According to these criteria, the time discretisation was set as shown in Figure 5-5.

5.4.2 Reference case #2: The clay system

The modelled domain considered for the reference case #2 is a 2D symmetric vertical cross section of a clay layer that may be present at the bottom of discharge areas present at Forsmark, like lakes and the Baltic Sea (see Figure 5-2). Based on the characterization of the lake sediments reported in /Johansson et al. 2005/, the thickness of the clay layer in the model was set to 1 m. The length of the X axis was set to 10 m.

In this case, the shallow groundwater flowing in the underlying till aquifer enters in the clay domain through the left and bottom boundaries (Figure 5-6). As explained above, the deep groundwater inflow for the reference case #2 will occur at the bottom right corner of the domain. The water flowing in this domain will flow out through the whole top boundary. Since the modelled domain in the reference case #2 is relatively small (1 m X 10 m), it was set a fine discretisation of 0.1 m along both axis for the whole domain (Figure 5-6).
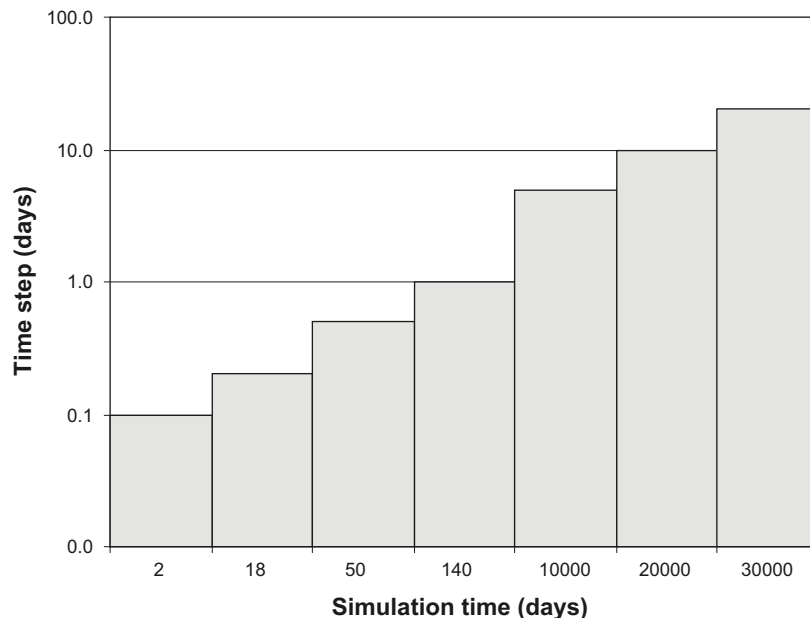

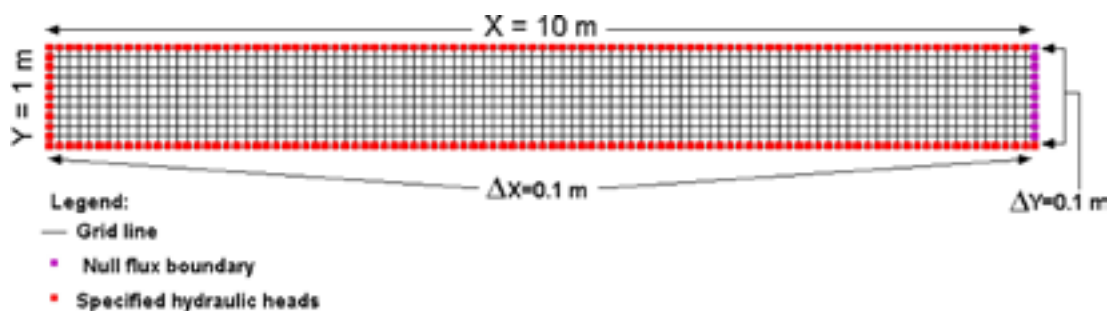*Figure 5-5. Time discretisation for reference case #1.*

Figure 5-6. Numerical grid showing the spatial discretisation of the modelled domain and the boundary conditions assigned to the clay system (reference case #2).

53

As in the previous reference case, it is expected that the higher chemical gradients will occur at the beginning of the simulation period, and therefore, more importnat changes of the water composition (aqueous species) and solid composition (composition of the illite exchanger, ferrihydrite surface, solid solutions and pure mineral phases) will also occur at the beginning of the simulation period. For these reasons, the time discretisation was finer at the beginning of the simulation period and made progressively coarser towards the end of the simulation period, as shown in Figure 5-7. To ensure stability in the numerical calculations, the Péclet criterion (Pe ≤ 2) is met for the maximum ΔX (maximum $\Delta X = 1$ m, and longitudinal dispersivity = 0.5 m) in both numerical models.

5.5 Initial and boundary conditons

5.5.1 Reference case #1: The till system

Hydrogeological initial and boundary conditons

According to the water balance calculations made with the MIKE SHE model for the Forsmark site /Johansson et al. 2005/, the shallow aquifers in the till deposits discharge 66 mm/year to the surface water bodies. Therefore, for the present numerical model, a flow of 66 mm/year has been prescribed in the top boundary of the modelled domain.

From the total length of the top boundary, only 80 m correspond to the recharge area, since the last 20 m correspond to the discharge area, and therefore, considering a surface of 80×1 m, the net recharge flow entering the system would be:

$$66 \times 10^{-3} \frac{m^3}{m^2 \times year} \times 80m \times 1m = 5.28 \frac{m^3}{year} = 14.5 \frac{L}{d}$$

As explained above, the net recharge flow of 14.5 L/d will be applied to the left boundary, in order to simulate a locally confined aquifer with a predominantly horizontal flow direction, before reaching the discharge area (Figure 5-8). The discharge area of the modelled domain is placed at the last 20 m of the top boundary, where a constant head of 3 m is set.

At the bottom boundary of the modelled domain, between X = 20 m and X = 20.2 m, the deep groundwater flows into the domain. The remaining bottom boundary (from X = 0 m to X = 19.9 m, and from X = 20.3 to X = 100 m) is set as impervious. The flux of deep groundwater
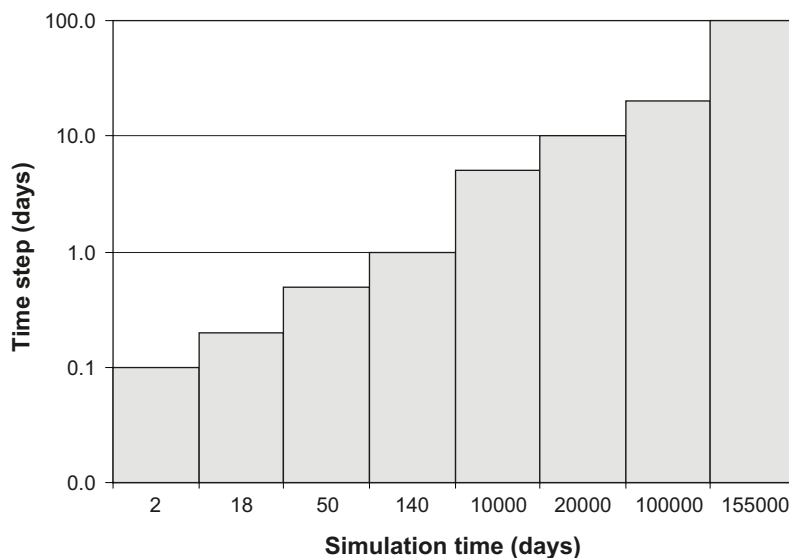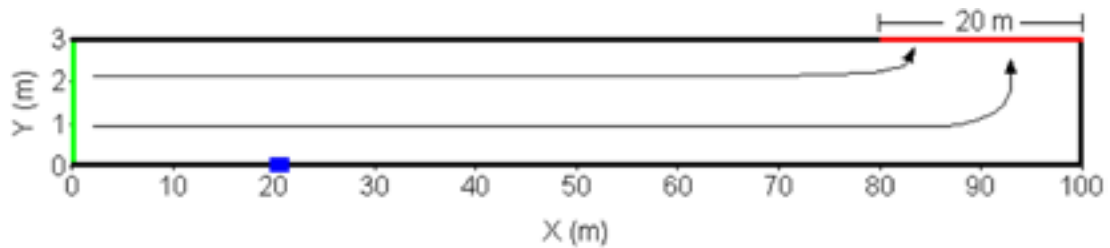

Figure 5-7. *Time discretisation for reference case #2.*

Legend:
— Till groundwater inflow: 14.5 L/d   — Null flux boundary
— Discharge area: Constant head of 3m   ■ Deep groundwater inflow: 0.5 L/d
→ Expected groundwater flow direction

Figure 5-8. *Boundary conditions for the numerical model applied in reference case #1.*

entering through the 0.2 m of the bottom boundary was calculated from the 2 mm/year of inflow across bottom boundary obtained in the water balance from the MIKE SHE model applied to the Forsmark area /Johansson et al. 2005/.

For the present model, the 2 mm/year were multiplied by the total bottom area of 100×1 m, and applied to the discrete deep inflow boundary of 0.2 m. Therefore, the total deep inflow passing through the 0.2 m is:

$$2 \times 10^{-3} \frac{m^3}{m^2 \times year} \times 100m \times 1m = 0.2 \frac{m^3}{year} = 0.5 \frac{L}{d}$$

Then, it is assumed that the simulated catchment has a deep inflow concentrated at a single point which would correspond to a hypothetical fracture zone.

Initial groundwater composition in the till

The chemistry of the groundwater in equilibrium with the till used in the simulations has been obtained after the equilibration of the SFM0002 shallow groundwater with $(Ca,Sr)CO_3$ solid solution, quartz and ferrihydrite (Table 5-8). As the groundwater is close to the equilibrium with these minerals, the resulting composition does not differ much from the sampled water. Iron concentration is slightly modified by the equilibrium with ferrihydrite, and strontium by the equilibrium with the solid solution. The redox state of the solution is controlled by the Fe^{2+}/Ferrihydrite pair.

Initially, uranium is found as U(VI) and is mainly speciated as carbonate complexes (mainly $UO_2(CO_3)_3^{4-}$). All uranium solid phases are far from saturation. Strontium is found almost completely as Sr^{2+} cation. The more abundant phases in nature, celestite $(SrSO_4)$, and strontianite $(SrCO_3)$ are clearly undersaturated, with saturation indexes (SI) of -4.05 and -3.20, respectively. The relatively low chloride content prevents a significant complexation of Cs, and, therefore, the free species Cs^+ is the dominant one in groundwater.

Initial radionuclide-bearing groundwater composition

The composition of radionuclide-bearing groundwater is rather similar to the original chemistry of the soil pipe SFM0023. It is considered that waters flowing through granitic rocks are in equilibrium with pyrite and calcite, and these equilibria control both the pH and the redox state of the water (Table 5-1).

Radionuclide concentrations have been increased to simulate the influence of a radionuclide plume coming from the repository. Uranium concentration has been fixed at 1.0×10^{-6} M. At this concentration, the solution is clearly oversaturated with crystalline U(IV) phases (uraninite

Table 5-8. Initial composition of till groundwater and deep groundwater in reference case #1. Concentrations of U, Sr and Cs in the deep groundwater have been increased to simulate the addition of radionuclides from the repository. Further explanation of these modified values is given in the following section.

	Till GW	Deep GW
pH	7.15	7.16
Eh(mV)	112	–150
Na	1.23×10^{-3}	6.93×10^{-2}
K	1.23×10^{-4}	1.67×10^{-3}
Ca	2.92×10^{-3}	1.35×10^{-2}
Mg	3.59×10^{-4}	7.18×10^{-3}
C(IV)	5.15×10^{-3}	2.56×10^{-3}
Cl	1.90×10^{-3}	1.07×10^{-1}
SO_4^{2-}	2.41×10^{-4}	3.73×10^{-3}
Si	1.34×10^{-4}	7.56×10^{-5}
Fe_{total}	1.44×10^{-4}	4.91×10^{-4}
Sr	2.72×10^{-7}	9.12×10^{-4} (*)
U	2.05×10^{-8}	1.00×10^{-6} (*)
Cs	6.52×10^{-11}	1.00×10^{-7} (*)
NH_4^+	6.66×10^{-6}	1.95×10^{-4}
PO_4^{3-}	1.39×10^{-7}	3.80×10^{-8}

Concentrations in $mol \cdot L^{-1}$.

(*) Increased concentrations.

and coffinite), and also moderately oversaturated with $UO_2 \cdot 2H_2O$ (SI = 1.74), which are more likely to be the solubility limiting phases. Strontium concentration in the deep groundwater (9.12×10^{-4} M) has been obtained from the equilibrium with the least soluble Sr solid phase (celestite), assuming that it is neither equilibrated with solid solutions nor with exchange surfaces (e.g. clay interlayers).

Finally, an arbitrary concentration of caesium of 1.0×10^{-7} M is set for the radionuclide-enriched deep groundwater, which is several orders of magnitude higher than that of the natural waters. All these radionuclide concentrations are very high taking into consideration that the engineered barriers and geosphere will be able to retain much of the hypothetical radionuclide release, preventing it from accessing the near-surface systems. Nevertheless, as the objective of the simulations is to evaluate the retention capacity of the Quaternary sediments, an extreme scenario has been assumed in this work.

Initial composition of the exchanger

The clay content in the till is usually more than 5 wt%, with illite being the most abundant clay mineral. For modelling purposes, it was considered an illite content of 10 wt%, which leads to a site density of 1.026 moles of sites per dm^{-3}. The total concentration of sites in illite is kept constant during the reactive transport simulations since it is assumed that this mineral does not dissolve (nor precipitate) in the environmental conditions considered in the model. Exchange constants have been implemented following the Gaines-Thomas convention and are shown in Table 5-5.

The composition of the exchangeable sites in the illite in the till at Forsmark is unknown. For this reason, the initial exchanger composition has been considered to be in equilibrium with the reference groundwater. This calculation has been conducted by using the **PHREEQC** code and the initial composition is shown in Table 5-9. From this calculation, the interlayer in the illite in

Table 5-9. Initial composition of the illite interlayer in reference case #1.

Site	Concentration (mol·L$_{water}^{-1}$)
Planar sites	
NaX	3.579×10^{-3}
KX	4.502×10^{-3}
CsX	7.557×10^{-9}
SrX$_2$	3.474×10^{-5}
CaX$_2$	3.757×10^{-1}
MgX$_2$	2.937×10^{-2}
Type II sites	
NaX^{II}	1.511×10^{-2}
KX^{II}	1.901×10^{-1}
CsX^{II}	3.191×10^{-6}
Frayed edge sites (FES)	
NaX^{FES}	5.860×10^{-5}
KX^{FES}	1.470×10^{-3}
CsX^{FES}	3.107×10^{-5}
NH$_4$X^{FES}	1.005×10^{-3}

equilibrium with the reference water is rich in calcium, which is the dominant cation in the illite exchanger, occupying approximately 73% of the total number of exchangeable sites.

On the planar sites, calcium is the dominant cation, occupying approximately 92% of this type of sites, with a concentration of 3.757×10^{-1} mol·L$_{water}^{-1}$. Magnesium is the second most important cation on these sites (occupying approximately 7% of the planar sites). On the planar sites, the magnesium concentration is one order of magnitude lower than that of calcium, while the concentrations of sodium and potassium are two orders lower than the concentration of calcium. Caesium is weakly retained on this type of sites (with a concentration of 7.557×10^{-9} mol·L$_{water}^{-1}$). In contrast, caesium is strongly retained (up to 3.1×10^{-5} mol L$_{water}^{-1}$) on the frayed edge sites ("FES") and "Type II" sites, despite the relative low site density.

On the Type II and frayed edge sites, potassium is the most abundant cation (up to 1.901×10^{-1} mol·L$_{water}^{-1}$ in Type II sites). Interestingly, ammonium is also abundant on the FES (up to 1.0×10^{-3} mol·L$_{water}^{-1}$)

Initial composition of the ferrihydrite surfaces

The initial composition of the ferrihydrite surface in equilibrium with the till system is shown in Table 5-10. The most abundant surface complex is the neutral ≡HFO^{s}OH, although surface carbonate complexes are also significant. Uranium is mainly sorbed as the carbonate complex ≡(HFO^{s}O)$_2$UO$_2$CO$_3^{2-}$ on the high affinity sites. The initial concentration of uranium sorbed is 1.14×10^{-4} mol·L$^{-1}_{water}$, corresponding to a uranium concentration in the till of 2.23×10^{-6} mol·kg$^{-1}_{till}$ if all immobilised uranium in the system is considered to be sorbed onto ferrihydrite.

The U/Fe molar ratios in the till range from 1.5×10^{-5} to 1.5×10^{-4} (Figure 2-15). In the numerical model, an initial ferrihydrite concentration of 0.1 wt% in the till has been considered, which corresponds to 1.1×10^{-2} mol Fe·kg$^{-1}_{till}$. Assuming that most Fe and U are linked to iron oxyhydroxides, which is a realistic approach, the resulting U/Fe molar ratio in the model is 1.98×10^{-4}, which is within the range of U/Fe ratios actually measured in the till.

Table 5-10. Initial concentration of the species adsorbed on ferrihydrite surfaces in reference case #1.

| Site	Concentration (mol·L_{water}^{-1})
Strong sites	
$\equiv HFO^sOH$	5.097×10^{-4}
$\equiv HFO^sOH_2^+$	6.116×10^{-5}
$\equiv HFO^sO^-$	1.019×10^{-5}
$\equiv (HFO^sO)_2UO_2$	6.328×10^{-6}
$\equiv (HFO^sO)_2UO_2CO_3^{2-}$	8.752×10^{-5}
$\equiv HFO^sCO_3H$	1.764×10^{-4}
$\equiv HFO^sCO_3^-$	4.869×10^{-5}
Weak sites	
$\equiv HFO^wOH$	2.760×10^{-1}
$\equiv HFO^wOH_2^+$	3.312×10^{-2}
$\equiv HFO^wO^-$	5.518×10^{-3}
$\equiv (HFO^wO)_2UO_2$	6.682×10^{-7}
$\equiv (HFO^wO)_2UO_2CO_3^{2-}$	3.853×10^{-6}
$\equiv HFO^wCO_3H$	9.556×10^{-2}
$\equiv HFO^wCO_3^-$	2.637×10^{-2}

5.5.2 Reference case #2: The clay system

Hydrogeological initial and boundary conditons

Reference case #2 simulates the water flow and geochemical processes that occur in a clay layer located immediately underneath a surface water body that constitutes a discharge area of the till aquifer, and therefore the flow conditions prescribed for the clay system depend on the flow conditions in the surrounding till aquifer. In order to evaluate the flow directions that occur in such a clay layer, a previous symmetric numerical model with a clay domain located at the right top corner of a till domain was used. In this previous model a shallow groundwater inflow of 14.5 L/d at the left boundary, and a deep groundwater inflow of 0.25 L/d (half of the total deep groundwater flow in reference case #1) was set (Figure 5-9).

After evaluating the flow directions and hydraulic heads attained in the previous numerical model, the final numerical model for the reference case #2 was built. The top boundary of this model is a constant head of 3 m, which represents the discharge area of the clay layer. The groundwater enters from the left and bottom boundaries, as specified by the heads previously computed. The last two nodes on the right side of the bottom boundary correspond to the area in contact with the radionuclide-bearing groundwater (Figure 5-9).

Initial groundwater composition

The redox state of clay porewaters is expected to be controlled by microbial activity. In some lakes similar to those at Forsmark, reducing conditions are indicated by the presence of biogenic pyrite /Percival et al. 2001, Outridge et al. 2005/. Given that a relatively reducing environment in the lake bottom sediments is expected, and that these sediments are relatively rich in quartz and calcite /Hedenström 2004/, the porewater in the clay layer has been considered to
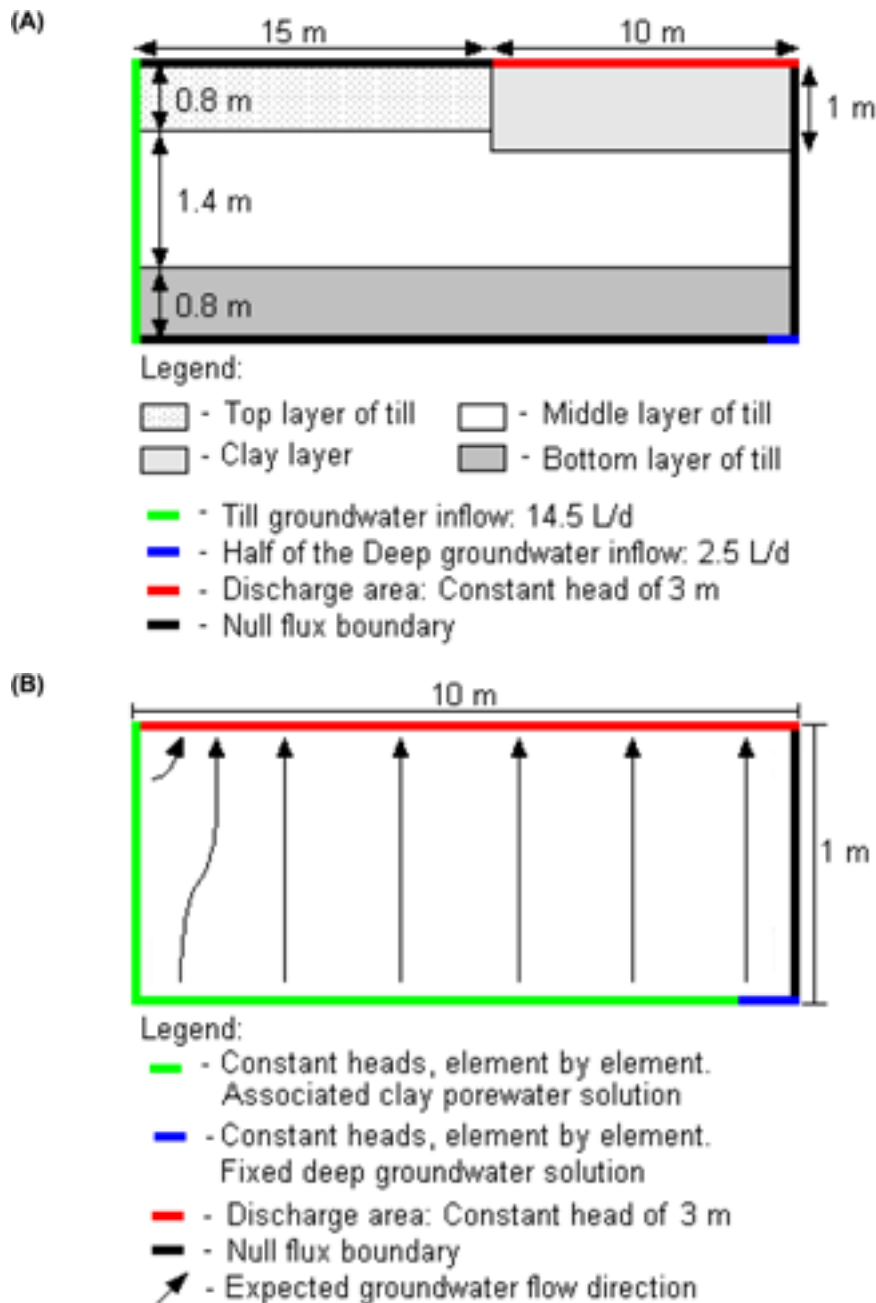
Figure 5-9. *Boundary conditions of (A) a previous numerical model built with a clay layer in the top right corner of a till aquifer, in order to get the prescribed heads for reference case #2, and (B) the numerical model built for reference case #2.*

be in equilibrium with pyrite, quartz and calcite, and therefore the composition of the initial porewater in reference case #2 results from the equilibration of the water sample collected at the bottom of Lake Eckarfjärden in sampling point PFM117 (the composition of which is shown in Table 5-1) with these minerals (Table 5-11). The deep groundwater has the same composition as in reference case #1.

Table 5-11. Initial composition of glacial clay porewater and deep groundwater (which is the same as in reference case #1). Humic acid concentration is 10% of the dissolved organic carbon (DOC) in bottom lake waters.

	Glacial Clay PW	Deep GW
pH	7.64	7.16
Eh(mV)	−210	−150
Na	2.58×10^{-4}	6.93×10^{-2}
K	5.07×10^{-5}	1.67×10^{-3}
Ca	1.12×10^{-3}	1.35×10^{-2}
Mg	1.10×10^{-4}	7.18×10^{-3}
C(IV)	2.43×10^{-3}	2.56×10^{-3}
Cl	1.53×10^{-4}	1.07×10^{-1}
SO_4^{2-}	6.39×10^{-5}	3.73×10^{-3}
Si	1.81×10^{-4}	7.56×10^{-5}
Fe_{total}	8.36×10^{-7}	4.91×10^{-4}
Sr	1.53×10^{-6}	9.12×10^{-4} (*)
U	1.36×10^{-9}	1.00×10^{-6} (*)
Cs	4.40×10^{-11}	1.00×10^{-7} (*)
NH_4^+	1.78×10^{-5}	1.95×10^{-4}
PO_4^{3-}	4.80×10^{-8}	3.80×10^{-8}
Humic acid	1.00×10^{-4} (**)	1.00×10^{-12} (**)

Concentrations in $mol \cdot L^{-1}$.

(*) Increased concentrations.

(**) Arbitrary value.

The presence of organic acids dissolved in the porewater is represented by 1.0×10^{-4} $mol\cdot L^{-1}$ of humic acid. This value corresponds to 10% of the total DOC in the lake bottom porewater. Under the pH and redox conditions of the clay porewater, the U(VI) dominant species are uranium carbonate complexes, namely $UO_2(CO_3)_3^{4-}$ and $UO_2(CO_3)_2^{2-}$. The main humate is the complex formed with Calcium ($CaHumate^+$) representing 97.5% of the dissolved humic.

Initial composition of the exchanger

The modelled domain of the clay system is composed of glacial clays that are rich in illite /Hedenström 2004/, and therefore an illite content of 50 wt% has been considered in the model, which leads to an exchange site density of 1.08 $mol\cdot dm^{-3}$. As in the previous reference case, the total concentration of sites in illite is kept constant during the reactive transport simulations, and the implemented exchange constants follow the Gaines-Thomas convention (Table 5-5). The initial composition of the exchangeable sites in the illite present in the glacial clays has been calculated by equilibrating these exchangeable sites with the glacial clays porewater, using the **PHREEQC** code. The resulting initial exchanger composition is shown in Table 5-12.

The illite exchanger composition resulting from the equilibration of the illite exchangeable sites with the glacial clays porewater may be summarised as follows: (1) the most abundant cation in the illite interlayer is calcium, which occupies 93% of the planar sites, with a concentration of 4×10^{-1} $mol\cdot L_{water}^{-1}$, followed by magnesium (which is the second most abundant cation on the planar sites), with a concentration one order of magnitude lower than that of calcium; (2) on the planar sites, caesium is the least abundant cation, while potassium and sodium and strontium show intermediate concentrations on this type of sites; (3) on the type II sites, potassium is the most abundant cation, while in the FES ammonium is the most abundant cation (Table 5-12). As may be seen in Table 5-12, caesium is most effectively retained on the FES, followed by the type II sites, as expected from the exchange constants given in Table 5-5.

Table 5-12. Initial composition of the illite interlayer in the glacial clay of reference case #2.

Site	Concentration (mol·L_{water}^{-1})
Planar sites	
NaX	1.292×10^{-3}
KX	3.191×10^{-3}
CsX	8.759×10^{-9}
SrX_2	5.970×10^{-4}
CaX_2	4.004×10^{-1}
MgX_2	2.740×10^{-2}
Type II sites	
NaX^{II}	8.404×10^{-3}
KX^{II}	2.076×10^{-1}
CsX^{II}	5.697×10^{-6}
Frayed edge sites (FES)	
NaX^{FES}	1.002×10^{-5}
KX^{FES}	4.940×10^{-4}
CsX^{FES}	1.707×10^{-5}
NH_4X^{FES}	2.179×10^{-3}

5.6   Numerical tool and thermodynamic database

The geochemical simulations have been performed with the reactive transport code **PHAST version 1.3.2** /Parkhurst et al. 2004/. This code is the result of coupling a transport code, **HST3D** /Kipp 1997/ and a geochemical code, **PHREEQC** /Parkhurst and Appelo 1999/. It is able to simulate multi-component, reactive solute transport in three-dimensional saturated groundwater flow systems. A number of boundary conditions are available (specified-head, flux and leakage conditions), and chemical reactions include homogeneous equilibria using an ion-association thermodynamic model, heterogeneous equilibria between the aqueous solution and minerals, gases, surface complexation sites, ion exchange sites, solid solutions, and kinetic reactions.

The reaction transport equations are solved by a sequential iteration approach in which solute transport and chemical reactions are decoupled into separate calculations for each time step. First, the primary species are transported and, then, the outcome of the geochemical reactions occurring in the cell is calculated. The transport and geochemical calculations are evaluated by an iterative approach until prescribed convergence criteria are fulfilled. **PHAST** uses porous media properties and boundary conditions defined by zones for a point-distributed finite-difference grid.

The database used in the present study is an extension of the NAGRA-PSI database, compiled by /Hummel et al. 2002. The extension was made in the frame of the SKB's project SKB-TDB /Duro et al. 2006b/. This database contains a large set of complexation reactions as well as pure mineral equilibrium reactions for many radionuclides and trace elements. Additional Fe(III) carbonate complexes have been added to the database due to the high bicarbonate content of the till groundwaters (see section 5.3.1). Data for humic complexes are not initially included in the database. As explained in section 5.3.2, thermodynamic data for complexation with humic acids was selected from /Choppin and Shanbhag 1981, Li et al. 1980, Shanbhag and Choppin 1981/.

6 Results

6.1 Reference case #1: The till system

6.1.1 Conservative transport

The transport of solutes is affected by the hydraulic gradient and groundwater flow geometry generated from the prescribed boundary conditions. Figure 6-1 shows the groundwater flow directions and hydraulic gradient obtained by the numerical tool. In this figure, it is possible to see that the groundwater entering through the left boundary moves horizontally through most of the domain, and then flows out through the last 20 m of the top boundary where a vertical upward flow is generated.

The conservative transport in reference case #1 has been studied by using chlorine as a tracer, with no retention processes implemented for this element. Initial chloride concentration in the till groundwater is 1.9×10^{-3} mol·L^{-1}, whereas in the deep groundwater [Cl$^-$] is 1.07×10^{-1} mol·L^{-1}. The tracer reaches the discharge area (X = 80 m, Y = 3 m) approximately 5 years after the intrusion of the deep groundwater (Figure 6-2).

Figure 6-3 shows the evolution of the chloride tracer through time. The tracer behaviour is reflecting the contrasting hydraulic conductivities of the till sedimentary layering and the difference between horizontal and vertical hydraulic conductivities. At the beginning of the simulation, the deep groundwater plume moves mainly vertically since the bottom layer of the till is relatively conductive. At longer times, however, the plume is diverted when it reaches the lower-conductivity middle layer.

The plumes generated by the intrusion of the deep groundwater in the modelled domain represent variable degrees of mixing between till and deep groundwaters. These mixtures plot within the range of concentrations measured in the shallow groundwaters in the Forsmark area.
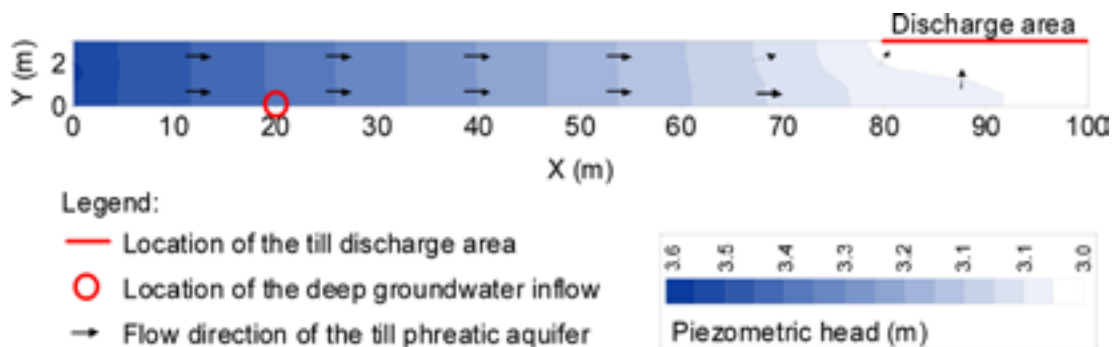
Figure 6-1. *Groundwater flow directions and hydraulic gradient obtained from the numerical tool transport simulation after setting the prescribed boundary conditions.*
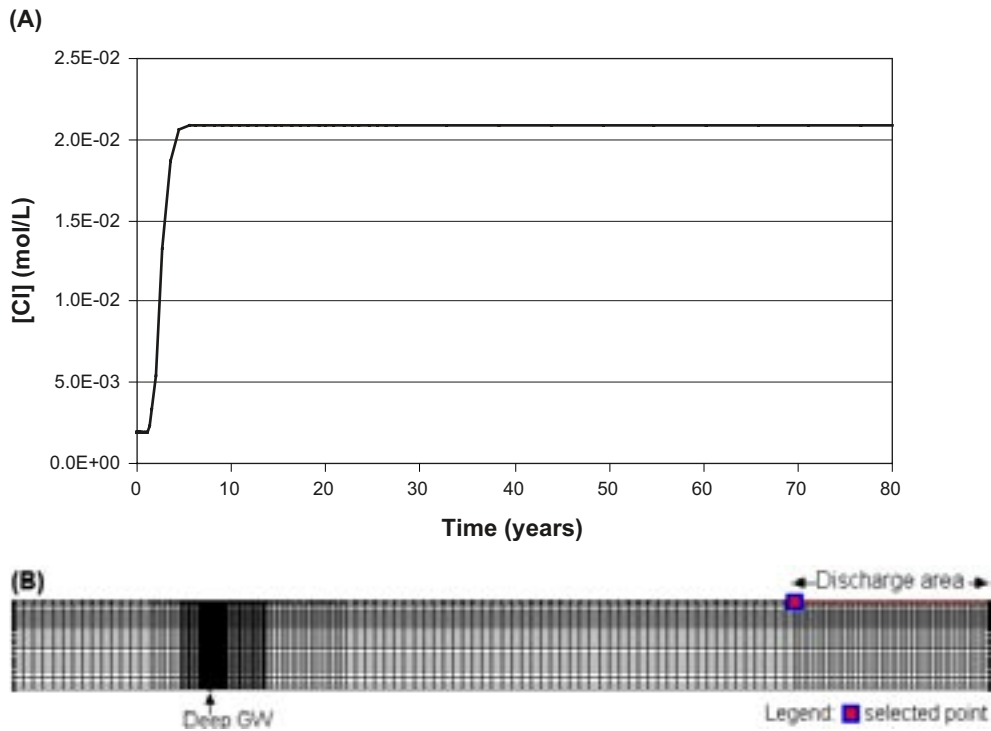
Figure 6-2. *(A) Breakthrough curve of [Cl⁻] in the node X = 80 m, Y = 3 m. The time needed to reach the stationary state of solute transport is approximately 5 years. (B) Location of selected point for the study of the evolution of the outflowing solution.*
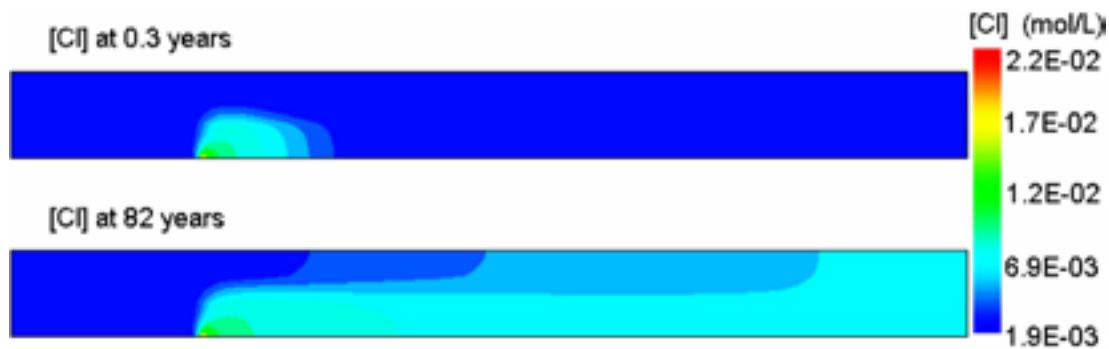
Figure 6-3. *Chloride concentration in the modelled domain through time.*

In Figure 6-4, concentrations of Na-Cl predicted by the numerical simulations at the stationary state (5 years) are plotted together with the concentrations measured in shallow groundwaters in the Lake Bolundsfjärden catchment. It is worth mentioning that Na^+ is a reactive ion as it is affected by cation exchange in illite interlayers. The modelled data plot in the range of the SFM0002 temporal variation, indicating, consequently, that the modelled data show realistic (natural) conditions.
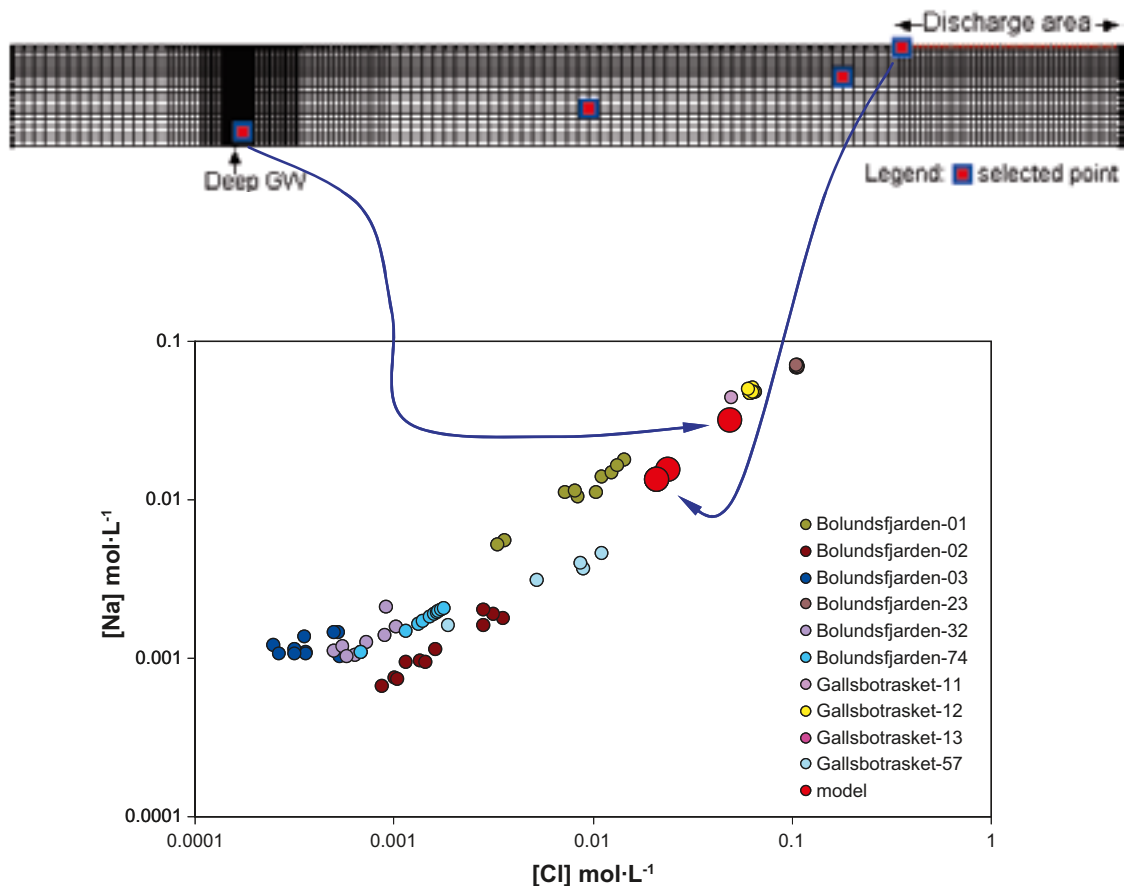
Figure 6-4. *Predicted Na-Cl concentrations in the numerical simulation in reference case #1, along with the compositions of the shallow groundwaters in the Lake Bolundsfjärden catchment.*

6.1.2 Reactive transport

Major ions (Na, Mg, Ca and HCO$_3^-$), pH and redox state

The initial equilibrium of many major constituents of the till groundwater with the solid materials is expected to be disturbed, at least temporarily, by the deep groundwater inflow. pH and Eh of the system are initially controlled by the equilibrium with Sr-bearing calcite and Fe(II)-ferrihydrite, respectively. Numerical calculations predict only slight modifications of the pH (Figure 6-5).

At the beginning of the simulation, pH decreases and a relatively low-pH plume (pH = 6.9) is developed, which quickly vanishes after 6 years. The reason for this initial pH decrease is a slight precipitation of the (Ca,Sr)CO$_3$ solid solution. After a few days, the solid solution dissolves, but at the same time it becomes enriched in Sr (cf below). The pH does not change much, as the precipitation of siderite supplies H$^+$ to the porewater compensating the dissolution of the Sr-bearing calcite (Figure 6-6). This precipitation is triggered by the inflow of deep groundwater with a much lower redox potential, leading to ferrihydrite dissolution and release of Fe^{2+} to the porewater.

The evolution of the redox potential is comparable to that of pH. The initial increase is caused by pH changes and subsequent siderite precipitation (Figure 6-7).
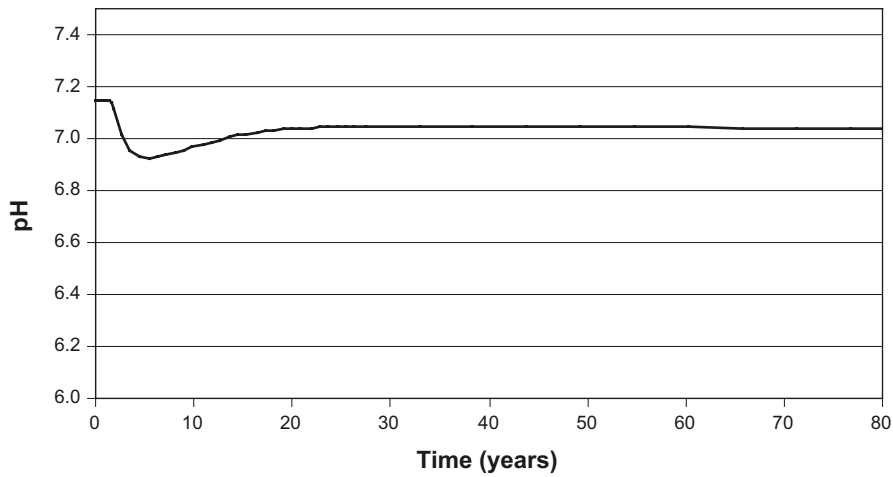
Figure 6-5. Evolution of pH in the discharge area (node located at X = 80 m and Y = 3 m). A slight pH decrease is seen at the beginning of the simulation time. After this first disturbance, the geochemical processes occurring in the modelled domain reach a new equilibrium.


Figure 6-6. Total moles of siderite precipitated after 82 years.
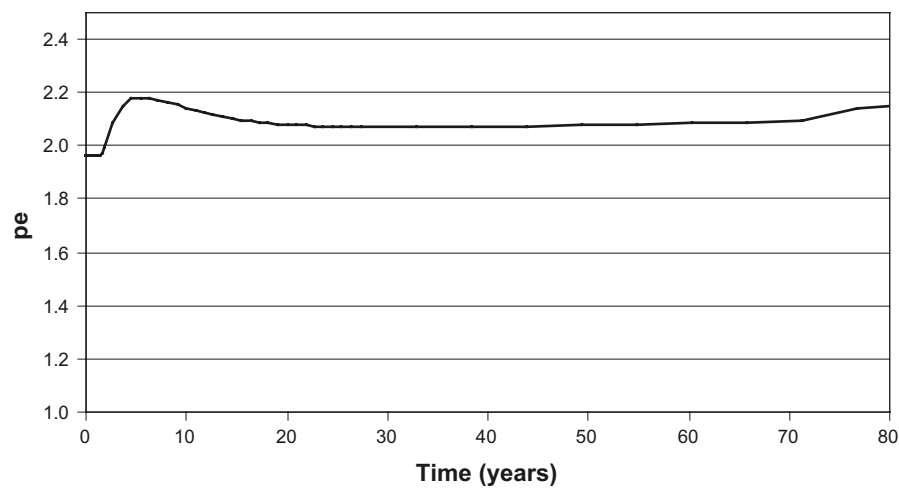

Figure 6-7. Evolution of pe (= Eh in mV/59.16) through time.

The transient pH decrease is buffered by the dissolution of $(Ca,Sr)CO_3$ solid solution leading to an increase of the calcium concentration in the till porewater. In addition to carbonate mineral dissolution, other geochemical processes can contribute to the increase of the aqueous calcium concentration, such as the cation exchange in the illite interlayer. The amount of sites occupied by calcium in illite decreases due to the Mg- and Sr-enrichment of the planar sites (Figure 6-8). This change in the interlayer composition is caused by the relative concentrations of Mg, Sr and Ca in the till porewater and in the deep groundwater.

Even though the inflow of deep groundwater is able to modify temporarily the calcium carbonate system, calcium and carbonate ion concentrations have not changed much at the end of the simulation period. Both ions plot in the range of shallow groundwater compositions in the Forsmark area (Figure 6-9).
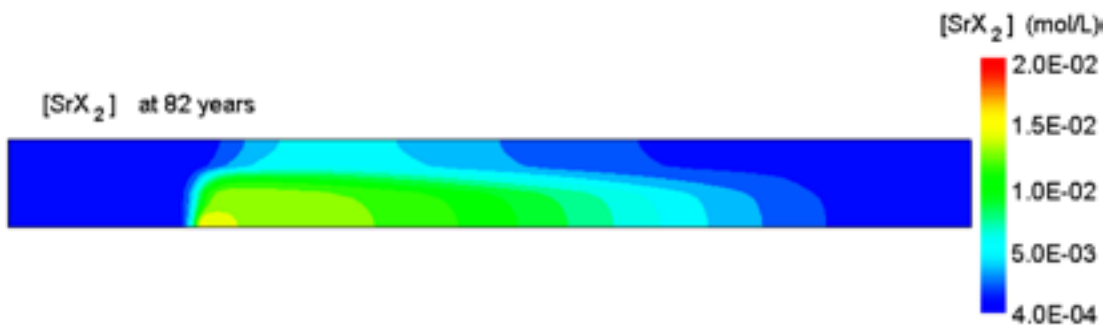
Figure 6-8. *Strontium concentration (mol·L^{-1}) of the illite interlayer at the end of the simulation period (after 82 years).*
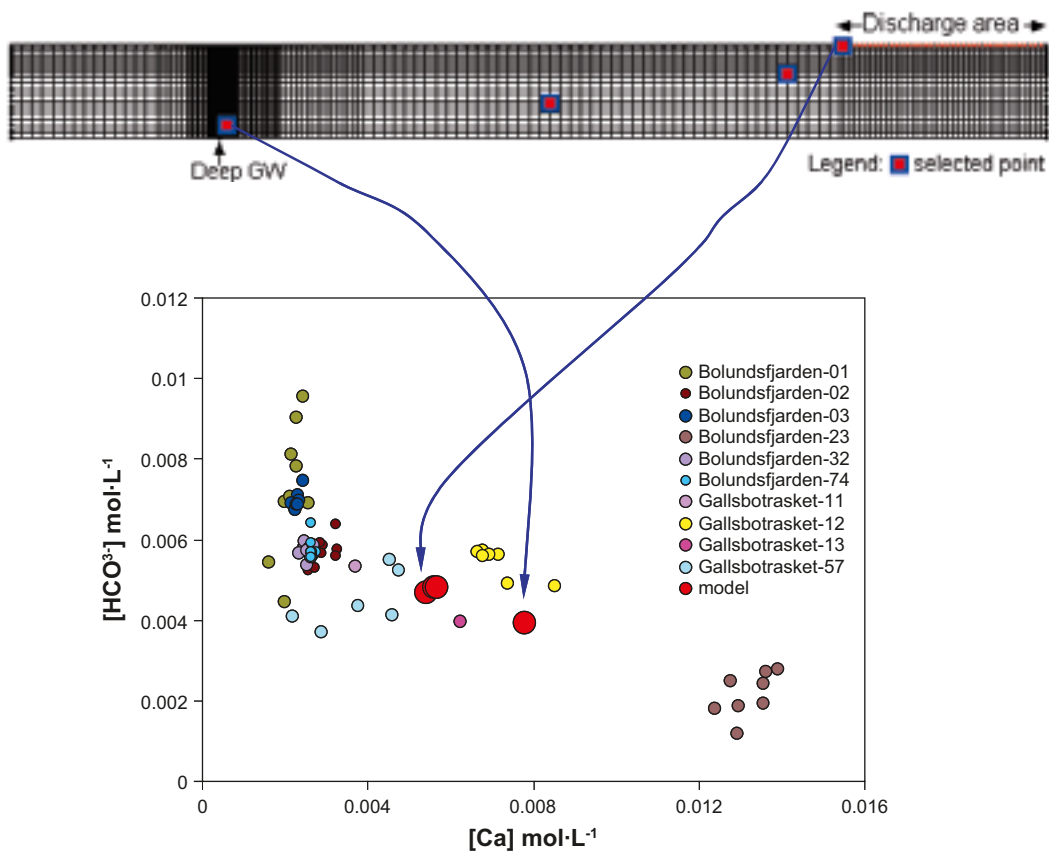
Figure 6-9. *Predicted Ca-HCO$_3^-$ concentrations in the numerical simulation in the reference case #1, along with the compositions of the shallow groundwaters in the Lake Bolundsfjärden catchment.*

Strontium

In the description of the geochemical processes (section 5.3), it is stated that the reactive transport calculations are done considering non-ideal solid solutions. However, the initial calculations perfomed showed that it was computationally very expensive to attain numerical convergence for the non-ideal solid solution. Very short time steps were required due to the strong non-linearity introduced by the non-ideal solid solution formulation.

For this reason, we faced the solid solution problem by considering an ideal solid solution. This approach resulted in a unrealistic strontium molar fractions in the solid solution, far above the miscibility limit reported for natural $(Ca,Sr)CO_3$ solid solution ($\chi_{Sr} = 3 \times 10^{-3}$, Figure 6-10). Consequently, we decided to improve the time discretisation in order to be able to consider a non-ideal behaviour of the solid solution.

When a non-ideal solid solution is considered, the till retention capacity is significantly reduced, because the solid solution is not capable of incorporating an unlimited amount of strontium, as observed in the ideal behaviour. The retention capacity of the till system is, actually, a combined effect of two processes: cation exchange in illite and strontium incorporation into $(Ca,Sr)CO_3$ solid solution.

According to the model results (considering non-ideal solid solutions), the illite exchanger becomes progressively enriched in strontium (Figure 6-11). The re-equilibrium of the exchange interlayer to the new conditions leads to a depletion of CaX_2 in the planar sites, being substituted by other divalent cations, mainly Mg^{2+} and, to a minor extent, Sr^{2+}.

On the other hand, $(Ca,Sr)CO_3$ solid solutions show an increase of the molar fraction of strontium, reaching values slightly lower than the maximum Sr content in this solid solution series limited by the miscibility gap ($\chi_{Sr} = 3 \times 10^{-3}$, Figure 6-12). Although there is an enrichment of Sr in the solid solution (limited by the miscibility gap), the overall solid solution dissolves. This leads to release of strontium to the aqueous phase (see Figure 6-20 below). Part of the dissolved moles precipitate back as a new solid solution which is richer in strontium, but most Sr initially present in the solid phase is dissolved. This is the reason for the increase of [Sr] compared with the conservative species (see next section).
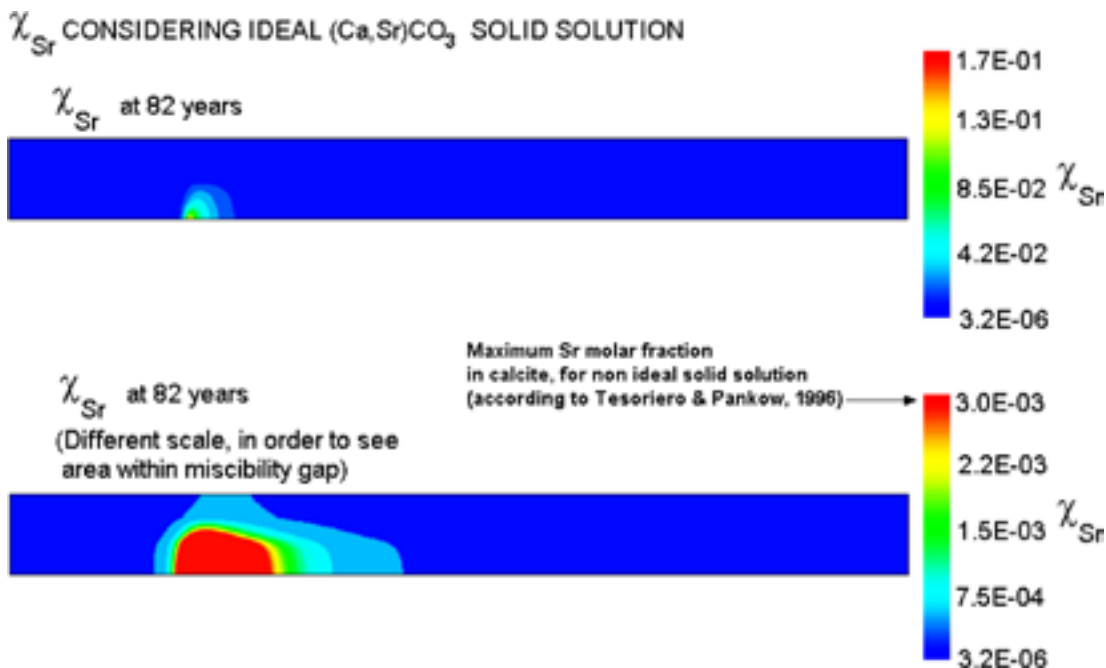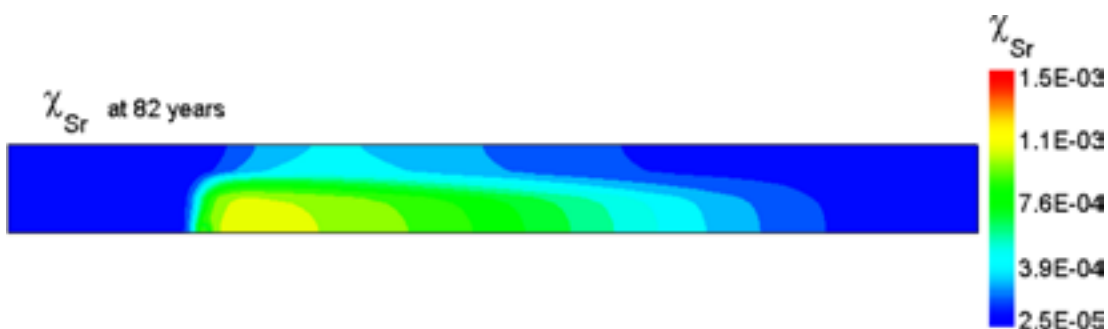

Figure 6-10. Molar fraction of Sr in the $(Ca,Sr)CO_3$ ideal solid solution. The predicted compositions of the solid solutions in the vicinity of the source of the deep groundwater are considered unrealistic.
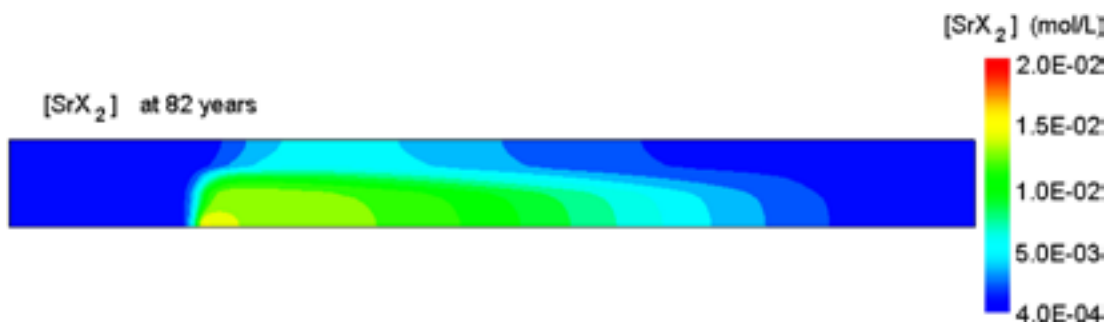
Figure 6-11. *Predicted concentration of strontium in the illite exchanger at the end of the simulation time (82 years).*

Figure 6-12. *Molar fraction of the strontianite end-member in the (Ca,Sr)CO₃ solid solution, at the end of the simulation period (82 years).*

Figure 6-13 shows the evolution of the concentration of aqueous strontium in the discharge area. The initial increase is related to the establishment of the transport steady state. The subsequent drop is reflecting the retention of strontium in the illite exchanger. From 50 years until the end of the simulation time, the aqueous strontium concentration increases in response to the release of this element from the solid solution. The overall effect of strontium release is a consequence of the reactive transport transient state triggered by the deep groundwater source.
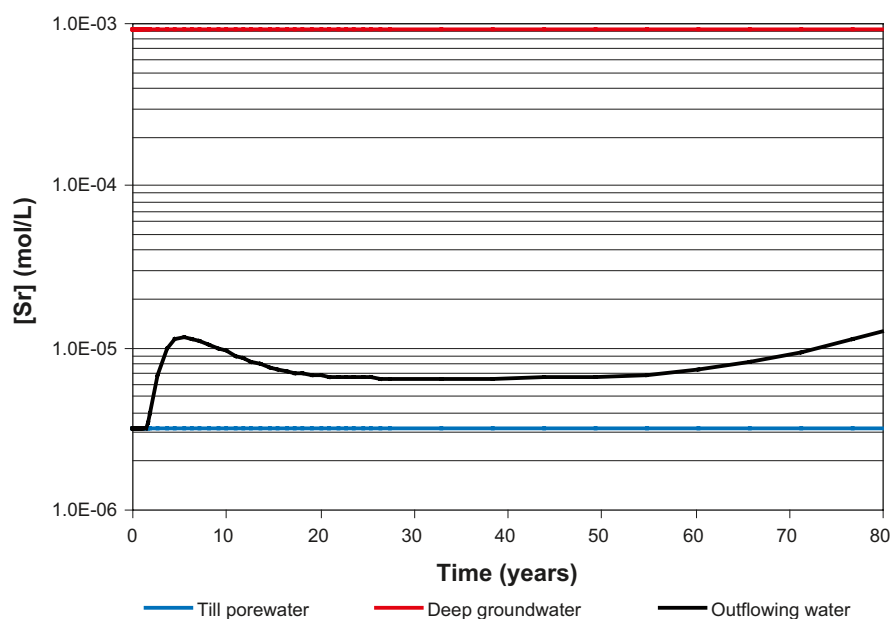
Figure 6-13. *Evolution of the concentration of aqueous strontium in the discharge area, during the reactive transport simulation of the till system (selected observation point located as in image B of Figure 6-2).*

Caesium

The reactive transport simulations predict that caesium is readily retained in the till due to the very high affinity of this element to the FES in the illite interlayer. This process occurs very close to the fracture, where the FES buffer the [Cs⁻] (Figure 6-14). Despite the high caesium concentration in the deep fluid (1.0×10^{-7} M), the concentration of this element in the modelled domain after 80 years has not increased much (see Figure 6-19).

Figure 6-15 shows the time evolution of the caesium aqueous concentration in the discharge area, compared to the initial caesium aqueous concentrations in both the till porewater and in the deep groundwater. In the discharge area (Figure 6-15) the concentration of caesium in the outflowing water is far from the concentration of this radionuclide in the deep groundwater, reflecting the potential of the geochemical processes to retard the transport of this radionuclide in the till between the rock and the discharge area.

Figure 6-14. *Concentration of Cs⁺ in the FES, at the end of the simulation period (82 years).*
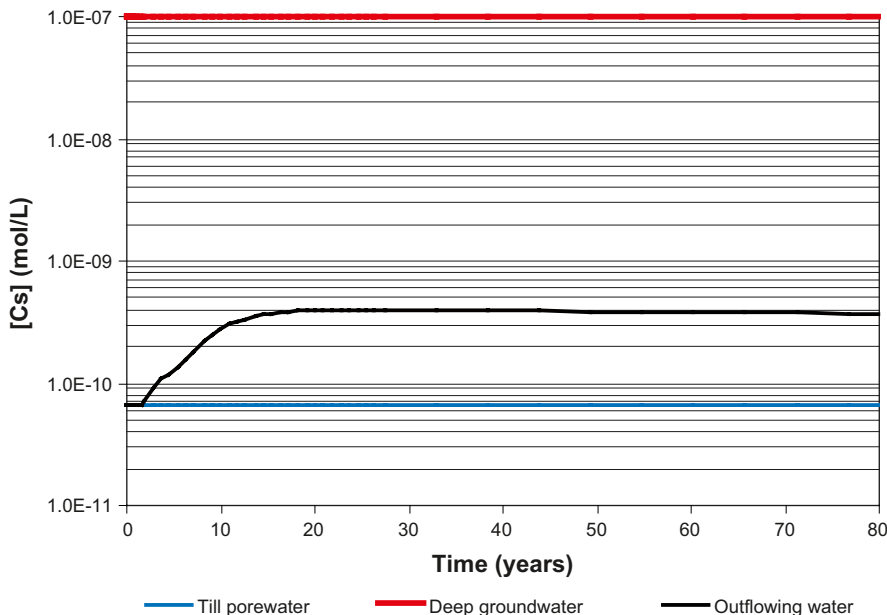

Figure 6-15. *Evolution of the concentration of aqueous caesium at the discharge area, during the reactive transport simulation in the till system (selected observation point located as in image B of Figure 6-2).*

Uranium

The uranium retention predicted in the numerical calculations indicates the relevance of adsorption of uranium on ferrihydrite (Figure 6-16). Evolution of the uranium concentration in the domain shows that [U] does not significantly increase with respect to the initial concentrations (Figure 6-17 and Figure 6-20). The initial decrease of the aqueous uranium concentration to values lower than the initial concentration in the till system (Figure 6-17) is reflecting the effective adsorption of uranium carbonate complexes on the ferrihydrite surface as a response of the deep groundwater intrusion.

On the other hand, no uranium is retained via precipitation of pure solid phases. The till porewater does not reach the saturation in any of the minerals considered in the model. U(IV) minerals are strongly subsaturated since the redox state in the domain is relatively oxidising, whereas the concentration of uranium is not high enough to allow the precipitation of U(VI) minerals.

Figure 6-16. *Predicted content of $UO_2CO_3^{2-}$ adsorbed on the ferrihydrite surface ($\equiv(HFO^sO)_2UO_2CO_3^{2-}$) after 82 years.*

Figure 6-17. *Evolution of the concentration of aqueous uranium in the discharge area, during the reactive transport simulation in the till system (selected observation point located as in image B of Figure 6-2).*
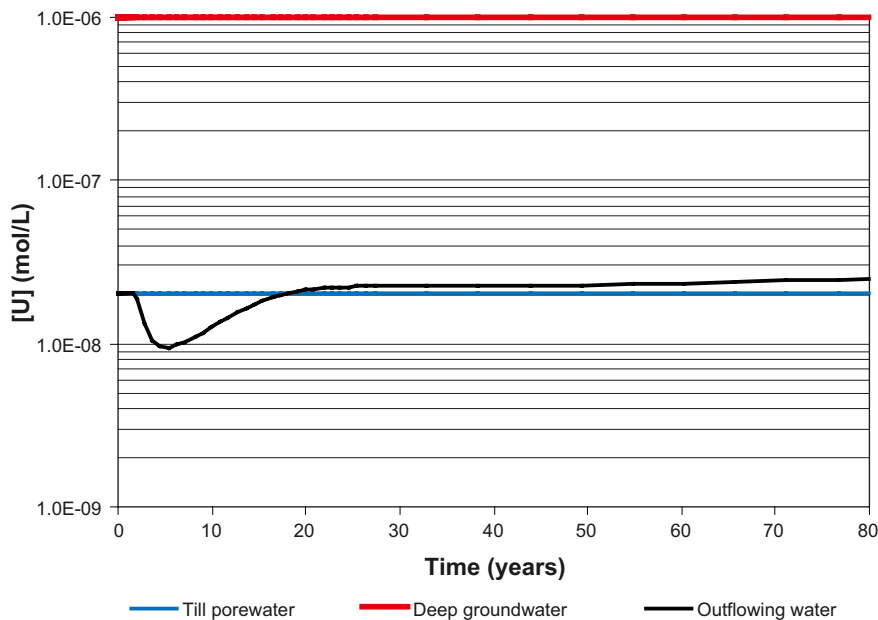
6.1.3 Conservative transport versus reactive transport

The geochemical processes considered to occur in the till system are able to effectively retain uranium and caesium, retarding their migration in the modelled domain. After the 82 years of reactive transport simulation time, the concentrations of U and Cs in the model domain are much lower than those observed that would be obtained in absence of retention, see Figure 6-18 and Figure 6-19. In these figures, the results of reactive transport modelling are compared with hypothetical corresponding cases of conservative transport; these are similar to the reactive cases, e.g. in terms of input concentrations, except that the retention processes are inactive.

For strontium, the dissolution of the solid solution leads to the release of strontium in the aqueous phase and to the increase of the [Sr] compared with the conservative behaviour (Figure 6-20).

Figure 6-18. *Comparison between the predicted uranium concentration in the modelled domain in reference case #1 and in the corresponding conservative case.*

Figure 6-19. *Comparison between the predicted caesium concentration in the modelled domain in reference case #1 and in the corresponding conservative case. Only a very small area near the source is affected in the reactive case.*
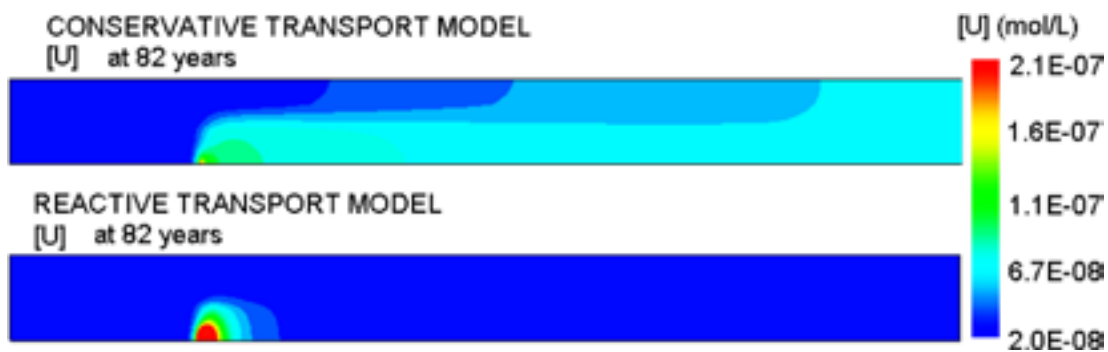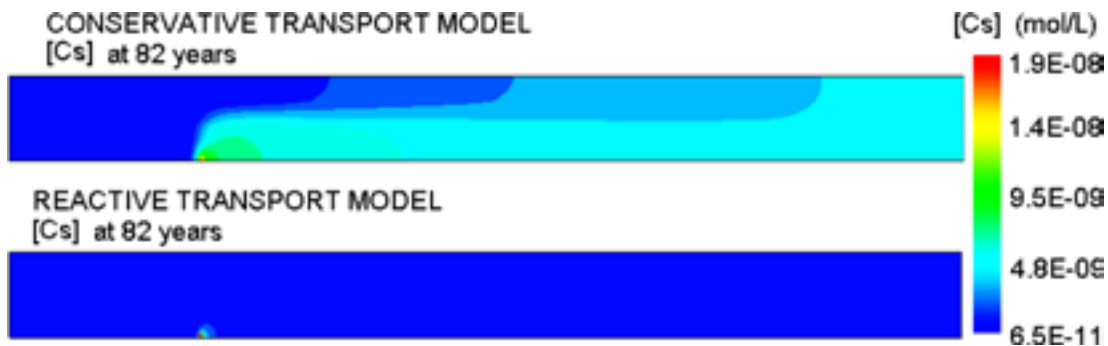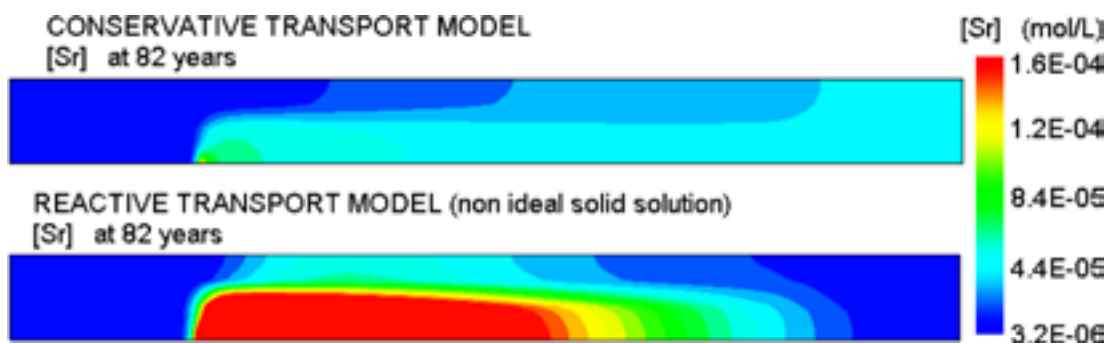

Figure 6-20. *Comparison between the predicted strontium concentration in the modelled domain in reference case #1 and in the corresponding conservative case.*

6.1.4 Quantitative assessment of the retention efficiency of the till system

The efficiency of the near-surface Quaternary system for radionuclide retention can be quantitatively evaluated by comparison of the computed conservative and reactive transport results. In the present case, the efficiency of the system will be assessed in the observation point shown in Figure 6-21, which corresponds to the point where the most rapid arrival of deep contaminants to the surface can be expected.

A relative (dimensionless) conservative concentration (C) can be defined at any point in the domain as:

$$C^\tau = \frac{(r)^\tau_c}{(r)^{ss}_c}$$

where (r) is concentration of a given radionuclide in the observation point, subscript c denotes conservative calculations, superscript τ and ss denote a given observation time and the time needed to reach the transport steady-state, respectively.

Similarly, a relative (dimensionless) reactive concentration (R) can be defined as:

$$R^\tau = \frac{(r)^\tau}{(r)^{ss}_c}$$

It should be noticed that the radionuclide concentration in the numerator corresponds to the computed results with the reactive model.

The radionuclide retention efficiency (E) of the system at a given time (τ) and a specific point can be quantitatively evaluated according to:

$$E^\tau = 100\left(1 - \frac{R^\tau}{C^\tau}\right)$$

According to this expression, a null relative reactive concentration (R) at a given time (τ) means that no mass of radionuclide is leaving the system at that time, resulting in a retention efficiency of 100%. On the other hand, a relative reactive concentration (R) equals to the relative conservative concentration means that no retention is occurring such that the corresponding retention efficiency would be 0%. Figure 6-21 shows the time evolution of retention efficiencies of the system computed for strontium, caesium and uranium.
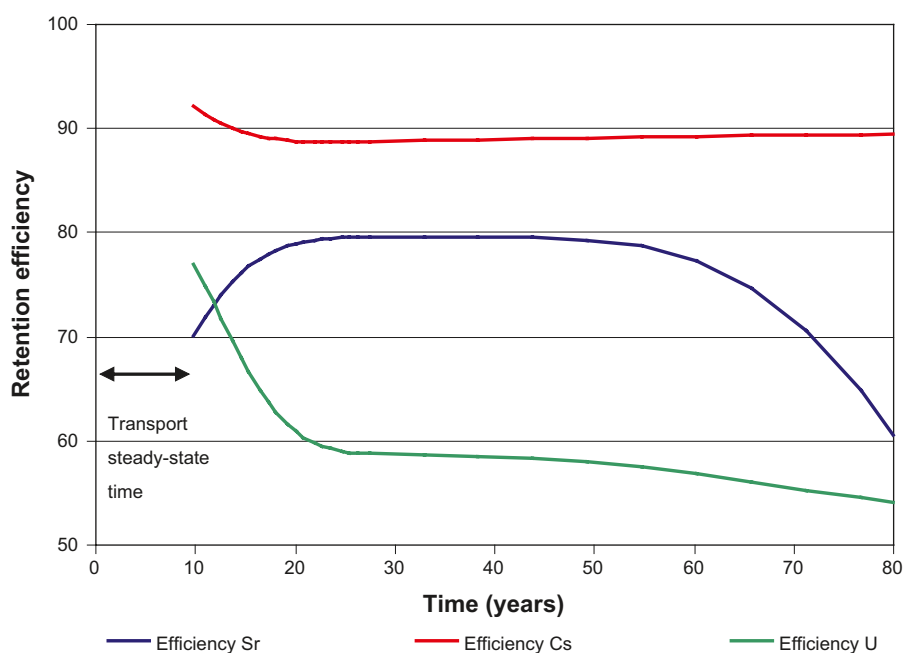

Figure 6-21. *Computed retention efficiencies for strontium, caesium and uranium.*

Figure 6-21 shows that computed retention efficiencies of the system are different for the 3 radionuclides considered. The till system exhibits a very high efficiency for retention of caesium (about 90%). After a short initial decrease, the efficiency of the system to retain caesium shows a slight but constant increase with time. This behaviour is due to the fact that caesium is very strongly absorbed into the illite interlayers, and the caesium plume moves very slowly within the aquifer. Then, the system still has the capacity to retain much more caesium as the slowly moving plume gets in contact with more aquifer material.

The behaviour of uranium is different. The till system shows a decrease of the retention efficiency with time, with different slopes in the time evolution pattern (Figure 6-21). The main process responsible for uranium retention is surface adsorption onto ferrihydrite. The different slopes of the retention efficiency pattern are reflecting the coupled effect of the saturation of the four different adsorption sites considered in the model, integrated in one observation point. The large initial decrease of retention efficiency is due to the fact that the chemical disequilibrium produced by the inflowing deep water during the time needed to reach the transport steady-state triggered the adsorption of a large amount of uranium.

This large amount of uranium adsorption is caused by the large natural amount of uranium in the till water. When steady-state transport is reached, the adsorption capacity of the system is reduced and, consequently, the retention efficiency of the system decreases. It is worth mentioning that the uranium retention capacity of the system remains higher than 50% after 80 years of simulation, and the final decreasing slope is very small (Figure 6-21).

Finally, the time evolution of the efficiency for strontium retention is reflecting a complex coupling between transport and the two different mechanisms for retention considered in the model. It can be seen in Figure 6-21 that the initial efficiency of the system increases as a result of the migration of the aqueous strontium plume. This is because a larger influence area (i.e. longer transport distances) implies a larger total retention capacity of the domain due to both solid solution and cation exchange processes.

A pseudo-equilibrium is temporarily attained in the system efficiency of strontium retention. After about 50 years, the dominating retention process is cation exchange. The illite interlayers of the till system could be progressively saturated, and strontium starts to be released due to dissolution of the solid solution. This results in a constant and pronounced decrease of the retention efficiency for strontium. At the end of the simulation time, the retention efficiency of the till system is still 60% for strontium. However, unlike the observed behaviour in the uranium case, the efficiency of the till system to retain strontium decreases at a high rate (c 1% per year) during the last part of the simulation time period (Figure 6-21).

6.2   Reference case #2: The clay system

6.2.1   Conservative transport

The groundwater flow directions and hydraulic gradients computed with the numerical model constitute the main physical driving force for the migration of radionuclides within the clay layers. As explained in section 5.5.2, the boundary conditions prescribed for reference case #2 were defined according to the heads obtained in a preliminary hydrogeological model that accounts for a layer of clay located immediately underneath the discharge area at the right top boundary of the till aquifer.

The preliminary hydrogeological model (picture A from Figure 6-22) reveals that the subhorizontal flow directions of the till aquifer tend to be subvertical near the discharge area, and are diverted close to the clay layer due to its low permeability. Since the groundwater has to pass through the clay layer to flow out from the modelled domain, it is established an upward vertical flow underneath and within the clay layer. The effect of the low permeability clay layer is clearly reflected by the high hydraulic gradients computed under the discharge area.

It is worth noting that a hydraulic "artefact" is produced in the left inflow boundary as a result of prescribing a constant flow rate in a layer system with different permeabilities. This produces local vertical flows between the three layers. However, such a flow distortion is equilibrated further away and do not affect the surroundings of the clay. It must be kept in mind that the objective of the preliminary hydrogeological model was to generate sound hydrogeological boundary conditions for the detailed reactive transport model of the clay system. In this way, the clay layer can be isolated and numerically optimized for reactive transport calculation purposes. This is why preliminary hydrogeological model results are perfectly valid both in terms of flow rates and heads in the clay surroundings, irrespectively of the details of the hydraulic conditions at the left boundary.

Figure 6-22 (Image B) shows the flow field computed with the isolated model of the clay by prescribing the flow boundary conditions previously computed with the preliminary hydrogeological model. In this figure it is possible to see that the flow directions are mainly vertical and upward. This flow conditions will be applied to the optimized reactive transport numerical model built for the reference case #2.

The conservative transport in reference case #2 has been studied using chloride as a tracer, since no retention processes have been implemented for this ion. The initial chloride concentration in the clay porewater is 1.5×10^{-4} mol·L^{-1}, whereas in the deep groundwater [Cl$^-$] is 1.07×10^{-1} mol·L^{-1}.
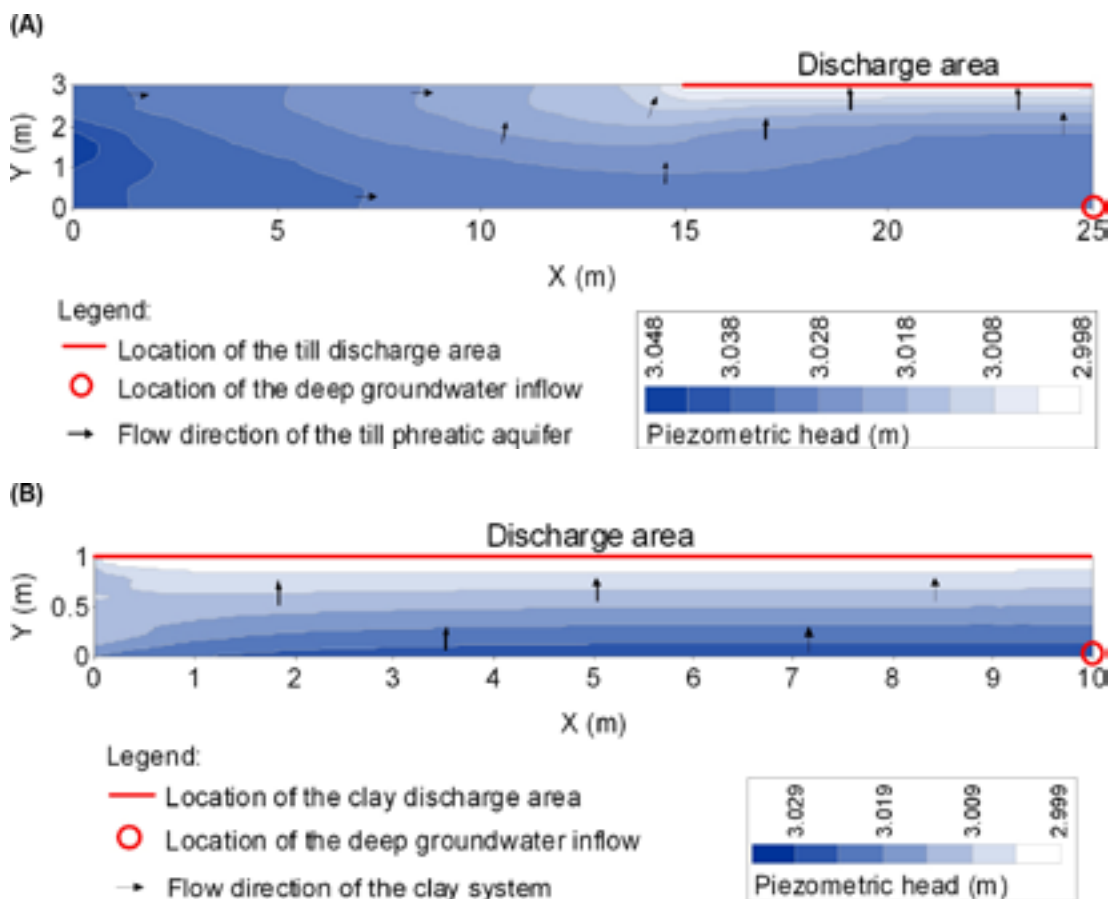
Figure 6-22. Groundwater flow directions and hydraulic gradients obtained from the numerical flow and transport simulation after setting the prescribed boundary conditions. A: Preliminary hydrogeological model composed of till and a 1 m thick clay layer underneath the discharge area; B: Detailed numerical model for reference case #2 (only the clay layer), using the previously computed boundary conditions.
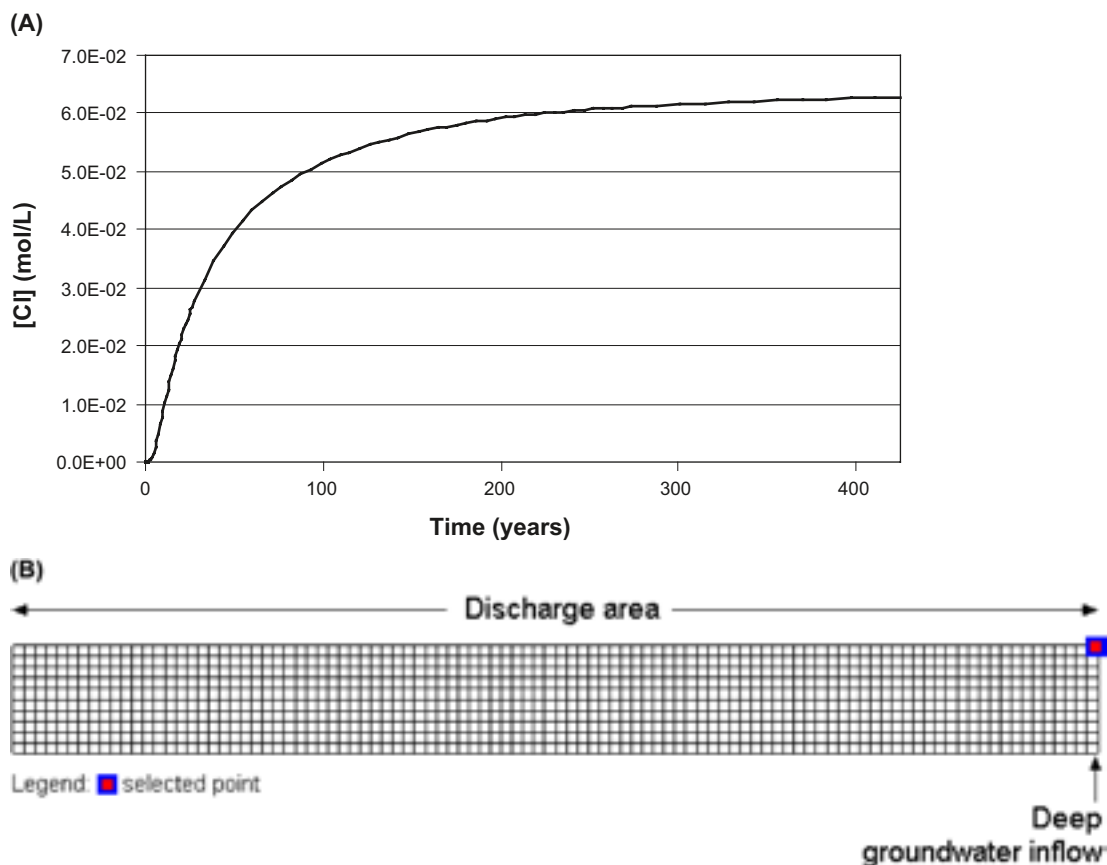
Figure 6-23 shows the evolution of chloride concentration at the top boundary. It can be seen that a conservative transport pseudo-steady state is reached in about 200 years. It is worth noting that the time needed to reach the transport steady state is much longer than in the previous reference case #1. The specific times needed to reach the transport steady state in each model reflect the contrasting hydrogeological media of each reference case. The first model simulates a relatively permeable medium (the till aquifer), with average porewater velocities on the order of 10^{-2} m·d^{-1}, while the second model simulates a low permeability medium (clay) with average porewater velocities of about 10^{-5} m·d^{-1}.

Figure 6-24 shows the evolution of the conservative chloride plume along the time. After 400 years the chloride plume reaches a pseudo-steady state. As it was expected, the quasi-concentric pattern of the computed concentration isolines indicates that molecular diffusion is a relevant transport process in this low permeability medium.

6.2.2 Reactive transport

Major ions (Na, Mg, Ca and HCO$_3^-$), pH and redox state

The initial equilibrium of the major constituents of the glacial clay porewater with the clayey sediments will be disturbed by the deep groundwater inflow. pH and Eh of the clay porewater are initially controlled by the equilibrium with $(Ca,Sr)CO_3$ solid solutions, siderite and pyrite.

Figure 6-23. *(A) Breakthrough curve of chloride concentration in an observation point located at the discharge area. (B) Location of selected observation point for the study of the evolution of the outflowing solution.*

Figure 6-24. *Evolution of the chlorine concentration in the modelled domain of the clay system. From 200 years until the end of the simulation time the chlorine plume does not change much, meaning that the transport steady state is reached.*

In the reactive transport model, the intrusion of a deep groundwater with a higher iron concentration ($[Fe_{TOT}] = 4.9 \times 10^{-4}$ mol L^{-1}) than the clay porewater ($[Fe_{TOT}] = 8.4 \times 10^{-7}$ mol L^{-1}) and a less reducing pe, triggers the precipitation of siderite in the vicinity of the deep groundwater inflow boundary (Figure 6-25), which leads to the decrease of pH from the beginning of the simulation till approximately 45 years (Figure 6-26). From this moment on, the other geochemical processes that occur in the domain and affect pH, namely the equilibrium with $(Ca,Sr)CO_3$ solid solution, drive the system towards a new equilibrium.

The redox state of the modelled domain is also disturbed by the intrusion of the deep groundwater inflow (Figure 6-27). The evolution of the redox potential is comparable to the pH evolution, reflecting their interdependency, and the participation of both H^+ and electrons when siderite precipitates. The first pe increase is mainly due to the intrusion of a less reducing deep groundwater concomitant to siderite precipitation, as a response to the intrusion. The smooth pe decrease from approximately 45 years until the end of the simulation reflects the evolution of the hydrogeochemical system towards a new equilibrium.

The intrusion of the deep groundwater leads to an increment of calcium, magnesium and sodium aqueous concentrations in the affected area, with a simultaneous increase of magnesium, sodium and strontium concentrations in the planar sites of the illite interlayer. At the same time, the calcium concentration on these sites is reduced.
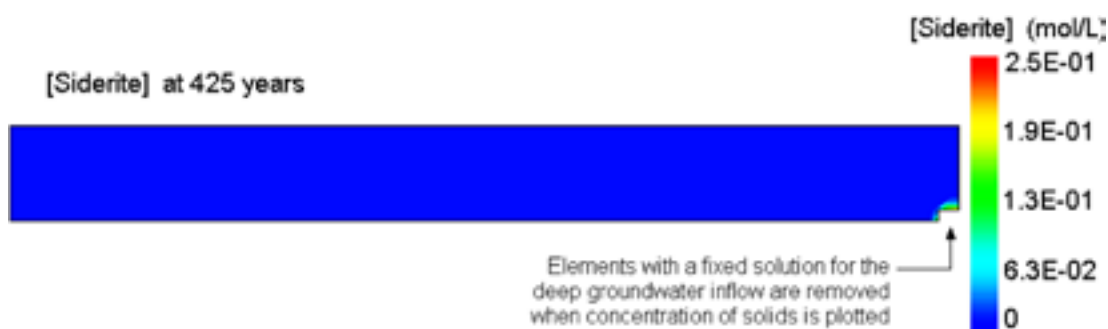
Figure 6-25. *Total moles of $FeCO_3$ precipitated close to the deep groundwater inflow, after 425 years.*
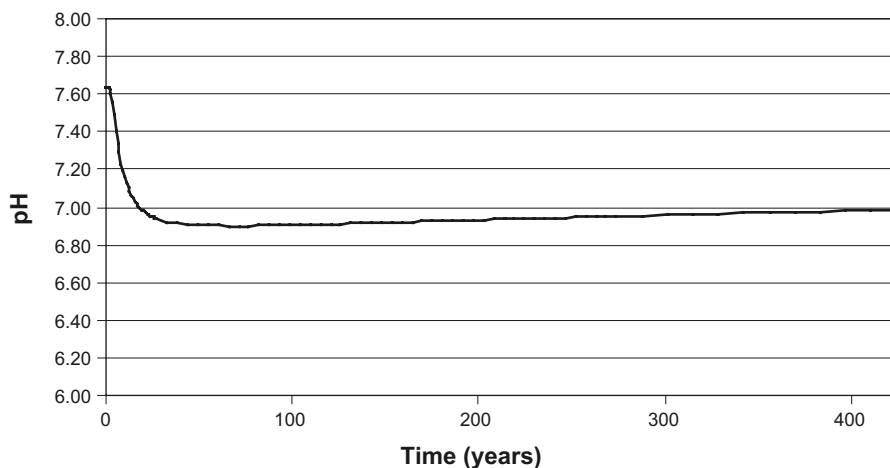
Figure 6-26. *pH evolution in the clay system during the simulation period. A visible decrease is predicted in this parameter, likely caused by siderite precipitation.*
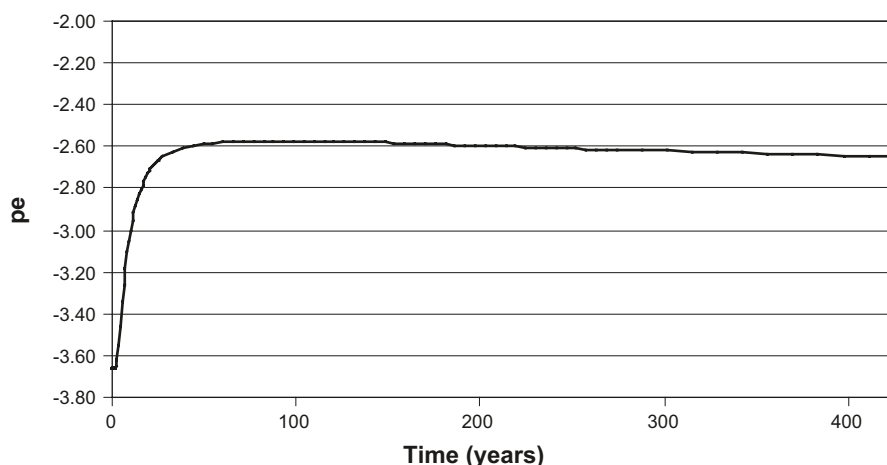
Figure 6-27. *Evolution of the redox state of the system through the simulation time (in terms of pe = Eh in mV/59.16).*

Strontium

The reactive transport simulation of the clay system predicts a significant retention of Sr in the planar sites of the illite interlayer which is compensated by a calcium depletion of these sites (Figure 6-28). A considerable increase of the Sr molar fraction in the $(Ca,Sr)CO_3$ solid solution can also be seen. This is due to the increment of aqueous strontium, as a consequence of the deep groundwater intrusion (Figure 6-28). The increment of the strontium molar fraction does not exceed the miscibility limit of 3×10^{-3} in the non ideal solid solution. Both processes, cation exchange and precipitation of solid solution with a higher Sr/Ca ratio, will contribute to the attenuation of strontium speading in the clay system.

Figure 6-29 shows the time evolution of the strontium aqueous concentration in the discharge area, compared to the initial strontium aqueous concentrations in both the clay porewater and in the deep groundwater. At the beginning of the simulation period, the concentration of strontium in the discharge area (selected point of image B from Figure 6-23) increases at a higher rate than at the end of the simulation period, reflecting the role of the geochemical processes that reduce strontium mobility (Figure 6-29).

78
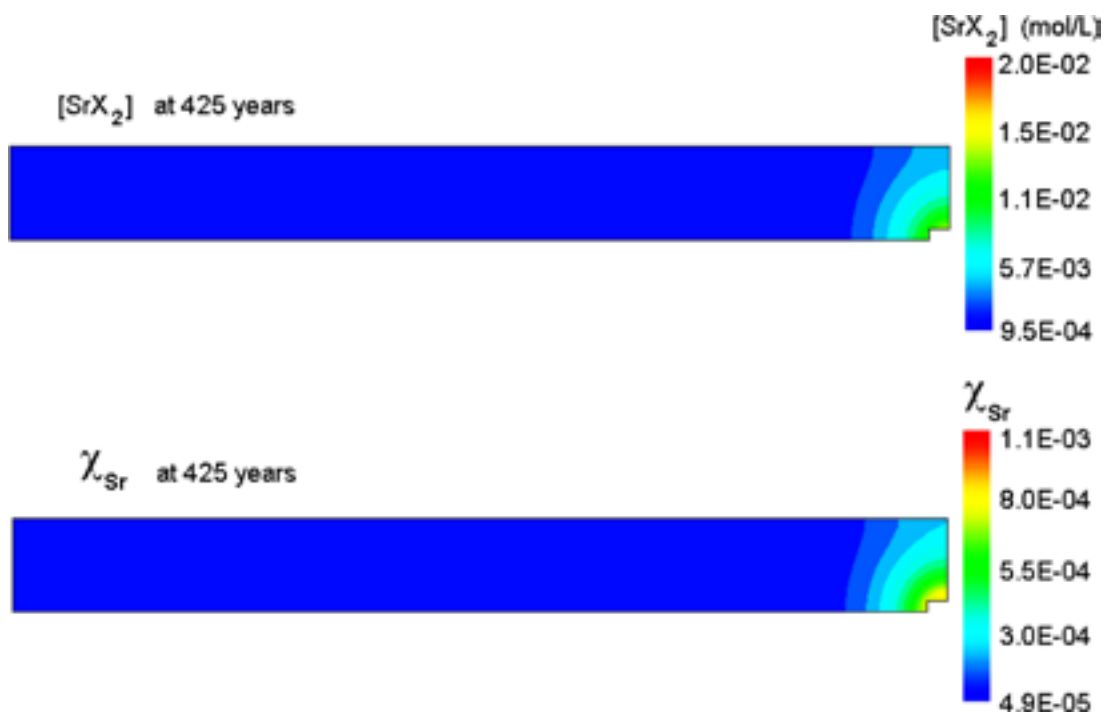
Figure 6-28. Strontium concentration in the planar sites of the illite interlayer, and strontium molar fraction in the (Ca,Sr)CO₃ solid solution, at the end of the 425-year simulation period.
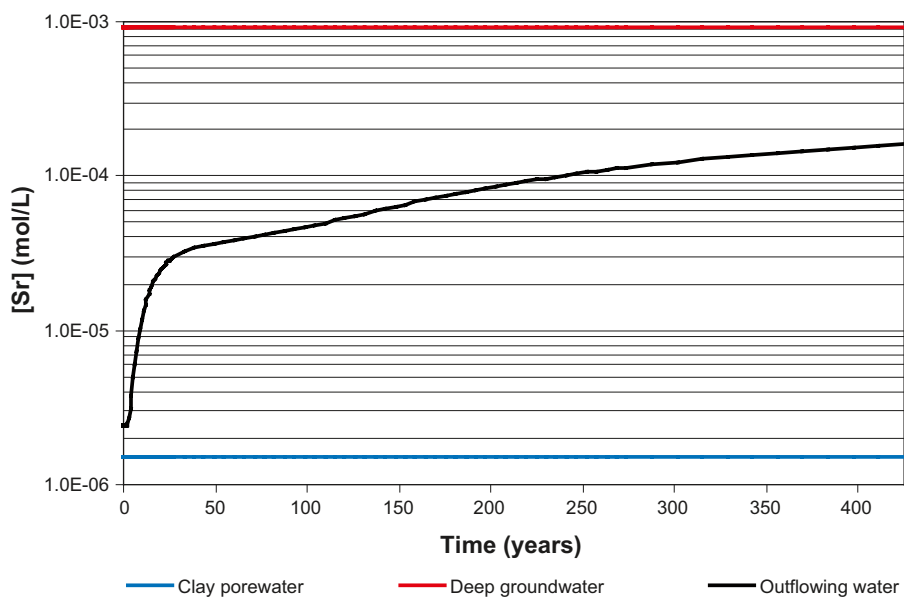
Figure 6-29. Evolution of the concentration of aqueous strontium in the discharge area, during the reactive transport simulation (selected observation point shown in image B of Figure 6-23).

Caesium

The main process retaining caesium is the sorption on the illite interlayer, namely in the FES, where its concentration increases during the simulation period (Figure 6-30). Simultaneously, the concentration of ammonium, which competes with caesium for the same sites, decreases in the exchanger.

Figure 6-30. *Concentration of caesium in the FES of the illite interlayer at the end of the 425-year simulation period. Only a very small area in the lower right corner is affected.*

Figure 6-31 shows the time evolution of the caesium aqueous concentration in the discharge area, compared to the initial caesium aqueous concentrations in both the clay porewater and in the deep groundwater. In the discharge area (Figure 6-31), it can be seen that the concentration of caesium in the outflowing water is far from the concentration of this radionuclide in the deep groundwater, reflecting the potential of the geochemical processes to retard the transport of this radionuclide towards the discharge area.

Uranium

Since ferrihydrite is absent in the modelled domain, the only process able to retain uranium in this reference case will be the precipitation of uranium solid phases. The only uranium phase that reaches oversaturation, and therefore precipitates, is $UO_2 \cdot 2H_2O_{(am)}$ (a U(IV) pure phase). Figure 6-32 shows the spatial distribution of precipitated $UO_2 \cdot 2H_2O_{(am)}$. The precipitation of $UO_2 \cdot 2H_2O_{(am)}$ in the vicinity of the deep groundwater inflow boundary will control the migration of this radionuclide through the clay system.
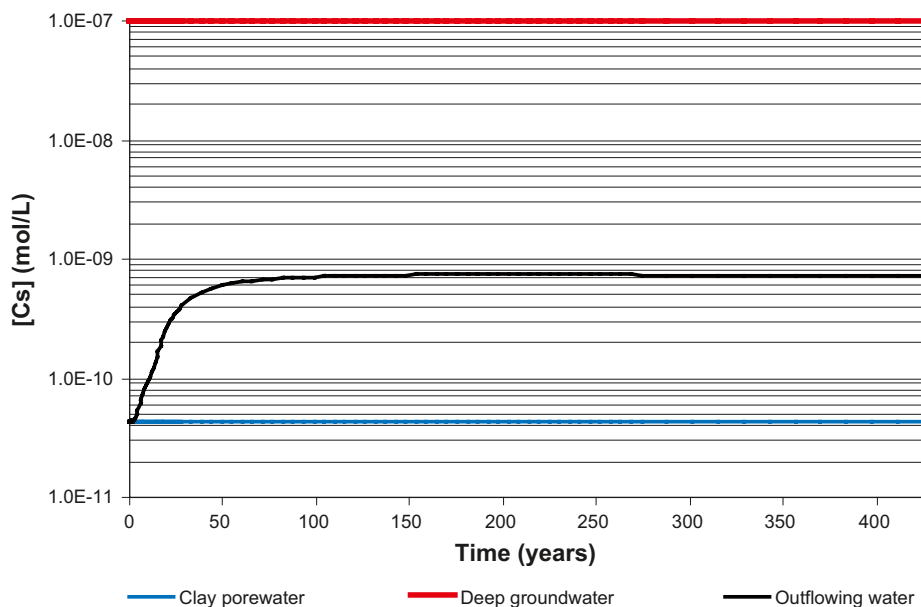
Figure 6-31. *Evolution of the concentration of aqueous caesium in the discharge area, during the reactive transport simulation (selected observation point shown in image B of Figure 6-23).*

Figure 6-32. Concentration of $UO_2 \cdot 2H_2O_{(am)}$ precipitated at the end of the 425-year simulation period.

Figure 6-33 shows the time evolution of the aqueous uranium concentration at the discharge area, compared to the initial uranium aqueous concentrations in both the clay porewater and in the deep groundwater. The evolution of the concentration of uranium in the discharge area indicates that the precipitation of $UO_2 \cdot 2H_2O_{(am)}$ limits the solubility of this radionuclide through the modelled domain, leading to a relatively low uranium concentration in the discharge area.

6.2.3   Conservative transport versus reactive transport

By comparing the amount of radionuclides in the modelled domain after the 425-year simulation period for both conservative and reactive transport simulations (cf section 6.1.3), it is possible to see that the geochemical processes considered to occur in the clay system are able to effectively retain the selected radionuclides, retarding their migration in the modelled domain. In Figure 6-34, it is observed that at the end of the simulation period the plume of strontium in the clay system is significantly reduced when cation exchange and $(Ca,Sr)CO_3$ solid solutions are considered (see Figure 6-28 for strontium concentrations retained in the solid phases).
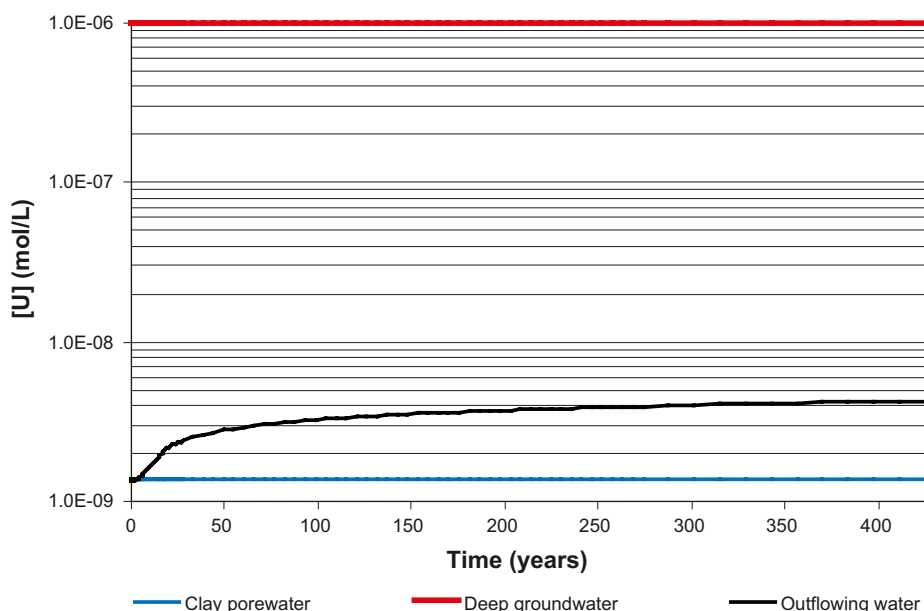

Figure 6-33. Evolution of the concentration of aqueous uranium in the discharge area, during the reactive transport simulation (selected observation point shown in image B of Figure 6-23).

CONSERVATIVE TRANSPORT MODEL
[Sr] at 425 years

REACTIVE TRANSPORT MODEL
[Sr] at 425 years

[Sr] (mol/L)
2.0E-03
1.5E-03
1.0E-03
5.0E-04
1.5E-06

Figure 6-34. Spatial distributions of computed strontium concentration in the conservative simulation (top) and the reactive transport simulation (bottom), reference case #2 after 425 years.

Figure 6-35 shows the predicted spatial distribution of dissolved caesium concentration both for conservative and reactive simulations. The plume of caesium is almost completely retained near the source of the radionuclides, indicating that cation exchange processes considered in the model are very effective in retaining caesium. As shown previously (Figure 6-30) almost all caesium entering the clay system is retained in the FES of the illite interlayer, just in the vicinity of the source of radionuclides.

Figure 6-36 shows the predicted spatial distribution of dissolved uranium concentration both for conservative and reactive simulations. As in the case of caesium, the plume of uranium is almost completely retained near the source of the radionuclides due to the oversaturation with respect to an amorphous uranium oxide which leads to the precipitation of this pure phase $(UO_2 \cdot 2H_2O_{(am)})$. The low concentrations of dissolved uranium are reflecting the spatial distribution of precipitated amorphous uranium oxide, as it was shown in Figure 6-32.

6.2.4 Quantitative assessment of the retention efficiency of the clay system

The efficiency of the near-surface Quaternary system for radionuclide retention can be evaluated quantitatively by comparison of the conservative and reactive transport computed results, as it was explained in section 6.1.4. The efficiency of the system can be assessed in any observation point. In the present study, we selected a point located in the discharge area, as shown at Figure 6-23.

CONSERVATIVE TRANSPORT MODEL
[Cs] at 425 years

REACTIVE TRANSPORT MODEL
[Cs] at 425 years

[Cs] (mol/L)
2.5E-07
1.9E-07
1.3E-07
6.3E-08
1.0E-10

Figure 6-35. Spatial distribution of computed caesium concentration in the conservative simulation (top) and the reactive transport simulation (bottom), reference case #2 after 425 years. Only a very small area in the lower right corner is affected in the reactive transport case.

Figure 6-36. Spatial distribution of computed uranium concentration in the conservative simulation (up) and the reactive transport simulation (down), reference case #2 after 425 years. Only a very small area in the lower right corner is affected in the reactive transport case.

In this observation point, the first arrival of deep contaminants to the surface can be recorded. Figure 6-37, Figure 6-38 and Figure 6-39 show C and R relative concentrations of strontium, caesium and uranium, respectively. The breakthrough curves correspond to the observation point located at the clay surface, as shown in Figure 6-23.

As expected, breakthrough curves of relative conservative concentrations (C) are identical for the three radionuclides. It can be seen that conservative transport steady-state is reached in about 400 years at the observation point located on the surface. Also, the relative reactive concentrations (R) are noticeably lower than the corresponding conservative concentrations (C) for the three simulated radionuclides. The larger the differences between R and C, the stronger the retention of the radionuclides in the clay. It is worth noting that R values are much higher for strontium than for both caesium and uranium, indicating that strontium retention processes are not as efficient as those for Cs and U.
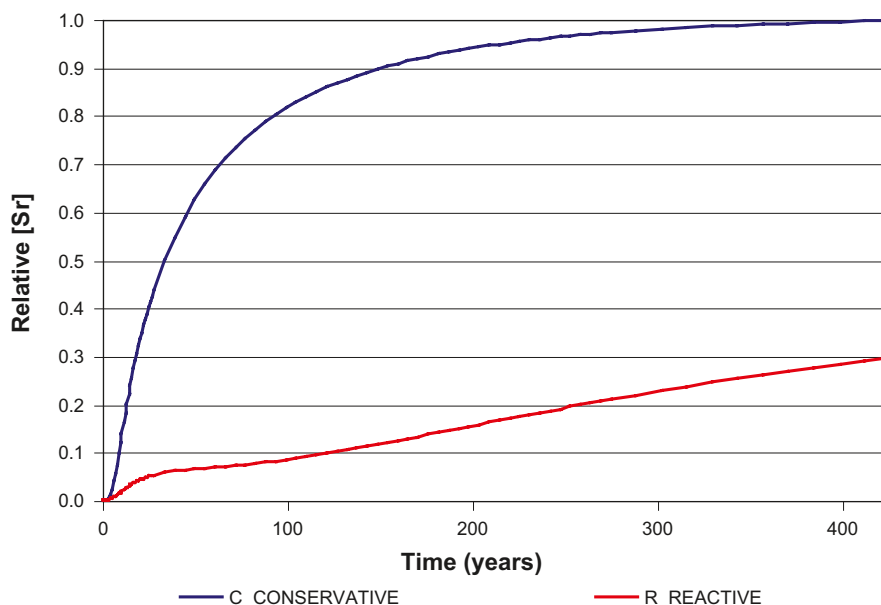
Figure 6-37. Breakthrough curves of relative C and R concentrations for Sr.
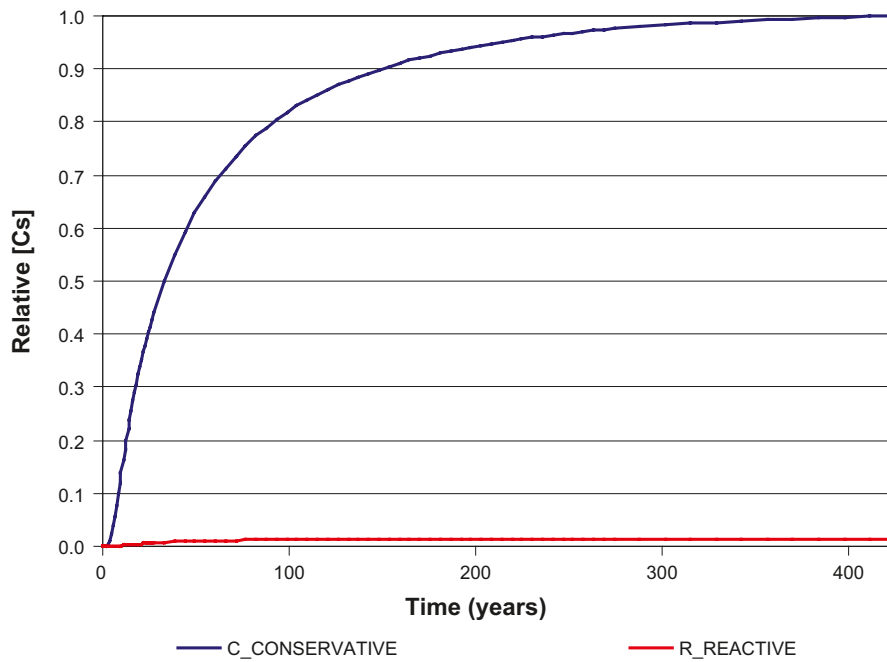
Figure 6-38. *Breakthrough curves of relative C and R concentrations for Cs.*
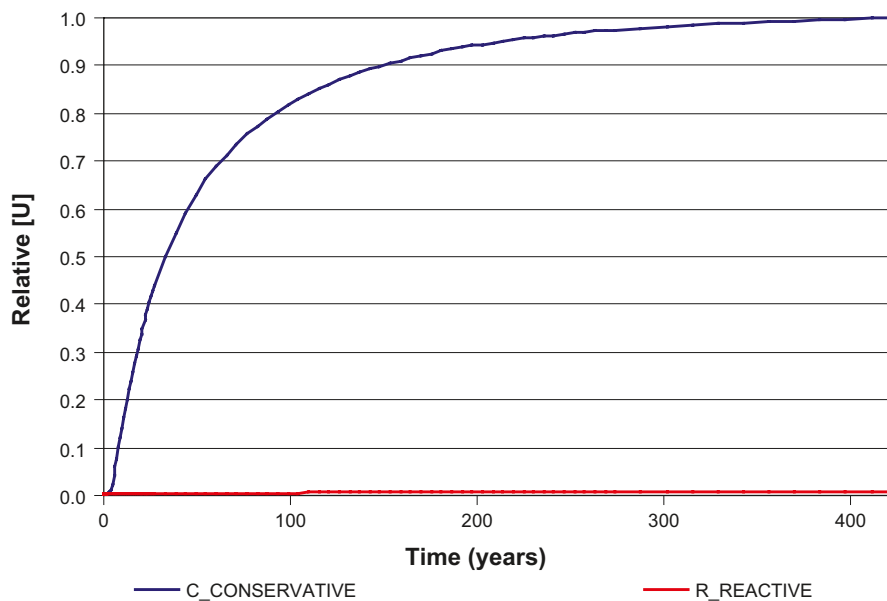
Figure 6-39. *Breakthrough curves of relative C and R concentrations for U.*

Figure 6-40 shows the time evolution of retention efficiencies of the system computed for strontium, caesium and uranium. The calculations of retention efficiencies are explained in Section 6.1.4.

The computed retention efficiencies of the system are very different for caesium and uranium compared with strontium. The clay system exhibits a very high efficiency for retention of uranium and caesium ($E > 95\%$) and this high efficiency remains constant during the simulated time period. The high retention efficiency of the system for uranium and caesium is a result of the fact that almost all the mass entering the system was fixed in the solid phase of the immediate surroundings of the radionuclide source.
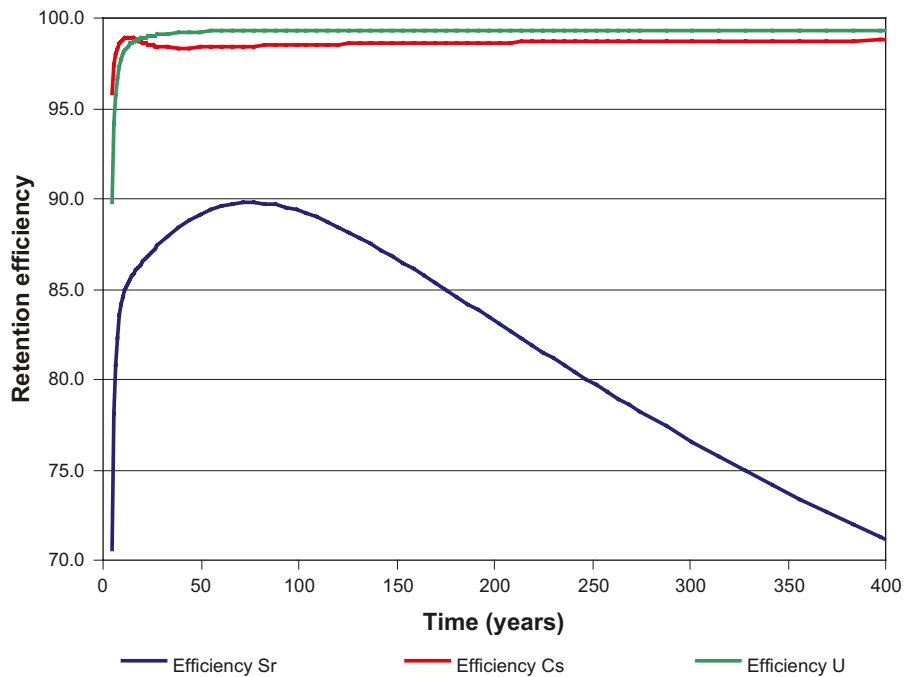
Figure 6-40. *Computed retention efficiencies for strontium, caesium and uranium.*

The uranium sink is a solid phase, $UO_2 \cdot 2H_2O$, which will precipitate as long as the solution is oversaturated; therefore, no limitations exist for its formation. The geochemical sink for caesium is the illite interlayer through cation exchange. This process is very favourable thermodynamically and the cation exchange sites are in excess with regards to Cs, which means that the process is highly efficient.

The calculated retention efficiency for strontium shows a different behaviour (Figure 6-39). The predicted efficiency increases up to 90% (after about 70 years) to decrease progressively from this time onwards. The initial increasing of the retention efficiency of the system is due to the fact that the radionuclide plume is migrating across the clay, so the amount of available clay to retain strontium increases. However, after reaching a maximum efficiency of the system, when all the clay in contact with radionuclide-bearing water is contributing to retention, the efficiency starts to decrease because the exchanger sites start to get saturated in strontium. Then, the solid solution approaches the miscibility limit of strontium, i.e. the maximum amount of strontium "accepted" as trace element in the solid solution.

Consequently, the efficiency of the system after the initial advective arrival time can only decrease progressively with time. It is worth noting that, according to the current model, the retention efficiency of the system is still 70% after 400 years of simulation time. The decrease of retention efficiency does not follow a constant slope pattern because it is the combined effect of 2 different processes. Initially, the cation exchange clearly dominates, but the effect of the solid solution is significant for longer times (see slope change in efficiency after 300 years in Figure 6-40).

7 Conclusions and future work

The main objective of the work presented in this report is the assessment of the migration behaviour of selected long-lived radionuclides through the near-surface system of the Forsmark Quaternary deposits, including lake and wetland sediments. The quantitative evaluation of the efficiency of the Quaternary system for radionuclide retention was also stated as a main objective.

An important effort has been devoted to construct a sound conceptual model based on the present-day state-of-the-art knowledge of geochemical behaviour of radionuclides. Moreover, the implementation of this conceptual model in reactive transport simulations has been successfully achieved.

This methodology has been proven to be a very powerfool quantitative tool for the assessment of the radionuclide retention capacity of the near-surface system present at Forsmark. The numerical simulations presented in this report aim at depicting a realistic evolution of the system and are based on site specific data whenever possible, although they consider hypothetical scenarios.

According to the results presented, Quaternary deposits and sediments at the Forsmark site are able to effectively retain radionuclides transferred from the deep bedrock. From the hydrogeological and reactive transport model results it is seen that the near-surface system at Forsmark constitutes a reactive geochemical barrier able to retain radionuclides by several key processes. Such retention mechanisms produce an effective overall retardation of radionuclide migration. In the calculations presented in this report, high initial radionuclide concentration in the deep groundwater have been considered as a first attempt assess the retention capacity of the system.

The ubiquity of illite in both the till aquifers and clay sediments allows a very strong retention of caesium. Most of the caesium mass entering the system from the deep bedrock is very efficiently retained in the close vicinity of the source, independently of the hydrogeological conditions. The overall retention efficiencies computed for caesium are close to 100% for both the till aquifers and the clay aquitards.

In the case of uranium, the most effective processes for retention are very different for the two considered hydrogeochemical systems. In the till aquifer, the dissolved uranium is mainly adsorbed onto the charged surfaces of ferrihydrite. It is seen that this dynamic aquifer system still exhibits a uranium retention efficiency of about 50% even after about 100 years of simulation time. The simulated clay system is much more efficient than the till aquifer for uranium retention due to the precipitation of amorphous uranium oxides. Uranium retention efficiencies higher than 95% are obtained for the clay system, even after more than 400 years. As in the case of caesium, most of the uranium mass entering the system from the deep source is effectively retained (in this case precipitated) in the vicinities of the source.

For strontium, the results indicate that this radionuclide is retained by two different geochemical processes: (1) cation exchange within illite interlayers and (2) precipitation as a $Sr_xCa_{1-x}CO_3$ solid solution. Even though there are 2 distinct retention mechanism affecting strontium, the clay system is less efficient retaining this radionuclide compared to the other two simulated radionuclides. It is noteworthy that numerical predictions, under the hypothetical assumptions considered in the modelling, indicate that strontium co-precipitation in calcite becomes a secondary retention mechanism together with the cationic exchange in the clays. In addition, the overall efficiency of both simulated systems to retain strontium shows a decrease with time.

The models and results presented in this report have some limitations that are summarized below, together with some suggestions for future work:

(1) Numerical models performed in this work are based on Forsmark Site Descriptive Model version 1.2. Major updates have been recently produced at the Forsmark site, mainly concerning the hydrogeological description. Current understanding indicates that deep groundwater discharge mainly occurs under the present Baltic Sea, and not in the present lakes, water courses and wetlands as initially thought. Thus, the models presented here should be updated to account for this new hydrogeological understanding and additional data collected at the site.

(2) As shown in Chapter 6 of this report, there are indications of that deep groundwater discharge into Quaternary deposits and sediments could trigger relatively long reactive transport transient states. Therefore, the numerical models should incorporate a generation of sound reactive transport natural conditions previously to the "injection" of radionuclides from the repository.

(3) The two hydrogeological systems studied in this work (i.e. till aquifer and clay aquitard) are actually not independent but connected at the Forsmark site. Clay layers are always overlying the till aquifer in the discharge areas. Then, the retention capacity of both systems are likely to be additive. More realistic and heterogeneous domains, including both till and clay system, could be simulated in future stages of this work.

(4) Co-precipitation of strontium in non-ideal carbonate solid solutions has been identified as a likely process able to retain dissolved strontium. However, the formulation of non-ideal solid solutions introduces an additional strong non-linearity in the reactive transport calculations. This fact leads to very expensive numerical simulations in terms of required CPU time. Some research on more efficient spatial and temporal discretization schemes could be very helpful to improve future numerical simulations.

(5) Coupled groundwater flow and reactive solute transport models involve a large number of processes and parameters. Consequently, the validity of model results is highly conditioned by the uncertainty in selected parameter values. Uncertainty can be properly studied and quantified by means of comprehensive and systematic sensitivity analyses. A methodology to study the retention efficiency of the systems (i.e. the reactivity of the systems) has been proposed in this work, which is based on the use of dimensionless (normalised) calculated conservative and reactive concentrations. It is thought that this methodology can be very useful also as a tool for systematic analysis of sensitivity exercises in the future.

(6) It is likely that reactive transport model results, and consequently the evaluated retention capacity, are sensitive to the hydrochemical boundary conditions prescribed in the deep groundwater source. Further evaluation and sensitivity analysis should be done as to reduce this source of uncertainty.

8　References

Abdelouas A, Lutze W, Gong W L, Nuttall E H, Strietelmeier B A, Travis B J, 2000.
Biological reduction of uranium in groundwater and subsurface soil. Sci. Total Env. 250, 25–31.

Albrecht J, 2005. Forsmark site investigation. Study of Quaternary sediments in connection with investigations of bedrock lineaments. SKB P-05-138, Svensk Kärnbränslehantering AB.

Alfthan G, Wang D, Area A, Soveri J, 1995. The geochemistry of selenium in groundwaters in Finland. The Science of the Total Environment, 162, 93–103.

Avery S V, 1996. Fate of caesium in the environment: Distribution between the abiotic and biotic components of aquatic and terrestrial ecosystems. Journal of Environmental Radiactivity, 30-2, 139–171.

Belzile N, Chen Y-W, Xu R, 2000. Early diagenetic behaviour of selenium in freshwater sediments. Applied Geochemistry, 15, 1439–1454.

Bostock A C, Shaw G, Bell J N B, 2003. The volatilisation and sorption of [129]I in coniferous forest, grassland and frozen soils. Journal of Environmental Radioactivity, 70, 29–42.

Boudreau B P, 1999. Metals and models: Diagenetic modelling in freshwater lacustrine sediments. Journal of Paleolimnology, 22, 227–251.

Bradbury M H, Baeyens B, 2000. A generalised sorption model for the concentration dependent uptake of caesium by argillaceous rocks. Journal of Contaminant Hydrology, 42, 141–163.

Bruggeman C, Maes A, Vancluysen J, Vandemussele P, 2005. Selenite reduction in Boom clay: Effect of FeS_2, clay minerals and dissolved organic matter. Environmental Pollution, 137, 209–221.

Bruno J, Sandino A, 1989. The solubility of amorphous and crystalline schoepite in neutral to alkaline aqueous solutions. Mat. Res. Soc. Symp. Proc, 127, 871–878.

Bruno J, Stumm W, Wersin P, Brandberg F, 1992. On the influence of carbonate in mineral dissolution: Part 1. The thermodynamics and kinetics of hematite dissolution in bicarbonate solutions at T = 25°C. Geochimica et Cosmochimica Acta, 56, 1139–1148.

Bruno J, Duro L, de Pablo J, Casas I, Ayora C, Delgado J, Gimeno M J, Peña J, Linklater C, Pérez del Villar L, Gómez P, 1998. Estimation of the concentrations of trace metals in natural systems. The application of codissolution and coprecipitation approaches to El Berrocal (Spain) and Poços de Caldas (Brazil). Chemical Geology, 151, 277–291.

Bruno J, Duro L, Grivé M, 2002. The applicability and limitation of thermodynamic geochemical models to simulate trace element behaviour in natural waters. Lessons learned from natural analogue studies. Chemical Geology, 190, 371–393.

Casas I, Bruno J, Cera E, Finch R J, Ewing R, 1994. Kinetic and thermodynamic studies of uranium minerals. Assessment of the long-term evolution of spent nuclear fuel. SKB TR-94-16, Svensk Kärnbränslehantering AB.

Casas I, Bruno J, Cera E, Finch R J, Ewing R C, 1997. Characterization and dissolution behaviour of a Becquerelite from Shinkolobwe, Zaire. Geochimica et Cosmochimica Acta, 61, 3879–3884.

Chabroullet C, Coppin F, Martin-Garin A, Floriani M, Tinseau E, Gaudet J-P, 2006.
Se-soil organic matter interactions: Direct or indirect association?. Goldschmidt Conference Abstract 2006, A93.

Choppin G R, Shanbhag P M, 1981. Binding of calcium with humic acid. J. Inorg. Nucl. Chemistry, 43, 921–922.

Chen C C, Hayes K F, 1999. X-ray absorption spectroscopy investigation of aqueous Co(II) and Sr(II) sorption at clay-water interfaces. Geochimica et Cosmochimica Acta 63(19-20), 3205–3215.

Cole T, Bidoglio G, Soupioni M, O'Gorman M, Gibson N, 2000. Diffusion mechanisms of multiple strontium species in clay. Geochimica et. Cosmochimica Acta 64, 385.

Comans R N J, Middelburg J J, Zonderhuis J, Woittiez J R W, De Lange G J, Das H, Van Der weijden C H, 1989. Mobilization of radiocesium in pore waters of lake sediments. Nature, 339, 367–369.

Couture R A, Seitz M G, 1983. Sorption of anions of iodine by iron oxides and kaolinite. Nucl. Chem. Waste Manag, 4, 301–306.

Cox J D, Wagman D D, Medvedev V A, 1989. CODATA Key Values for Thermodynamics, Hemisphere Publishing Corp, New York.

Davis J-A, Meece D-E, Kohler M, Curtis G, 2004. Approaches to surface complexion modelling of Uranium(VI) adsorption on aquifer sediments. Geochimica et Cosmochimica Acta, Vol. 68, 18: 3621–3641.

Dhakar S P, Burdige D J, 1996. A coupled, non-linear, steady state model for early diagenetic processes in pelagic sediments. Am. J. Sci. 296: 296–330.

Duc M, Lefevre G, Fedoroff M, Jeanjean J, Rouchaud J C, Monteil-Rivera F, Dumonceau J, Milonjic S, 2003. Sorption of selenium anionic species on apatites and iron oxides from aqueous solutions. Journal of Environmental Radioactivity, 70, 61–72.

Duff M C, Urbanik-Coughlin J, Hunter D B, 2002. Uranium co-precipitation with iron oxide minerals Geochimica et Cosmochimica Acta, 66-20, 3533–3547.

Dumat C, Staunton S, 1999. Reduced adsorption of caesium on clay minerals caused by various humic substances. Journal of Environmental Radioactivity, 46, 187–200.

Duro L, Grivé M, Cera E, Gaona X, Domènech C, Bruno J, 2006a. Determination and assessment of the concentration limits to be used in SR-MET. SKB TR-06-32, Svensk Kärnbränslehantering AB.

Duro L, Grivé M, Cera E, Domènech C, Bruno J, 2006b. Update of a thermodynamic database for radionuclides to assist solubility limits calculation for performance assessment. SKB TR-06-17, Svensk Kärnbränslehantering AB.

Finch R J, 1994. Paragenesis and crystal chemistry of the uranyl oxide hydrates. Ph.D. Thesis, University of New Mexico, 257 p.

Finch R J, Murakami T, 1999. Systematics and paragenesis of uranium minerals. In: Uranium: Mineralogy, geochemistry and the environment. (eds.) P. Burns and R. Finch, Reviews in Mineralogy, 38, 91–180.

Fuller C C, Bargar J R, Davis J A, Piana M J, 2002. Mechanisms of uranium interactions with hydroxyapatite: Implications for groundwater remediation. Environ. Sci. Technol, 36, 158–165.

Garbisu C, Ishii T, Leighton T, Buchanan B B, 1996. Bacterial reduction of selenite to elemental selenium. Chemical Geology, 132. 199–204.

Goldhaber M B, Hemingway B S, Mohagheghi A, Reynolds R L, Northrop H R, 1987. Origin of coffinite in sedimentary rocks by a sequential adsorption-reduction mechanism. Bulletin de Minéralogie, 110, 131–144.

Grenthe I, Fuger J, Konings R J M, Lemire R J, Muller A J, Nguyen-Trung C, Wanner H, 1992. Chemical Thermodynamics of Uranium. Elsevier, Amsterdam.

Grivé M, 2005. The linkage between uranium, iron and carbon cycling. Processes at interfaces: evidences from combined solution chemical and spectroscopic studies. PhD. Thesis, Universitat Politècnica de Catalunya, 341 pp.

Gu B, Chen J, 2003. Enhanced microbial reduction of Cr(VI) and U(VI) by different natural organic matter fractions. Geochimica et Cosmochimica Acta, 67-19, 3575–3582.

Guggenheim E A, 1937. Theoretical basis of Raoult's law. Trans. Faraday Soc, 33, 151–159.

Guillaumont R, Fanghänel J, Neck V, Fuger J, Palmer D A, Grenthe I, Rand M H, 2003. Chemical Thermodynamics 5. Update on the Chemical Thermodynamics of Uranium, Neptunium, Plutonium, Americium and Technetium. NEA OECD, Elsevier.

Hedenström A, 2003. Forsmark site investigation. Investigation of marine and lacustrine sediment in lakes. Field data 2003. SKB P-03-24, Svensk Kärnbränslehantering AB.

Hedenström A, 2004. Forsmark site investigation. Investigation of marine and lacustrine sediment in lakes. Stratigraphical and analytical data. SKB P-04-86, Svensk Kärnbränslehantering AB.

Hird A B, Rimmer D L, Livens F R, 1995. Total caesium-fixing potentials of acid organic soils. Journal of Environmental Radioactivity, 26, 103–118.

Hsi C-K D, Langmuir D, 1985. Adsorption of uranyl onto ferric oxyhydroxides: Applications of the surface complexation site-binding model. Geochim. Cosmochim. Acta 49, 1931–1941.

Hu Q, Zhao P, Moran J E, Seaman J, 2005. Sorption and transport of iodine species in sediments from the Savannah River and Hanford Sites. Journal of Contaminant Hydrology, 78, 185–205.

Hummel W, Berner U, Curti E, Pearson F J, Thoenen T, 2002. Nagra/PSI Chemical Thermodynamic Data Base 01/01. ISBN: 1-58112-620-4. 565 p.

Jerden J L, Sinha A K, Zelazny L, 2003. Natural immobilization of uranium by phosphate mineralization in an oxidizing saprolite–soil profile: chemical weathering of the Coles Hill uranium deposit, Virginia. Chemical Geology, 199, 129–157.

Johansson P O, Werner K, Bosson E, Berglund S, Juston J, 2005. Description of climate, surface hydrology, and near-surface hydrogeology Preliminary site description. Forsmark area – version 1.2. SKB R-05-06, Svensk Kärnbränslehantering AB.

Johnson J, Anderson G, Parkhurst D, 2000. Database from "thermo.com.V8.R6.230" prepared by at Lawrence Livermore National Laboratory (revision 1.11). LLNL report.

Kaplan D I, Serne R J, Parker K E, Kutnyakov I V, 2000. Iodide sorption to subsurface sediments and illitic minerals. Environ. Sci. Technol. 24-3, 399–405.

Kipp K L, 1997. Guide to the revised heat and solute transport simulator HST3D-Version 2. U.S. Geological Survey Water-Resources Investigations Report, 97-4157, 149 p.

Köhler S J, Dufaud F, Oelkers E H, 2003. An experimental study of illite dissolution kinetics as a function of ph from 1.4 to 12.4 and temperature from 5 to 50°C. Geochimica et Cosmochimica Acta, 67-19, 3583–3594.

Krestou A, Xenidis A, Panias D, 2004. Mechanism of aqueous uranium(VI) uptake by hydroxyapatite. Minerals Engineering, 17, 373–381.

Lamble G M, Lee J F, Staudt W J, Reeder R J, 1995. Structural studies of selenate incorporation into calcite crystals. Physica B 208&209, 589–590.

Langmuir D, 1997. Aqueous environmental geochemistry. Prentice-Hall Inc. Upper Saddle River, NJ.

Li W C, Victor D M, Chakrabati C L, 1980. Effect of pH and uranium concentration on interaction of uranium(VI) and uranium (IV) with organic ligands in aqueous solutions. Anal. Chem. 52, 520–523.

Lenhart J J, Cabaniss S E, MacCarthy P, Honeyman B D, 2000. Uranium (VI) complexation with citric, humic and fulvic acids. Radiochimica Acta, 88, 345–353.

Lippmann F, 1980. Phase diagrams depicting aqueous solubility of binary mineral systems. Neues Jahrb. Mineral. Abh, 139, 1–25.

Loft S, Tipping E W, Sanchez A L, Dodd B A, 2002. Modelling the role of humic acid in radiocaesium distribution in a British upland peat soil. Journal of Environmental Radioactivity, 61, 133–147.

Lokrantz H, Hedenström A, 2006. Forsmark site investigation: Description, sampling and analyses of Quaternary deposits in connection with groundwater monitoring wells, pumping wells and BAT filter tips. SKB P-06-92, Svensk Kärnbränslehantering AB.

Lorens R B, 1981. Sr, Cd, Mn and Co distribution coefficients in calcite as a function of calcite precipitation rate. Geochim. Cosmochim. Acta 45, 553–561.

Losi M E, Frankenberger Jr W T, 1998. Reduction of selenium oxyanions by Enterobacter cloacae strain SLDa-1. In: Frankenberger Jr, W.T., Engberg, R.A. (Eds.), Environmental Chemistry of Selenium. Marcel Dekker, New York, pp. 515–544.

Lu N P, Mason C F V, 2001. Sorption-desorption behavior of strontium-85 onto montmorillonite and silica colloids. Applied Geochemistry 16-14, 1653–1662.

Martens D A, Suarez D L, 1999. Soil Transformations of volatile methylated selenium in soil. Biology and Biochemistry, 31, 1355–1361.

Masscheleyn P H, Delaune R D, Patrick W H, 1991. Biogeochemical behaviour of selenium in anoxic soils and sediments: An equilibrium thermodynamics approach. J. Env. Sci. Health, A26(4), 555–573.

Murakami T, Ohnuki T, Isobe H, Sato T, 1997. Mobility of uranium during weathering. Am. Min., 82, 888–889.

Muramatsu Y, Yoshida S, 1995. Volatilization of methyl iodide from the soil–plant system. Atmos. Environ. 29, 21–25.

Muramatsu Y, Yoshida S, Fehn U, Amachi S, Ohmomo Y, 2004. Studies with natural and anthropogenic iodine isotopes: iodine distribution and cycling in the global environment. Journal of Environmental Radioactivity, 74, 221–232.

Nguyen N S, Silva R J, Weed H C, Andrews Jr J E, 1992. Standard Gibbs free energies of formation at the temperature 303.15K of four Uranyl silicates: soddyite, uranophane, sodium boltwoodite and sodium weeksite. J. Chem Thermodyn, 24, 1, 359–376.

Nordstrom D K, Plummer L N, Langmuir D, Busenberg E, May H M, Jones B F, Parkhurst D L, 1990. Revised chemical equilibrium data for major water-mineral reactions and their limitations. In R.L. Bassett and D. Melchior, (eds.), Chemical modeling in aqueous systems II: Washington D.C., American Chemical Society Symposium Series 416, Chapter 31, 398–413.

Ohnuki T, Yoshida T, Ozaki T, Samadfam M, Kozai N, Yubuta K, Mitsugashira T, Kasama T, Francis A J, 2005. Interactions of uranium with bacteria and kaolinite clay. Chemical Geology, 220, 3-4, 237–243.

Olin A, Noläng B, Osadchii E G, Öhman L-O, Rosén E, 2005. Chemical Thermodynamics vol. 7: Chemical Thermodynamics of Selenium. NEA OECD, Elsevier.

Oremland R S, Hollibaugh J T, Maest A S, Pressor T S, Miller L G, Culbertson C W, 1989. Selenate reduction to elemental selenium by anaerobic bacteria in sediments and culture: biogeochemical significance of a novel, sulfate-independent respiration. Appl. Environ. Microbiol. 55, 2333–2343.

Outridge P M, Stern G A, Hamilton P B, Percival J B, McNeely R, Lockhart W L, 2005. Trace metal profiles in the varved sediment of an Arctic lake. Geochimica et Cosmochimica Acta, 69-20, 4881–4894.

Pabalan R T, Turner D R, Bertetti F P, Prikryl J D, 1998. Uranium(VI) sorption onto selected mineral surfaces: key geochemical parameters. In: Jenne, E.A. (Ed.), Adsorption of Metals by Geomedia: Variables, Mechanisms, and Model Applications. Academic Press, San Diego, pp. 99–130.

Payne T E, Davis J A, Waite T D, 1996. Uranium adsorption on ferrihydrite – effects of phosphate and humic acid. Radiochim. Acta 74, 239–243.

Payne T E, Lumpkin G R, Waite T D, 1998. Uranium(VI) adsorption on model minerals: controlling factors and surface complexation modeling. In: Jenne, E.A. (Ed.), Adsorption of Metals by Geomedia: Variables, Mechanisms, and Model Applications. Academic Press, San Diego, pp. 75–97.

Parkhurst D L, Appelo C A J, 1999. User's guide to PHREEQC (version 2) – A computer program for speciation, batch-reaction, one-dimensional transport and inverse geochemical calculations. U.S. Geological Survey Water Resources investigations report 99-4259.

Parkhurst D L, Kipp K L, Engesgaard P, Charlton S R, 2004. A program for simulating ground-water flow, solute transport, and multicomponent geochemical reactions. U.S. Geological Survey Techniques and Methods 6-A8, 154 pp.

Peak D, 2006. Adsorption mechanisms of selenium oxyanions at the aluminium oxide/water interface. Journal of Colloid and Interface Science, 303, 337–345.

Percival J B, Hunt P, Wygergangs M, 2001. Mineralogical investigations of Canadian till and lake- and stream-sediment reference materials: Part 1. Standardized X-ray diffraction and scanning electron microscope methods. Geol. Surv. Can. Curr. Res. 2001-E9, 8 p.

Pérez I, Casas I, Torrero M E, Cera E, Duro L, Bruno J, 1997. Dissolution studies of soddyite as long-term analogue of oxidative alteration of spent nuclear fuel matrix. Mater. Res. Soc. Symp. Proc., 465, 565–572.

Plummer L N, Busenberg E, 1982. The solubilities of calcite, aragonite and vaterite in CO_2-H_2O solutions between 0°C and 90°C, and an evaluation of the aqueous model for the system $CaCO_3$-CO_2-H_2O. Geochimica et Cosmochimica Acta 46-6: 1011–1040.

Plummer L N, Busenberg E, 1987. Thermodynamics of aragonite–strontianite solid solutions: results from stoichiometric solubility at 25 and 76°C. Geochimica and Cosmochimica Acta 51, 1393–1411.

Poinssot C, Baeyens B, Bradbury M H, 1999. Experimental and modelling studies of caesium sorption on illite. Geochimica et Cosmochimica Acta, 63(19-20), 3217–3227.

Puigdomènech I, 2002. MEDUSA: Make Equilibrium Diagrams Using Sophisticated Algorithms. Software based on: Puigdomenech, I (1983). INPUT, SED and PREDOM: computer programs drawing equilibrium diagrams. Report TRITA-OOK-3010, Dept. Inorg. Chem. Royal Institute of Technology, Stockholm.

Rädlinger G, Heumann K G, 2000. Transformation of iodide in natural and wastewater systems by fixation on humic substances. Environ. Sci. Technol. 34-18, 3932–3936.

Redlich O, Kister A T, 1948. Algebraic representation of thermodynamic properties and the classification of solutions. Ind. Eng. Chem., 40-2, 345–348.

Reiller P, 2005. Pronosticating the humic complexation for redox sensitive actinides through analogy, using the charge neutralisation model. Radiochimica Acta, 93, 43–55.

Robie R A, Waldbaum D R, 1968. Thermodynamic properties of minerals and related substances at 298.15°K (25°C) and one atmosphere (1.013bars) pressure and at high temperatures, U.S. Geological Survey Bulletin, 1259.

Robit-Pointeau V, Poinssot C, Vitorge P, Grambow B, Cui D, Spahiu K, Catalette H, 2006. Assessment of the relevance of coffinite formation within the near-field environment of spent nuclear fuel geological disposals. Materials Research Society Symposium Proceedings, 932, 489–496.

Roden E E, Leonardo M R, Ferris G, 2002. Immobilization of strontium during iron biomineralization coupled to dissimilatory hydrous ferric oxide reduction. Geochimica et Cosmochimica Acta, 66-16, 2823–2839.

Sandino A, Bruno J, 1992. The solubility of $(UO_2)_3(PO_4)_2 \cdot 4H_2O(s)$ and the formation of U(VI) phosphate complexes: Their influence in uranium speciation in natural waters. Geochim. Cosmochim. Acta 56, 4135–4145.

Sawhney B L, 1972. Selective sorption and fixation of cations by clay minerals: a review. Clays and Clay Minerals, 20, 93–100.

Seaman J C, Meehan T, Bertsch P M, 2001. Immobilization of Cesium-137 and uranium in contaminated sediments using soil amendments. Journal of Environmental Quality, 30, 1206–1213.

Shanbhag P M, Choppin G R, 1981. Binding of uranyl by humic acid. J. Inorg. Nucl. Chem. 43, 3369–3372.

Shaw G, Bell J N B, 1991. Competitive effects of potassium and ammonium on caesium uptake kinetics in wheat. Journal of Environmental Radioactivity, 13, 283–296.

Shenber M A, Eriksson A, 1993. Sorption behaviour of caesium in various soils. J. Environ. Radioactivity, 19, 41–51.

Sheppard M I, Hawkins J L, 1995. Iodine and microbial interactions in an organic soil. J. Environ. Radioactivity, 29-2, 91–109.

Siddique T, Zhang Y, Okeke B C, Frankenberger W C, 2006. Characterization of sediment bacteria involved in selenium reduction. Bioresource Technology, 97, 1041–1049.

SKB, 2005. Preliminary site description. Forsmark area – version 1.2. SKB R-05-18, Svensk Kärnbränslehantering AB.

SKB, 2006. The biosphere at Forsmark. Data, assumptions and models used in the SR-Can assessment. SKB R-06-82, Svensk Kärnbränslehantering AB.

Sohlenius G, Hedenström A, Rudmark L, 2004. Forsmark site investigation. Mapping of unconsolidated Quaternary deposits 2002–2003. Map description. SKB R-04-39, Svensk Kärnbränslehantering AB.

Staunton S, Dumat C, Zsolnay A, 2002. Possible role of organic matter in radiocaesium adsorption in soils. Journal of Environmental Radioactivity, 58, 163–173.

Strömgren M, Brunberg A-K, 2006. Elemental composition of a deep sediment core from Lake Stocksjön in the Forsmark area. SKB R-06-96, Svensk Kärnbränslehantering AB.

Stumm W, Morgan J, 1996. Aquatic chemistry. 3rd Ed. New York: John Wiley.

Templeton A S, Trainor T P, Spormann A M, Brown G, 2003. Selenium speciation and partitioning within *Burkholderia cepacia* biofilms formed on α-Al_2O_3 surfaces. Geochimica et Cosmochimica Acta, 67-19, 3547–3557.

Tesoriero A J, Pankow J F, 1996. Solid solution partitioning of Sr^{2+}, Ba^{2+}, and Ca^{2+} to calcite. Geochim. Cosmochim. Acta 60-6, 1053–1064.

Ticknor K V, Cho Y H, 1990. Interaction of iodide and iodate with granitic fracture-filling minerals. Radioanal. Nucl. Chem. 140-1, 75–90.

Tikhomirov F A, Kasparov S V, Prister B S, Sal'nikov V G, 1980. Role of organic matter in iodine fixation in soils. Sov. Soil Sci. 2, 54–62.

Tournassat C, Gailhanou H, Crouzet C, Braibant G, Gautier A, Lassin A, Blanc Ph, Gaucher E C, 2007. Two cation exchange models for direct and inverse modelling of solution major cation composition in equilibrium with illite surfaces. Geochimica et Cosmochimica Acta, 71, 1098–1114.

Trivedi P, Axe L, 1999. A comparison of strontium sorption to hydrous aluminum, iron, and manganese oxides. Journal of Colloid and Interface Science 218, 554–563.

Tröjbom M, Söderbäck B, 2006. Chemical characteristics of surface systems in the Forsmark area. Visualisation and statistical evaluation of data from shallow groundwater, precipitation, and regolith. SKB R-06-19, Svensk Kärnbränslehantering AB.

Turner G D, Zachara J M, McKinley J P, Smith S C, 1996. Surface-charge properties and UO_2^{2+} adsorption of a subsurface smectite. Geochim. Cosmochim. Acta 60, 3399–3414.

Van Beinum W, Hofmann A, Meeussen J C L, Kretzschmar R, 2005. Sorption kinetics of strontium in porous hydrous ferric oxide aggregates. I. The Donnan diffusion model. Journal of Colloid and Interface Science 283, 18–28.

Van Geen A, Robertson A P, Leckie J O, 1994. Complexation of carbonate species at the goethite surface: Implications for adsorption of metal ions in natural waters. Geochimica et Cosmochimica Acta, 58, 2073–2086.

Vikström M, 2005. Modelling of soil depth and lake sediments. An application of the GeoEditor at the Forsmark site. SKB R-05-07, Svensk Kärnbränslehantering AB.

Wang X, Liu X, 2005. Sorption and desorption of radioselenium on calcareous soil and its solid components studied by batch and column experiments. Applied Radiation and Isotopes, 62, 1–9.

Waite T D, Davis J A, Payne T E, Waychunas G A, Xu N, 1994. Uranium (VI) adsorption to ferrihydrite: Application of a surface complexation model. Geochimica et Cosmochimica Acta, 58, 5465–5478.

Zachara J M, Smith S C, Liu C, McKinley J P, Serne R J, Gassman P L, 2002. Sorption of Cs+ to micaceous subsurface sediments from the Hanford site, USA. Geochimica et Cosmochimica Acta 66, 193–211.

Zhang Y Q, Moore J N, 1996. Selenium fractionation and speciation in a wetland system. Environ. Sci. Technol. 30, 2613–2619.

Zhang Y Q, Moore J N, 1997. Reduction potential of selenate in wetland sediment. J. Environ. Qual. 26, 910–916.